



NTNU – Trondheim
Norwegian University of
Science and Technology

Condition Assessment of Wind Farm Medium Voltage Cable Joints

Hans Lavoll Halvorson

Master of Science in Electric Power Engineering

Submission date: June 2012

Supervisor: Frank Mauseth, ELKRAFT

Co-supervisor: Sverre Hvidsten, Sintef

Norwegian University of Science and Technology
Department of Electric Power Engineering

Project description

Condition Assessment of Wind Farm Medium Voltage Cable Joints

To estimate the degree of ageing is at present the most important tasks of non-destructive diagnostic testing. By such knowledge condition based maintenance actions can be planned, hopefully resulting in reduced number of unexpected failures and reduced maintenance cost.

Current loading of wind farm cable systems is very different from that observed in traditional distribution systems. Variations in wind power will give huge number of current cycles during service. The current load can vary from maximum permitted load (equivalent to 90 °C at the conductor) to zero within minutes and vice versa. This makes high demands on e.g. the quality of the electrical connections such as the metallic contacts in cable joints. The contact resistance should be low to avoid critical temperatures even higher than 90 °C for such installations. Any high temperatures can cause large cyclic temperature gradients inducing significant thermo-mechanical forces. High temperatures also result in severe oxidation of the insulation materials, cracking of brittle oxidized materials, partial discharges and finally a breakdown likely even after only a few years of service.

The project work will be mainly experimental. The main purpose of the work will be to examine wind farm service conditions in the laboratory simulating badly installed cable joints, and to examine the applicability of a Sweeping Frequency PD (SFPD) method to assess non-destructively the insulation condition. An ageing set-up should be designed and built, as well as a reproducible "bad" metallic joint connection. The SFPD measurements should be done in a broad but practical frequency range. A high voltage source is available (high voltage amplifier), but in order to perform sensitive measurements a low pass filter has to be built and tested on cable joints. The filter should be further improved to reduce the noise level. The PD activity in the joints should also be localized and the cable joints dissected in order to determine the real cause of the ageing and any discharge activity.

*Frank Mauseth, Ph.D.
Associate Professor
Norwegian University of Science and Technology
Department of Electric Power Engineering
O.S. Bragstads Plass 2E
7491 Trondheim, Norway
Phone: +47-735-94234*

Preface

This report is a summary of the lab work and literature study completed in my master thesis during the spring of 2012 at NTNU. The work has been carried out at the Department of Electric Power Engineering. I would like to thank my supervisor Frank Mauseth and co-supervisor Sverre Hvidsten for their great help and insightful guidance during the master thesis work. Also Horst Førster, Erik Bjerrehorn, Odd Lillevik, Vladimir Klubicka and Bård Almås should be mentioned for their contributions on practical matters in the laboratory.



Hans Lavoll Halvorson

Student

Trondheim

June 2012

Abstract

Rapid aging and failure in wind-farm collector systems has become an issue for grid owners. PD measurements of the cable systems can give good diagnostics, detect aging and pinpoint faults. Different PD measuring techniques are used today and the results will vary with applied voltage and frequency. This master thesis deals with preparation, electrothermal aging and characterization of XLPE cable joints. Dissection of the test objects was performed after aging and characterization.

For characterization a variable frequency PD measurement setup has been built. The setup is defined by being able to detect PD with high accuracy in test objects at $\pm 17 \text{ kV}_{\text{peak}}$ using Omicron MPD600 measuring equipment at variable frequencies between 10 mHz and 100 Hz. A PD-free low-pass RLC filter had to be used in the setup to reduce noise from the high-voltage source.

The most important findings are that PD measurement results will vary significantly with regards to measuring technique. Aging may not be detected when measuring with too low frequency or voltage.

Content

- Project description I
- Preface II
- Abstract III
- Content.....IV
- 1. Introduction..... 1
 - 1.1 Perspectives 1
 - 1.2 Objectives and approach..... 2
 - 1.3 Structure of the thesis..... 3
- 2. Theory 4
 - 2.1 Test objects..... 4
 - 2.1.1 XLPE cable 4
 - 2.1.2 Cable joint 4
 - 2.1.3 Cable termination 4
 - 2.2 Characterization of test objects 5
 - 2.2.1 Condition assessment and aging..... 5
 - 2.2.2 Partial discharge definition 6
 - 2.2.3 Effects of frequency..... 6
 - 2.2.4 Location of PD 9
 - 2.2.5 Detection of PD 10
 - 2.2.6 Noise..... 12
 - 2.2.7 Low-pass filter 13
 - 2.2.8 PD data handling and statistics 15
 - 2.3 Aging procedure 17
- 3. Experimental 19
 - 3.1 Test objects..... 19
 - 3.1.1 XLPE cable 20
 - 3.1.2 Simulation of contact failure..... 20
 - 3.1.3 Raychem joint..... 21
 - 3.1.4 PD free cable termination..... 22
 - 3.1.5 Finding physical properties 23

3.2	Characterization of test objects	25
3.2.1	PD detection	25
3.2.2	Coupling Capacitor C_k	26
3.2.3	Low pass filter	26
3.2.4	Variable frequency PD measurement setup.....	30
3.2.5	PD detection at different frequencies and voltages	30
3.2.6	Finding inception/extinction voltage.....	31
3.2.7	Dissection	32
3.3	Aging procedure	33
3.3.1	Heat cycling setup	33
4.	Results and observations	34
4.1	Test objects.....	34
4.1.1	Finding physical properties (joint # 4).....	34
4.1.2	Simulation of contact failure and electrothermal aging	35
4.2	Characterization of test objects	37
4.2.1	PRPDA plots.....	38
4.2.2	Inception/extinction voltage as a function of frequency	38
4.2.3	PD count and charge per cycle as a function of frequency and voltage	39
4.2.4	Mean charge as a function of frequency and voltage.	41
4.2.5	Charge amplitude distribution	43
4.2.6	Weibull distributions	45
4.2.7	Acoustic analysis of test objects	46
4.2.8	Dissection of joints	47
5.	Conclusions and further work	51
6.	References	53
7.	Appendices.....	56
A.	Statistical results	56
B.	Inception voltage results	61
C.	PRPDA plots	63
D.	Histogram plots	78

E. Weibull plots	92
F. Dissection photos	106
G. Equipment lists	112
H. Export data from MTRONIX to MATLAB	115
I. Driving capacitive load	117
J. Joint ferrule replacement	119
K. Temperature sensor placement in joint #4	120
L. Labview aging program	121
M. Wiring diagram aging setup	124

1. Introduction

1.1 Perspectives

Wind farm collector systems experience a very demanding load on cables and accessories compared to utility distribution systems. Temperature cycles caused by fast changing load profiles between 0 and 1 PU and long periods of full load contrast the calm 24 h sinusoidal loading cycle of a small cluster of domestic homes. Fast deterioration of cables and cable accessories has been reported at wind farms. PD measurements and diagnostic tools are now being used to determine aging and deterioration of medium voltage cable systems in wind farms [1] [2] [3] [4].

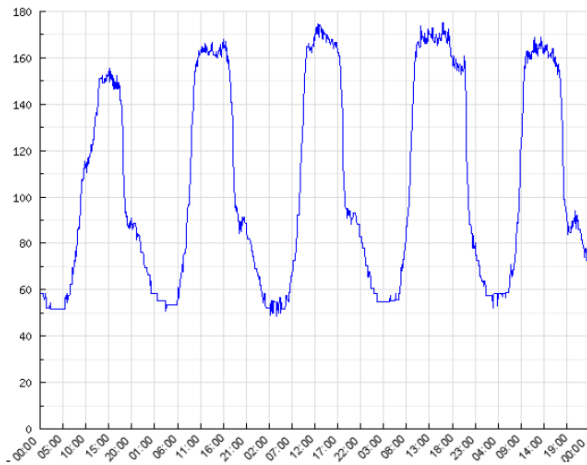


Figure 1. Typical load profile (over 5 days) of a normal distribution cable [4]

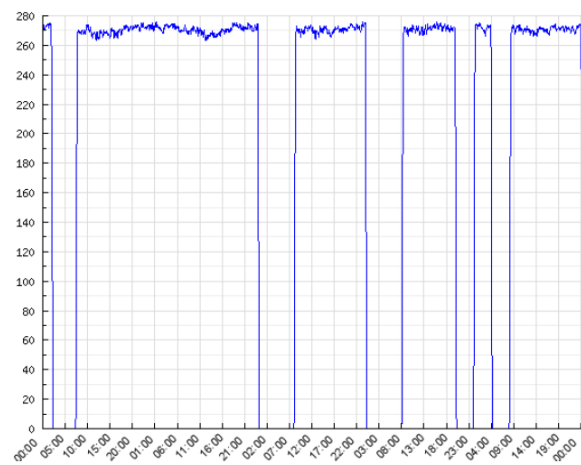


Figure 2. Typical load profile (over 5 days) of a wind farm collector system [4]

Joints are known to be a weak point in a cable system since it is an area which has been worked on by tools and hands. Reports suggest that failed joints are over represented compared to the cable itself in failure statistics. Typical causes of failure are moisture ingress, heating in joint ferrule and partial discharges in cracks and voids. Compression type ferrules, more often than others, have caused heating in joints by heightened contact resistance [5] [6] [7] [8].

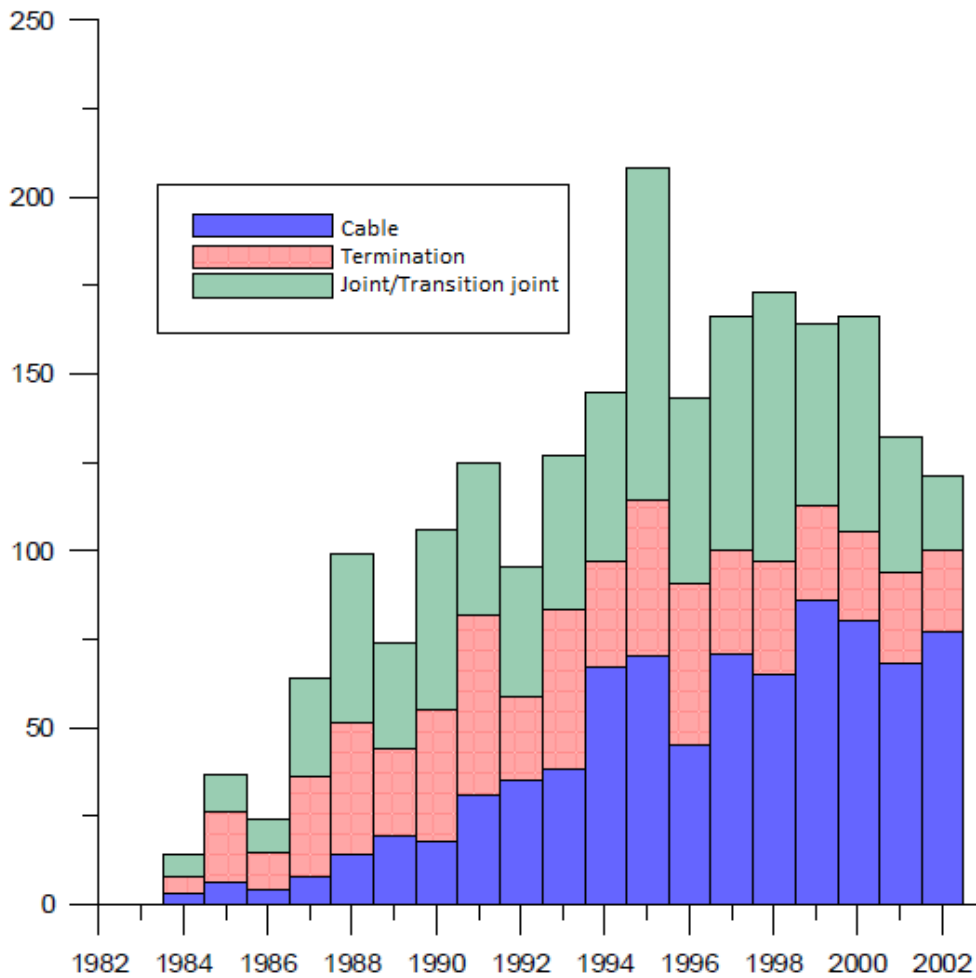


Figure 3. Failure statistics for Norwegian grid owners. XLPE cables and accessories [9].

1.2 Objectives and approach

Precise condition assessment is a prerequisite to perform maintenance and make appropriate reinvestment decisions. Partial discharge (PD) measurements in cable joints can be utilized as such an assessment tool. PD measuring results will vary with characteristics of the applied voltage (frequency, amplitude and phase relation), the material in question, chemistry, type of fault, pressure, temperature, start electrons, measuring device and statistical properties. New knowledge about frequency dependent PD activity can help improve condition assessment.

The main objectives in this master thesis have been to:

- Create test objects to simulate contact failure in joints which results in deteriorating materials caused by high temperatures and mechanical strain.
- Measure accurate PD in test objects at frequencies between 10 mHz and 100 Hz and voltage up to $2 \times U_0$ (17 kV_{peak}).
- Detect aging in cable joints by performing PD measurement.
- Compare PD measurement done at different frequencies and voltages.

1.3 Structure of the thesis

Chapter 1 of this report includes a short introduction and the most important motivations. Chapter 2 deals with theory pertaining to different aspects of the project. An overview of the different experiments and simulations is presented in chapter 3. Results and discussions are collected in chapter 4. Chapter 5 offers conclusions and suggestions for further work. All appendices containing detailed results, equipment lists and additional information are placed at the end.

2. Theory

2.1 Test objects

An underground transmission system will consist of cables, joints and terminations. All components must allow nominal current at nominal voltage and withstand all short circuits and temporary over voltages that may occur, without excessive temperatures or power loss. In this thesis the focus has been on modern XLPE cables and heat shrinkable joints. These technologies make up a large part of the equipment in use and will continue to dominate for many years to come. A short description of the most important features follows.

2.1.1 XLPE cable

The cable most often consists of the following components: conductor, inner semiconducting screen, insulation, outer semiconducting screen, screen wires/lead sheath, metal armoring and outer sheet. Water ingress creating water trees in the insulation has been a dominating aging phenomenon for XLPE cables. New water tight constructions have improved XLPE cable performance in later years [5].

2.1.2 Cable joint

The joint is the insulated and fully protected connection between two lengths of cable. The conductors are joined by a metal ferrule that is pressed or screwed. Bad contact between metal ferrule and conductor is a common source of failure in joints. This can be caused by poor installation, incorrect use of tools or wrong equipment. The different cable layers of semiconductors, insulation, screen wires and outer sheet are built around the metal ferrule. The joint must continue the moisture barrier in the cable so that water ingress is stopped. Electric field control in the joint is essential to avoid PD in enhanced electric fields.

2.1.3 Cable termination

A termination is the connection between a cable and other electrical equipment. The termination must act as a moisture barrier and continue the conductor through to the cable lug. Electric field control around the termination of metal screens and semiconductors is also very important to avoid PD in enhanced electric fields. With no field control the enhanced field at the screen termination may become too high

and PD may be initiated. The most vulnerable spot is where the insulation screen is ended. The semiconductor must have a smooth and clean transition.

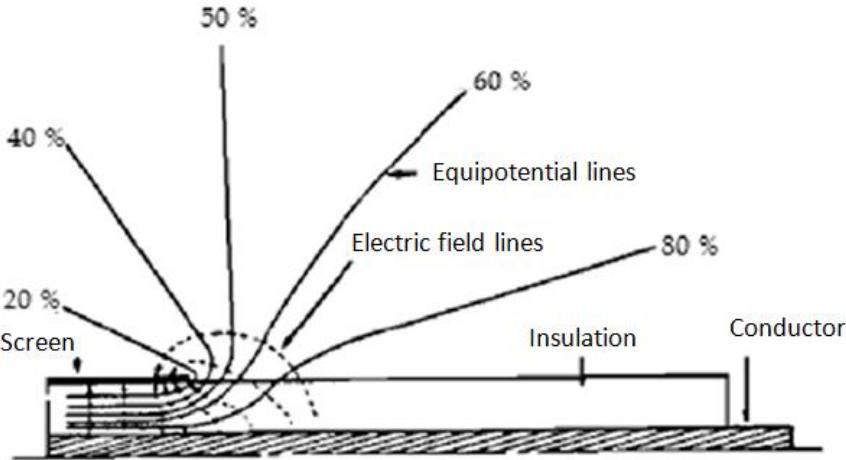


Figure 4. Electric field distribution with no field control at cable termination [10].

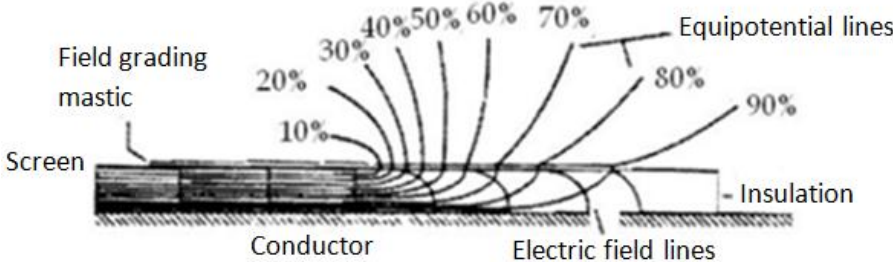


Figure 5. Electric field distribution with field controlling mastic at cable termination [10].

2.2 Characterization of test objects

2.2.1 Condition assessment and aging

The motivation to do condition assessment is to be able to utilize the full real life time of a component. Wear and tear of a component will ultimately lead to failure. According to the well-known “bath tub curve” [8] the failure rate will increase as the age increases. Many aging mechanisms such as temperature, electric stress, humidity, chemical contaminants, mechanical stress and environmental conditions such as oxygen work together on the power apparatus. The condition assessment aims to estimate the residual lifetime and degree of aging by taking a snapshot of the present condition, and/or combining this with several snapshots taken over time. Many methods of cable condition assessment are used today. Nondestructive

condition assessment is preferable over destructive tests for obvious reasons. Visual inspections, thermal surveillance, megging, dielectric response measurements, PD measurements and voltage withstand tests are examples [8].

In later years PD measurement equipment has become more available for condition assessment and is used in different ways on power apparatus like cables, generators, GIS and transformers. Acoustic, chemical and electric methods are utilized to measure PD. With electric measurements and Phase Resolved Partial Discharge Analysis (PRPDA) one can measure the PD in relation to the applied voltage and characterize the PD fault signature. Even though it may be difficult to determine the exact aging based on a single measurement, continuous measurement may reveal a trend and signal the need to perform maintenance. Evaluating whether a cable accessory is very good or very bad is certainly possible. With acoustic detection the position(s) of the discharge can be located by moving microphones around the object being tested.

2.2.2 Partial discharge definition

At least two conditions must be fulfilled to get PD: high enough electric field and a start-electron. The IEC [11] defines PD in this way: “**Partial Discharge (PD)** localized electrical discharge that only partially bridges the insulation between conductors and which can or can not occur adjacent to a conductor. Partial discharges are in general a consequence of local electrical stress concentrations in the insulation or on the surface of the insulation. Generally, such discharges appear as pulses having a duration of much less than 1 μ s.(...) Partial discharges are often accompanied by emission of sound, light, heat and chemical reactions.”

2.2.3 Effects of frequency

PD strongly depends on the testing voltage characteristics such as magnitude, frequency and waveform. These factors must be taken into account when comparing measurement results from the different techniques. When considering frequencies and waveforms applied to the test object there are four basic measurement techniques used today [12]:

- Online AC 50 Hz / 60 Hz
- Offline AC 20 – 300 Hz

- VLF (Very Low Frequency) 0.01 – 1 Hz
- DAC (Damped AC, oscillating wave) 20 – 500 Hz

There are some fundamental differences between online and offline measurements. Online is limited to nominal voltage and frequency values. Offline allows finding the exact inception/extinction voltages. Since voltage can be adjusted, faults only visible at elevated voltages can be found. Frequency can in offline measurements be set to any desired value. Low frequency makes it easier to achieve high voltages with less power (smaller equipment) as the capacitance of the test object draws less current. However, the test must be done over a longer time period in order to attain an adequate amount of voltage cycles. Reflection patterns are easier to separate when using VLF and for that reason PD site location becomes easier.

For the DAC method, limited size equipment is required. The decaying AC voltage is created by first applying a rising DC voltage to the test object thereby charging its capacitance until the desired voltage level is reached. The object is then short circuited across an inductive test circuit. A decaying voltage will oscillate between the capacitive test object and the inductive test circuit making it possible to detect PD in the stressed insulation. DAC PD testing conforms to power frequency PD testing up to about 500 Hz relative to inception behavior. However, only the first voltage cycle in DAC has a controllable voltage magnitude. When comparing results to power frequency measurements, only the first half waveform can be used. The rest of the PD patterns will contain information in relation to a decaying voltage waveform after the first cycle [13].

The dielectric loss factor, $\tan \delta$, varies with frequency (and temperature). At low frequency the loss factor increases inversely proportional to the frequency. This means that $\tan \delta$ is larger at 0.1 Hz compared to power frequency [14]. It has been reported that the electrical tree growth rate undergoing partial discharge can be higher at VLF compared to power frequency. A tree initiated at a VLF test may weaken the objects voltage withstand strength. It has not been proven that VLF testing has a lower initiation voltage for electric trees [15] [16] [17].

Edin [18] [19] has a short qualitative discussion on 4 frequency dependent mechanisms in HV insulation:

Statistical time lag (Δt_{lag}), which is the time lag between when inception voltage is reached and the start-electron is present at the right place. Hereunder he differentiates between two types of lag: The first, being the time delay between when inception voltage is reached and the first discharge occurs. The second, being the time delay between when inception voltage is reached and the discharge occurs after previous discharges already have taken place. This delay is much shorter since more free electrons are available. Δt_{lag} is considered to be constant, which means that phase lag ($\Delta\phi_{lag}$) will decrease with decreasing frequency and cause an increasing number of discharges within each cycle.

$$\text{Phase lag: } \Delta\phi_{lag} = \frac{\Delta t_{lag}}{T} \cdot 360^\circ \text{ [deg]} \quad (\text{eq. 1})$$

Dispersion in permittivity. One source of frequency dependent inception voltage is the dispersion of permittivity caused by frequency. The electric field enhancement in gas-filled voids and the resulting inception voltage is dependent on frequency across the test object.

Influence of bulk conductivity. With very low frequency (close to DC condition), the voltage across a delamination is mostly determined by the test objects conductivity. This affects the recharge time-constant of the delamination after a preceding discharge. Decreasing frequency will lead to increasing PD activity if the bulk has increased conductivity or has a permittivity with a strong dispersion.

Influence of surface conductivity. Lower frequency will have a screening/shielding effect in spherical voids, preventing any buildup of charge and therein reducing partial discharges. Chemical by-products produced by the PD increase the surface conductivity.

Bodega, Cavallini and Wester [20] have found that the frequency of the applied voltage influences the PD activity in air filled voids. This was studied in lab as well as simulated mathematically for frequencies from 0.1 to 1000 Hz. The frequency does not directly influence the discharge events since duration of a PD is much shorter than the applied voltage time period. It is the conductivity of the surface in the void

that will cause changes in the charge decay time. A polymer suffering PD activity will have higher conductivity than a fresh polymer.

2.2.4 Location of PD

PD will occur where the electric field is sufficiently high. The electric field has two contributions: the local enhancement caused by the defect and the local space and surface charges [20]. As illustrated in Figure 6, PD occurs at different locations in and around an electric component. **a)** Corona discharges **b)** Surface or sliding discharge **c)** Discharges in laminated material **d)** Cavity discharges **e)** Partial discharges in solid insulation materials (treeing channels).

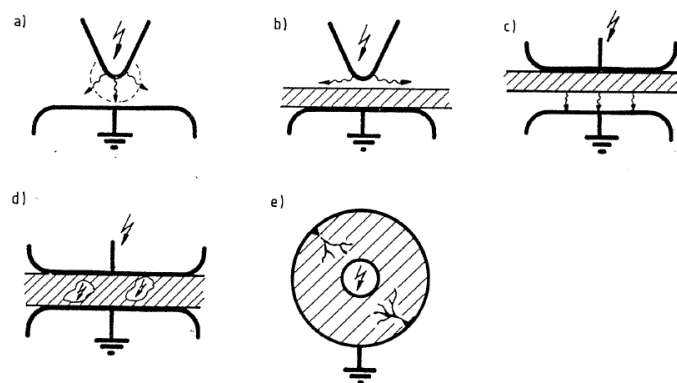


Figure 6. Partial discharges on simple insulation arrangements [21].

PD in a solid insulation material will cause deterioration and aging of the material. According to Ildstad [14] there are three causes of deterioration:

1. Bombardment of the insulation around the discharge region by ions and electrons accelerated in the discharge path.
2. Chemical reactions in the surrounding materials because of the discharges and corresponding rise of temperature (particularly for organic insulating materials).
3. Radiation from discharges. Ultraviolet radiation has sufficient energy to break up bonds in organic substances.

Paper-oil insulation is able to withstand a certain amount of PD because oil permeates and moves within the insulation thereby concealing emerging faults caused by PD. XLPE insulation tolerates no PD since it will definitely deteriorate the insulation. In cable joints PD will occur in voids or in the interface between different material layers. Such defects are most often caused by the jointer during installation

as a result of: knife cuts, bad fitting of the different parts, degradation of gradient paint, absorption of silicone grease and instability in voids inside soft mastic material [22].

2.2.5 Detection of PD

PD can be compared to a conventional discharge in gas when an adequate electric field and start-electron is present. Each discharge has a distinctive current pulse depending on the electric field, gas type and surrounding surface (e.g. glow, streamer, Townsend and leader discharges). This means that the different types of discharge can be characterized and differentiated if measured properly [23]. For example, discharges in cavities often occur on the applied voltages sharpest slope. Corona discharges often occur at the top value of the voltage [24].

Modern digital measuring devices detect the current and voltage pulse that results from the PD (the PD pulse). Some quantities related to measuring partial discharge pulses are listed:

Apparent charge	q
Pulse repetition rate	n
Pulse repetition frequency	N
Phase angle and time of occurrence of PD pulse	ϕ_i, t_i
Average discharge current	I
Discharge power	P
Inception voltage	U_i
Extinction voltage	U_e
Lower and upper limit frequencies	f_1, f_2
Mid-band frequency and bandwidth frequency	$f_m, \Delta f$
Scale factor	k

The complete list can be found in IEC60270 [11]. The norm contains recommendations as to how to measure and designate PD.

Quite often the ABC model is used to understand how electric detection of PD is possible (See Figure 7). It describes a conventional measuring technique where the

apparent charge (q_m) is measured and the real charge (q) is calculated. The test object (TO) is subjected to an AC voltage. The TO can be regarded as a capacitance **a**. Capacitance **a** can be related to the capacitance of the void **c** in the TO and the remaining capacitance **b1** and **b2** of the TO in series with the void (**b=b1+b2**). The voltage applied to the TO can be related to the voltage across the void through calculations. When PD occurs in the void, voltage across it falls from ignition voltage (U_{ig}) to remanent voltage (U_r). This can happen many times within each voltage cycle as seen in Figure 8. C_k will compensate by releasing charge in the outer circuit for each voltage collapse. When measuring the transient current and voltage (apparent charge) in the outer circuit impedance (Z_m), the real charge in the void can be calculated by using the found voltage and capacitance relationships [14]. The term quadripole often replaces Z_m . A quadripole is a four-terminal network which converts the input currents to output voltage signals [11].

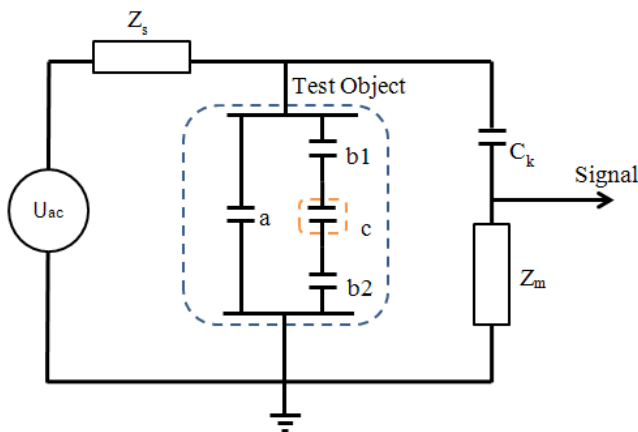


Figure 7. ABC model in test circuit [10].

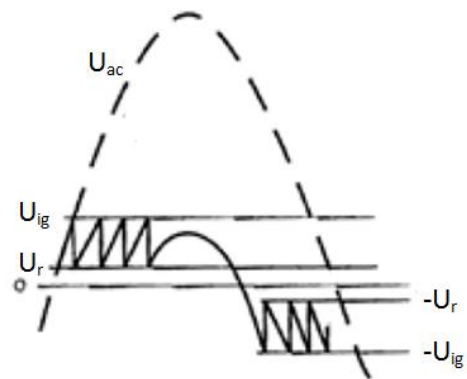


Figure 8. Voltage over the test object and in void [10].

The test capacitance (C_k) should be equal to or larger than the test objects capacitance ($C_{t.o}$) in order to achieve accuracy and sensitivity when measuring the apparent charge (q_m) [24]. For large capacitance test objects the apparent charge will be limited by the capacitance relationship in equation 2:

$$\frac{q_m}{q} = \frac{C_k}{C_{t.o} + C_k} \quad (\text{eq. 2})$$

When gradually increasing the voltage across the test object, one reaches inception voltage (U_i) at a certain point. It is at this point that PD occurs in voids or on surfaces. Raising the voltage further will increase PD activity. When lowering the voltage

gradually from above inception voltage the PD will decrease. However, PD will not disappear until the extinguish voltage (U_e) is reached. This is below inception voltage.

In order to detect PD accurately the test equipment must be calibrated with a known charge injected over the test object. The test equipment detects the known charge and the user must define the size so that a correct scale factor is calculated. The calibration charge should be in the same size range (50 - 200%) as the PD. If the test circuit is changed or the capacitance of different test objects exceeds $\pm 10\%$ a new calibration should be performed. If the same circuit is meant to measure voltage and phase relation, the voltage must also be calibrated in the detection equipment.

The measured PD in a certain object will vary with time since the material will be changed by the PD activity itself, temperature variations and pressure [23]. Further, PD in cavities may not occur at each voltage cycle if there are no start electrons to initiate the electron avalanche. This shows that PD is a complex stochastic process since it varies in properties like pulse amplitude, shape and time of occurrence. This means one must measure over a certain time period or sufficient voltage cycles in order to be certain to achieve results that are statistically correct.

2.2.6 Noise

Signals detected during a PD test which do not originate in the test object, are considered background noise [11]. Typical sources of noise in laboratory conditions are illustrated in Figure 9.

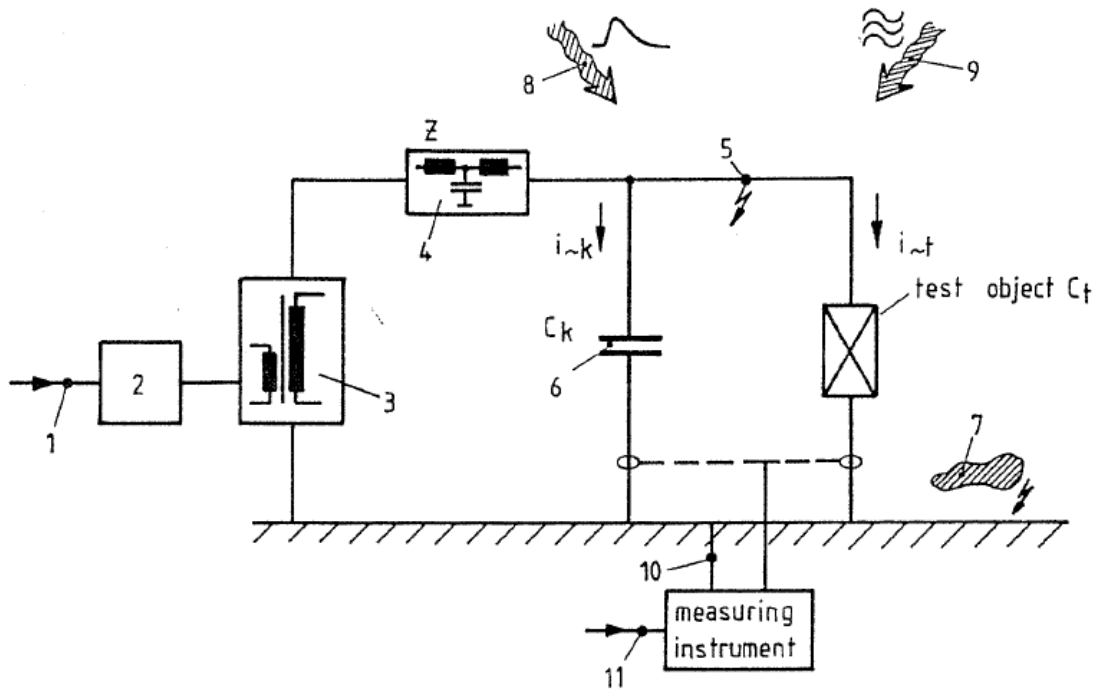


Figure 9. Typical sources of noise when measuring PD in laboratory: 1/11. Power supply 2. Variac or voltage regulator 3. High voltage source 4. Filtering of the HV source 5. Feeder line and electrodes 6. Coupling capacitor 7. Loose conductive objects in the vicinity of the test location 8. Pulse-shaped interferences 9. Electromagnetic waves by radio transmitters 10. Interference currents in the ground system of PD measuring instrument [21].

In order to assure accurate measurements, actions must be taken to reduce all the noise sources mentioned above. There is a big difference between doing experiments in controlled lab conditions as opposed to conditions in the field. For example, a lab can be electro-magnetically shielded and, prior to assembly, all single components in the setup can be tested separately under high voltage thereby eliminating them as a source of PD. This includes the coupling capacitor, resistors and capacitors of the low-pass filter, voltage sources, oscilloscope and internal wiring. All sharp edges are either avoided or covered by a toroid to even out the electric field thereby making corona charges less probable.

In field conditions where the surroundings may be irregular one must trust the measuring device. Balanced circuits, electronic processing, gating, polarity discrimination, pulse averaging and frequency selection are all methods listed in [11].

2.2.7 Low-pass filter

The high voltage amplifier, power supply and voltage regulator may all be sources of noise. Frequencies relevant to the test object are between 0.01 and 100 Hz. Higher

frequencies should be filtered out from the test circuit. In order to achieve this a low-pass filter is needed between the high voltage source and the test object. The three stage RLC low-pass filter presented in Figure 10 is based on Edin [19].

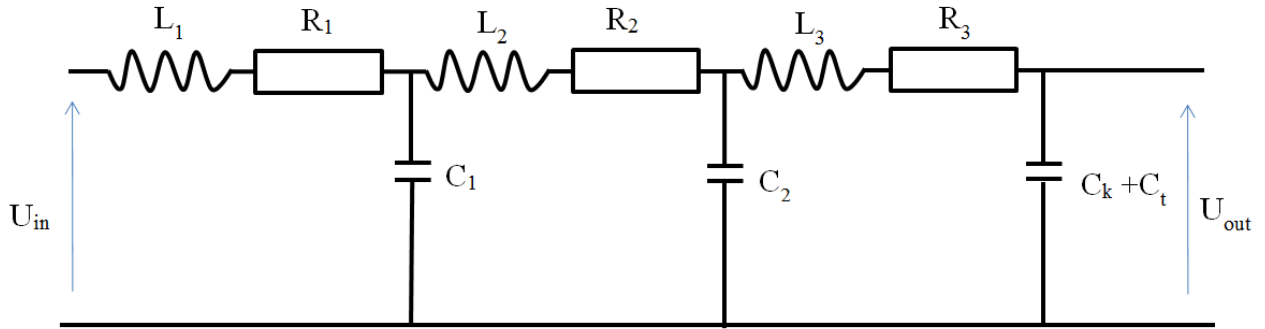


Figure 10. Low-pass filter circuit diagram. R1, R2, R3, L1,L2,L3,C1,C2 = filter components. C_k= coupling capacitor, C_t=capacitance of test object.

L₁, R₁ and C₁ in series act as the first filter. L₂, R₂ and C₂ act as the second filter. L₃, R₃ and C_k+C_t act as the third and last low-pass filter. The low-pass filter is load dependent since C_k+C_t make up the last filter leg. The ideal resistor stays unchanged for all frequencies. For zero frequency the inductor impedance is zero thereby acting as a short circuit. For increasing frequencies from zero, the inductor impedance increases relative to the impedance of the resistors. For infinite frequency the inductor impedance is infinite and the inductor acts as an open circuit. For zero frequency the capacitor impedance is infinite and the capacitor acts as an open circuit. For increasing frequencies from zero, the capacitor impedance decreases relative to the impedance of the resistors. For infinite frequency the capacitor impedance is zero and the capacitor acts as a short circuit. The component size in the circuit must be matched together to achieve the correct threshold for low-pass, high attenuation. This threshold is found at the cutoff frequency ω_c . The qualities of the filter can be expressed in a transfer function. The most important qualities are unity gain and a small phase shift within the pass band.

Transfer function frequency domain:
$$H(s) = \frac{V_{out}}{V_{in}} = \frac{1/LC}{s^2 + \frac{R}{L}s + \frac{1}{LC}} \quad (\text{eq. 3})$$

Cut-off frequency:
$$\omega_c = \frac{1}{\sqrt{LC}} \quad (\text{eq. 4})$$

Gain between input and output:
$$\text{gain} = 20 \times \log \left(\frac{V_{out}}{V_{in}} \right) \text{ [dB]} \quad (\text{eq. 5})$$

Phase shift between input and output:
$$\theta(j\omega) = \theta_{out}(j\omega) - \theta_{in}(j\omega) \quad (\text{eq. 6})$$

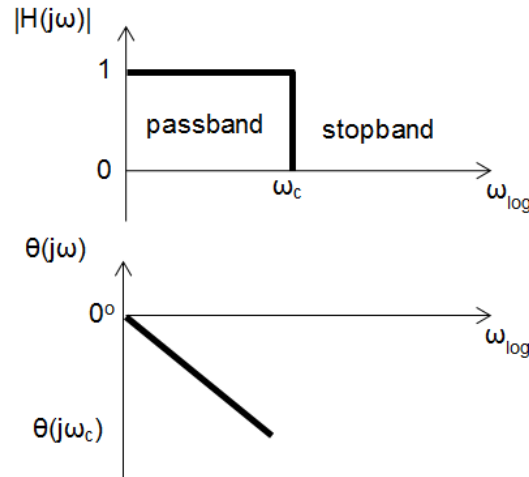


Figure 11. Ideal frequency response plots for low-pass filter [25].

2.2.8 PD data handling and statistics

Large quantities of data are created when measuring PD. In modern PD measurement equipment, data for each individual PD can be recorded. As mentioned in chapter 2.2.5, many attributes of the PD can be measured. In the Mtronix software used in this project, one can create MATLAB files containing discharge amplitude, discharge polarity, timestamp, phase relation and voltage level. A numerical tool like MATLAB is useful for dealing with large quantities of PD data. Codes for extracting interesting time intervals from longtime measurements, data preparation for statistical considerations and presentation of PD in phase resolved plots are examples of MATLAB functionality. The code prepared in this project is presented in appendix H.

There are several basic statistical quantities which can be used for easy comparison among test objects subjected to different voltage levels, frequencies and different stages of the aging process. The following quantities are inspired by Edin [18] [19]:

$$\text{Positive charge per cycle} = \frac{Q_p}{N_c} \quad (\text{eq. 7})$$

$$\text{Negative charge per cycle} = \frac{Q_n}{N_c} \quad (\text{eq. 8})$$

$$\text{Positive PD count per cycle} = \frac{N_{qp}}{N_c} \quad (\text{eq. 9})$$

$$\text{Negative PD count per cycle} = \frac{N_{qn}}{N_c} \quad (\text{eq. 10})$$

$$\text{Mean positive charge} = \frac{Q_p}{N_{qp}} \quad (\text{eq. 11})$$

$$\text{Mean negative charge} = \frac{Q_n}{N_{qn}} \quad (\text{eq. 12})$$

$$\text{Max positive charge} = \frac{0.01 \times \max(Q_p)}{0.01 \times N_{qp}} \quad (\text{eq. 13})$$

$$\text{Max negative charge} = \frac{0.01 \times \max(Q_n)}{0.01 \times N_{qn}} \quad (\text{eq. 14})$$

$$\text{Positive charge} \quad Q_p$$

$$\text{Negative charge} \quad Q_n$$

$$\text{Positive PD count} \quad N_{qp}$$

$$\text{Negative PD count} \quad N_{qn}$$

$$\text{Cycles} \quad N_c$$

By studying the Partial Discharge Height Distribution (PDHD) detected during aging, important information about the aging process will become apparent thereby identifying PD source typologies. The two-parameter Weibull distribution has been shown to correlate with PD pulse amplitude levels when only one type of PD phenomenon occurs. The distribution will follow a straight line as in Figure 12. The five-parameter distribution has been used to determine two or more simultaneous PD phenomena. The charges distribute along two or more straight lines as in Figure 13. Studying the development of parameters α (scale) and β (shape) in the Weibull distribution can say much about the condition of the test object [26] [27] [28]. The two-parameter distribution parameters can be extracted from a Weibull plot by the use of Matlab.

$$\text{Two-parameter Weibull function:} \quad F(q) = 1 - \exp\left(-\frac{q}{\alpha}\right)^\beta \quad (\text{eq.15})$$

$$\text{Five-parameter Weibull function:} \quad F(q) = p \cdot F_1(q) + (1 - p) \cdot F_2(q) \quad (\text{eq.16})$$

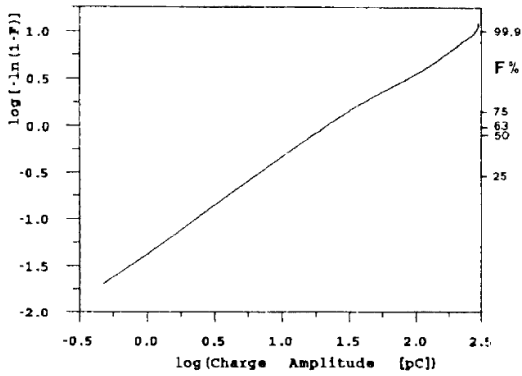


Figure 12. Weibull distribution, one PD mechanism [28].

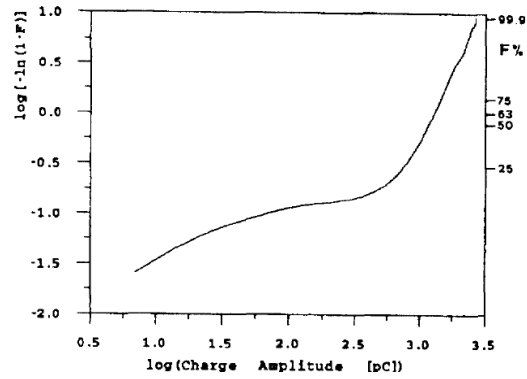


Figure 13. Weibull distribution, two PD mechanisms [28].

2.3 Aging procedure

A simple way of aging a polymeric test object is by subjecting it to heat. Susceptibility of cables and cable accessories to oxidative embrittlement increases with operational temperature [29]. Expansion and contraction of the polymers caused by thermal cycling can also precipitate micro-cracks, especially if the material is becoming brittle by oxidation. PD is more likely to occur when voids and cracks are created within the insulation thereby accelerating the aging by deteriorating the polymer.

Arrhenius models can be used to estimate and predict the oxidative life of a polymer [29]. The problem is simplified by assuming that heating and oxidative/thermal embrittlement is the only aging mechanism present in the test object, disregarding failure modes such as electrical treeing or water treeing. The relationship between temperature, activation energy and lifetime is given by the following formula:

$$\ln\left(\frac{t_n}{t_a}\right) = \frac{E_a}{k_0} \left(\frac{1}{T_1} - \frac{1}{T_2}\right) \rightarrow t_a = t_n e^{-\frac{\left(\frac{1}{T_1} - \frac{1}{T_2}\right) E_a}{k_0}} \quad (\text{eq.16})$$

Activation energy	Ea [ev]
Boltzman's Constant	k ₀
Accelerated Aging Temperature	T ₁ [K]
Nominal Operating Temperature	T ₂ [K]
Time to embrittlement at accelerated aging temperature T1	t _a
Failure time at operating temperature T2	t _n

Ontario Hydro Technologies [29] reports different activation energies for cable materials such as XLPE and EPDM ranging from 0.99 to 1.29 eV. Calculating the expected lifetime of an XLPE cable aged with 180 °C gives times between 80 to 250 h. These results can be used to predict how long aging can persist before failure becomes imminent.

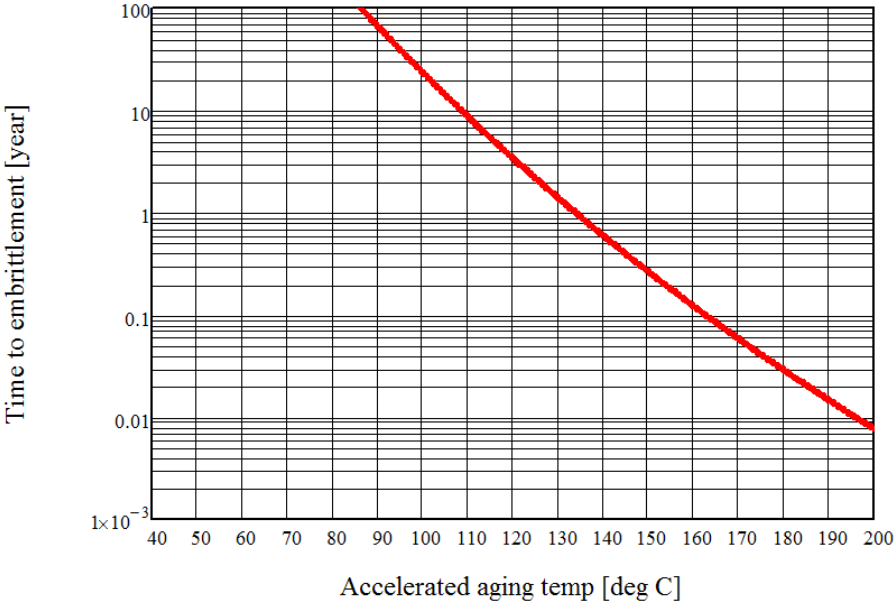


Figure 14. Example of Arrhenius aging model calculation. Insulating screen material. $E_a = 1.22 \text{ eV}$

It should be noted that oxidation will commence faster on XLPE test plaques (dog bones) compared to complete cables and joints. Oxygen must diffuse through many layers of different materials in real test objects. Also different adjacent materials inside the test object may influence how oxidation progresses by diffusing gases into each other changing the material properties.

3. Experimental

A total of four joints were made in the project. Joints # 1, 2 and 3 were electrothermally aged, characterized by PD measurements and dissected. Prior to this, joint # 4 was used to find the physical properties of the joints in order to calibrate the aging setup. In addition one dummy cable was made to exclude the possibility of PD in cable and terminations.

The experimental process followed five main steps:

Step 1 – Create test objects

Step 2 – Find inception/extinction voltage. If no PD go to step 4

Step 3 – Characterize the test objects by measuring PD at different frequencies and voltages.

If no breakdown, go to step 4.

If breakdown, go to step 5

Step 4 – Aging cycling, then go to step 2.

Step 5 – Dissection of joint.

Some additional tests and experiments had to be performed in order to build the variable test setup and the aging setup. They are all explained in this chapter.

3.1 Test objects

The test objects were made by using XLPE cables with a reduced cross section inside a complete Raychem joint. Each object became approximately 2 m long including two cable lugs, PD free terminations and the joint. The copper mesh between the joint body and insulating tubing determined ground potential in the joint. A thermocouple sensor was placed over the copper mesh to determine the temperature inside the joint. It was placed outside the ground potential so as not to interfere with PD measurements. The dummy cable had no joint, only cable terminations and cable lugs.

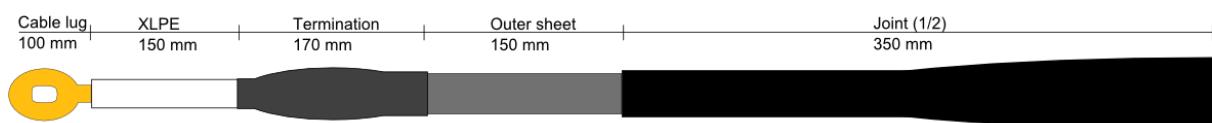


Figure 15. Size of test objects. Figure showing one half of a complete test object.

For test object capacitance calculation, see appendix I

3.1.1 XLPE cable

The cable used in the experiments is a XLPE insulated 95 mm² AL conductor with a strippable outer semiconducting screen. All other parts of the cable such as outer sheet and cu-wires were removed prior to the experiment.

Table 1. XLPE cable nominal electrical and dimensional data.

U _m - Highest r.m.s. voltage for equipment	12 kV
U ₀ - Rated r.m.s. voltage between conductor and screen	6 kV
U - Nominal system r.m.s. voltage	10 kV
Conductor diameter	11.4 mm
Insulation thickness	3.4 mm
Diameter over insulation	19.5 mm
Reduced conductor diameter	7 mm

3.1.2 Simulation of contact failure

The aim was to simulate heating in joints caused by reduced contact/high contact resistance between cable conductor and joint ferrule. The elevated temperature should accelerate the aging of the materials. It was decided to age the test objects at 180 °C. This temperature was calculated to give an aging time within the project timeframe.

Real joint ferrules were not used because of problems in making all specimens equal. Reproducible results could be achieved better by reducing the conductor cross-section within the joint to create heat. One layer of conductor strands were removed, reducing the cross section from 95 to 38.5 mm². A spliced metal cylinder was made to replace the joint ferrule so that thermal and electric field conditions would be as real as possible. The metal piece was insulated from the conductor with PTFE (teflon) to avoid actually increasing the cross-section. A small area was left to make electrical contact between the conductor and metal piece. PTFE was chosen because of its ability to withstand high temperatures.

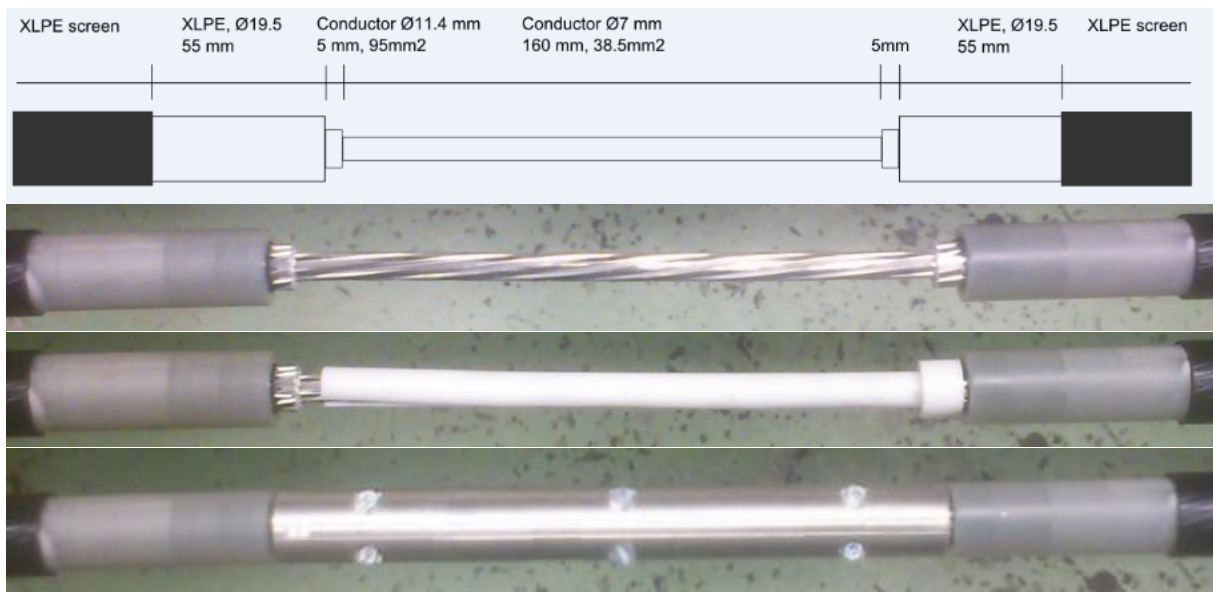


Figure 16. Joint ferrule replacement simulating contact failure. From the top: -Dimension drawing -XLPE cable with reduced cross section - Insulating teflon piece - Metal cylinder.

3.1.3 Raychem joint

The Raychem RTK-S1P-B/L joint and the MB203-04/2009 ESD-2368-NO-04/09 fitting instruction was used in the project. It is a heat-shrinkable elastomeric joint designed for 12 kV 95-185 mm² or 24 kV 35-95 mm² TSLE cables. The different components were shrunk using a Sievert 2944 propane blow torch burner. A short description of the different materials is found in Table 3. Some of the nominal electrical values from the datasheet are listed in Table 2.

Table 2. Raychem joint nominal values and performance [<http://www.te.com/en/industries/energy/>].

Test sequence	Voltage	Criteria
Highest voltage for cable U_m	24 kV	Phase to phase
AC voltage withstand 1 min	55 kV	No breakdown
AC voltage withstand 4h	48 kV	No breakdown
Impulse voltage withstand	150 kV	No breakdown
DC voltage withstand	96 kV	No breakdown
Partial discharge	15 kV	< 3 pC
Partial discharge	24 kV	< 20 pC
Load cycling. 63 cycles (5 h heating & 3 h cooling), 95 °C conductor.	30 kV	No breakdown

Table 3. Raychem joint material description provided by Ensto [30].

Stress relief tape (mastic)	Oil resistant, good flow properties, sealing and filling function
Stress-Control tubing (JSCR)	Stress control function for cable joints, replaces conventional tape or moulded stress cones, precisely defined impedance characteristic which smooths the electrical field
Copper mesh	Tinned copper to maintain screen area and ground potential through joint
Insulating joint (ECIC/ERIC)	Screened insulating composite tubing, inner layer (red) of insulating material, outer layer (black) of conductive/screening material
Insulating tubing (MWTM)	General purpose medium wall tubing, oversheath replacement, sealing and corrosion protection, with adhesive coating
Wraparound (CFSM/RFSM)	Repair wraparound system, outer protection, with AL-foil and glue for water sealing



Figure 17. Raychem RTK-S1P-B/L joint [<http://www.te.com/en/industries/energy/>]

3.1.4 PD free cable termination

A PD free cable termination had to be made on both sides of the test object. This was done to ensure that voltage could be applied to the test object without creating discharges at the XLPE screen cut. By using the following method only PD from inside the test object would be measured:

Strip or peel the external semiconducting layer. Make sure the final cut into the outer jacket is as clean and straight as possible. Proper cable stripping and cutting tools should be used. The whole XLPE surface must be clean and free from any cuts, cracks, dust or particles. Sandpaper and wash with isopropanol or other cable

cleansing liquid and dust-free cloth if necessary. Apply a 2 mm wide belt of semiconducting paint at the transition between the outer layer and XLPE. To make the edge between paint and XLPE perfect, use a glue-free masking tape. Then apply a field grading mastic. This should overlap about 2 cm over the semiconductor and 8-10 cm along the XLPE. Make sure it is free from any dust, contamination or air pockets. Apply 6 layers of stretched tape beginning and ending on the inside of the termination. This tape should remove the last of the air pockets by compressing the field grading mastic.

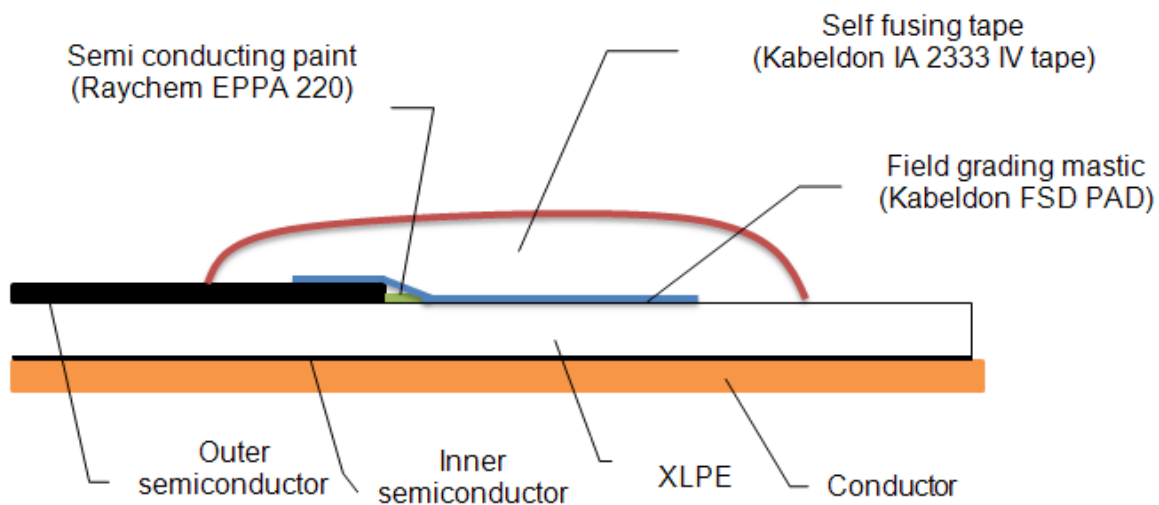


Figure 18. Drawing of XLPE cable termination. The design has been tested showing PD well below 1 pC up to 35 kV_{peak} [31].

3.1.5 Finding physical properties

One of the joints (#4) was used to determine the various physical properties needed to build the aging setup. Important properties to find were:

- Time needed for attaining desired aging temperature (180 °C)
- Amount of current needed to establish and maintain a stable temperature in joint
- Time needed for cooling down to ambient temperature.
- Establishing the temperature differences between various layers of the joint in stable conditions.

Joint # 4 was mounted on XLPE cable, approx. 3 m long. It was thermally insulated by 3 layers of 12 mm foam sheets. Thermocouple sensors were incorporated in different layers of the joint in order to measure the temperature gradients. In addition,

the cable and cable core temperature outside the joint were measured. A last thermocouple was installed to control the ambient temperature.

Temperature sensor placement:

1. Ambient air
2. Cable core
3. Cable surface
4. Metal piece in middle of joint
5. Between stress control tube and insulating joint (R/B)
6. Between insulating joint (R/B) and insulating tubing (copper-mesh)
7. Between wraparound and thermal insulation foam

See figure of temperature sensor placement in appendix K.

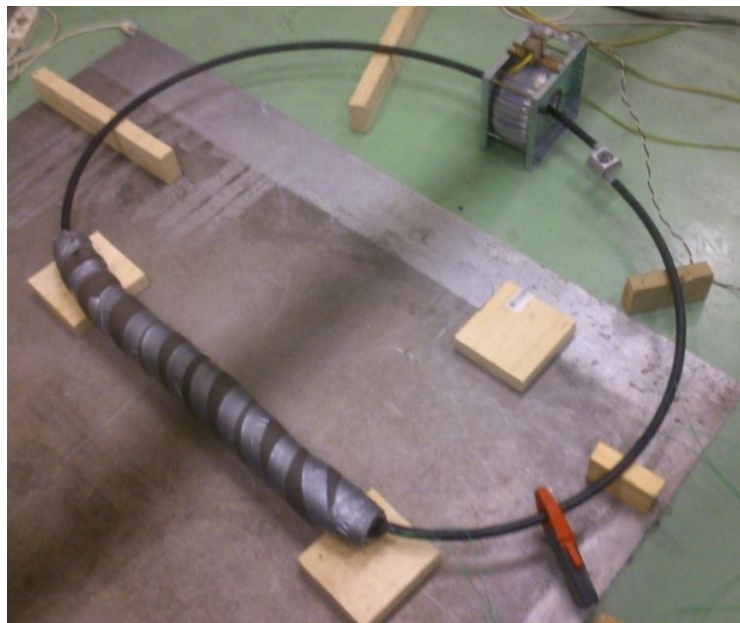


Figure 19. Testing to find the physical properties of the joint. Ring transformer induced current in the loop. Handheld ammeter read current level. Seven thermocouples placed in joint, cable and ambient air.

A visual estimation of the degree of aging could be performed after the physical properties were found. Thin PTFE sheets were placed between all layers of the joints to make dissection easier.

3.2 Characterization of test objects

3.2.1 PD detection

The PD detection device used in this project is the Omicron MPD600. The general setup is shown in Figure 20. The fiber optics controller MCU502 (1) is powered by and communicates through USB to the laptop running the Mtronix software (6). It is connected by a fiber optic cable (7) to the acquisition unit MPD600 (2). One can choose either battery power (3) or a voltage source connected to the 230 V grid. The battery power option is preferable because the voltage source generates more noise. Two BNC cables (8) connect to the measuring impedance (quadripole) CPL542 (5) to transfer PD and voltage signals. The quadripole is properly grounded and connects to the bottom of the coupling capacitor.

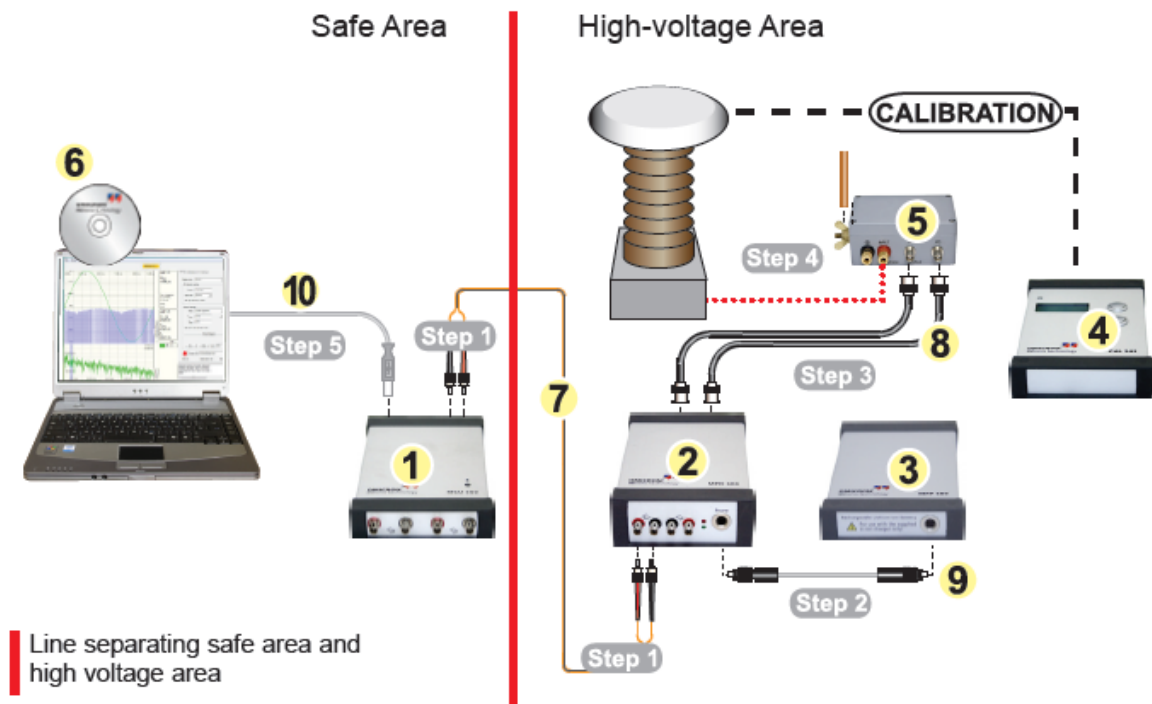


Figure 20. Omicron MPD600 PD detection system [32].

To calibrate the MPD600 a known charge (4) is injected between earth and the top of the coupling capacitor C_k . In the Omicron software the user can automatically calibrate by measuring the known charge, comparing it to the user input and finding the dividing factor. The same is done for calibration of voltage amplitude. The CPL542 unit in the Omicron software performs frequency and voltage

measurements. The general noise level is quite low in the laboratory where only about 500 fC is detected. Anything under 1 pC is considered acceptable.

When measuring PD an internal switching can be heard in the quadripole device at certain voltage levels, as the gain value is changed between the two highest sensitivity settings. PD measurements can be falsified by large quantities of noise-PD introduced by this auto switching. If auto gain is acting up, the user solves the problem by setting the gain to manual in the specific measurement.

Because PD measurements create large quantities of data, it is essential to establish correct threshold in the measurement phase. For example, preliminary testing will establish the noise level. Being able to exclude all discharges below this level will help tremendously.

3.2.2 Coupling Capacitor C_k

The coupling capacitance C_k is a 150 kV 800 pF HV capacitor mounted on an earthed steel plate. The capacitance should be equal to or larger than the test objects capacitance in order to achieve accuracy and sensitivity when measuring PD. A trade off must be done since a large capacitance will draw a large current at high frequency. If the coupling capacitor together with the test object draws too much current it may be difficult to reach the desired voltage levels. The test object is calculated to be about 500 pF.

3.2.3 Low pass filter

A low-pass filter has been designed and built to handle noise from the voltage source, signal generator and HV amplifier. The individual filter components have been matched to the electrical qualities of the test circuit to determine the right size. The following circuit has been designed and simulated to work for both a small capacitance load (400 pC) and a big capacitance load (4000 pC). The test object and C_k is about 1300 pF.

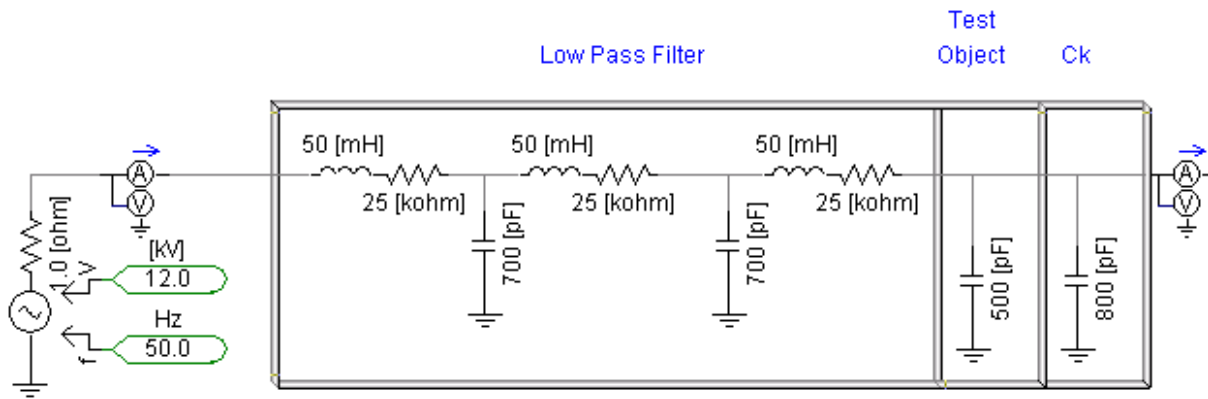


Figure 21. Low-pass filter, single line diagram from PSCAD simulation tool.

The low-pass filter has been built into a perforated metal box. The metal box controls stray capacitance and is properly grounded. 5 x 5 kΩ resistors and a 50 mH choke were placed in series inside perforated polycarbonate tubes. Perforation was needed to transfer heat efficiently to the ambient air. The resistor and choke legs were modified/bent aside and soldered together so they would fit inside the tubes.

Semiconducting tape was placed over the soldered legs to increase the circumference and reduce risk of corona. The 700 pF capacitors were mounted between the resistor tubes and the metal box with round conductors. Toroids and round conductors were used to even out the electric field thereby avoiding corona discharges at sharp points.

In order to avoid flashovers, there has to be a certain distance between HV parts and the metal enclosure. For practical reasons 5 cm was chosen as the minimum clearing distance between HV and ground inside the filter box. This secured an average electric field strength well below 0.5 kV/mm. Figure 24 to Figure 27 shows drawings of the individual filter components and the complete low-pass filter.

Simulation results on the low-pass filter show that gain and phase shift is minimal within the necessary frequency range from 10 mHz to 100 Hz. The cutoff frequency will be within 200-800 Hz depending on the size of the capacitive load. A higher capacitive load lowers the cutoff frequency. The results are presented in Figure 22 and Figure 23.

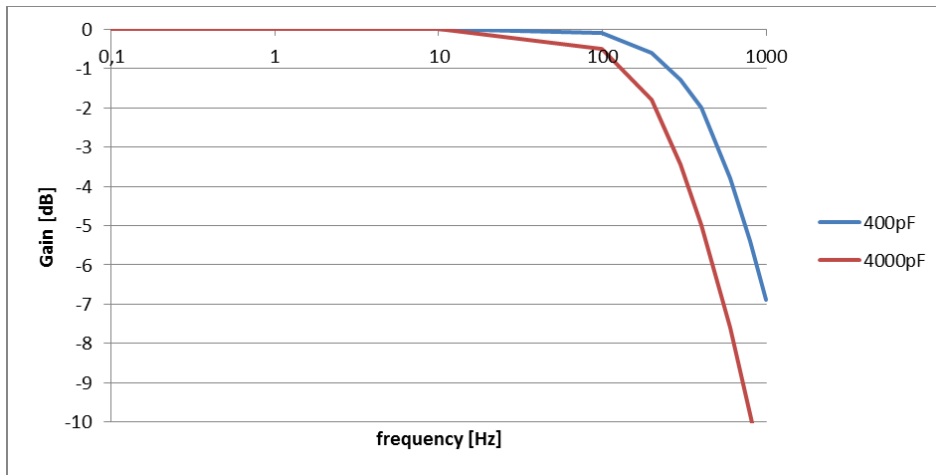


Figure 22. Simulated low-pass filter gain for small and large capacitive load. Unity gain up to above 100 Hz as needed in the measurement setup.

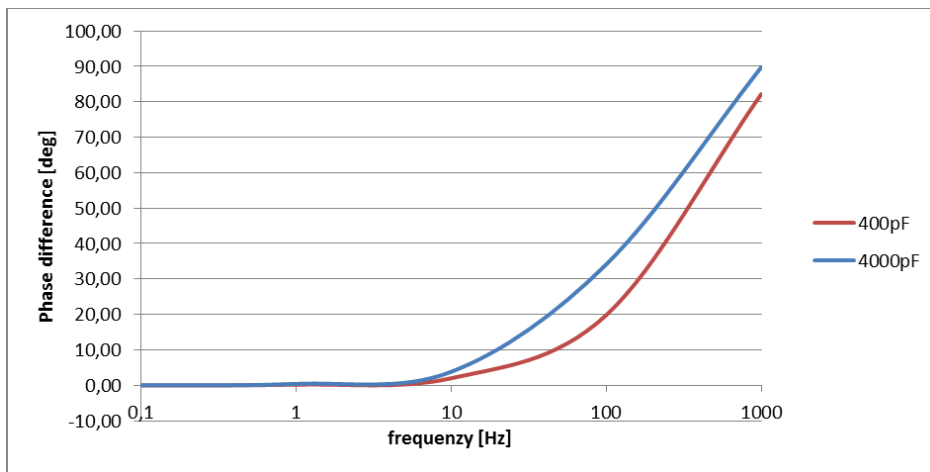


Figure 23. Simulated low-pass filter phase shift for small and large capacitive load. This does not influence the measurements, since PD and voltage is measured at the same place (at the test object).

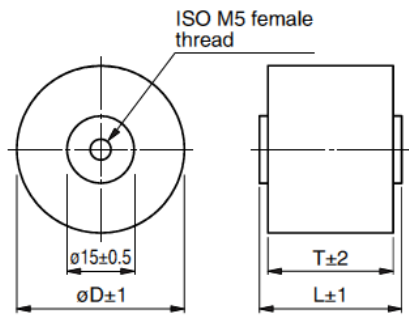


Figure 24. Capacitor UHV-7A. 700pF. D=38 mm T= 28 mm L= 32mm. (www.farnell.com)

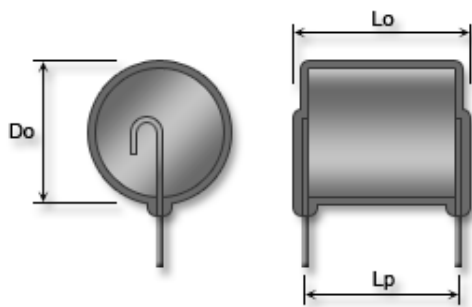
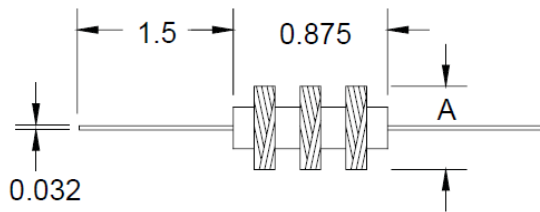


Figure 26. Resistor AB664. 5k Ω . $D_o=26$ mm $L_o=55$ mm $L_p= 50.5-52$ mm (www.hvrint.com)



Dimensions: Inches

Figure 27. Choke 6310-RC. 50mH. A = 0.63 (www.bourns.com)



Figure 25. Complete low-pass filter

3.2.4 Variable frequency PD measurement setup

A digital variable signal generator and HV amplifier (TREK) was connected as shown in Figure 28. The objective was to measure PD in the test object at frequencies between 0.01 and 100 Hz. The low pass filter was placed between the HV amplifier and C_k to stop noise from entering the test object from the HV amplifier. The output voltage from the signal generator and the high voltage applied to the test object were measured with the oscilloscope. The Omicron PD detection equipment was set up and calibrated as described in chapter 3.2.1.

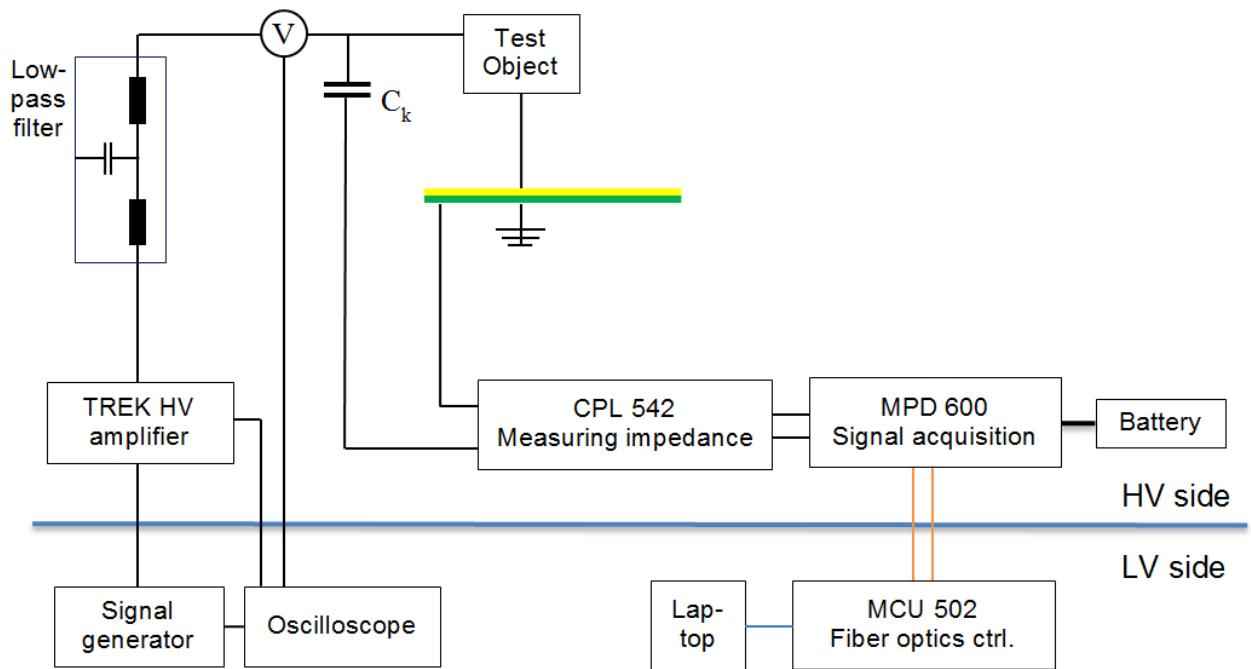


Figure 28. Variable frequency PD measurement setup.

Complete equipment can be found in appendix F. Current calculation for driving capacitive loads with the TREK HV amplifier is placed in appendix I.

3.2.5 PD detection at different frequencies and voltages

The variable frequency test setup was capable of detecting PD in test objects up to $17 \text{ kV}_{\text{peak}}$ for frequencies between 10 mHz and 100 Hz with PD accuracy down to 5 pC. This meant that test objects could be characterized up to $2 \times U_0$ ($2 \times 6 \text{ kV}_{\text{rms}} = 12 \text{ kV}_{\text{rms}} = 17 \text{ kV}_{\text{peak}}$).

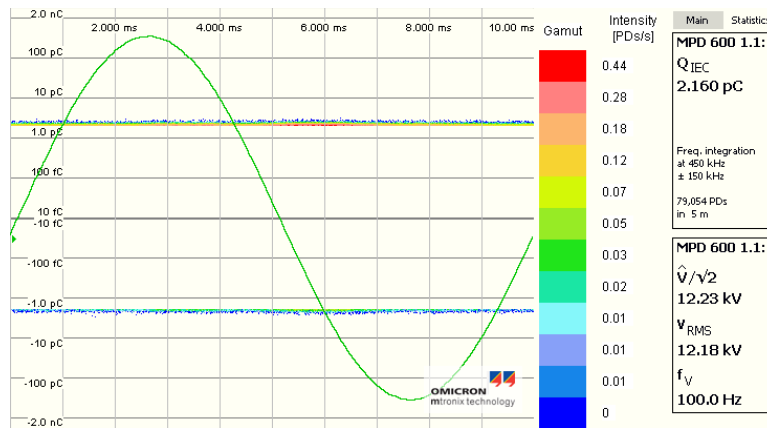


Figure 29. PD measurement on dummy cable. No PD above the noise level at 2-3pC. 17 kV_{peak} 100 Hz.

Measuring series were performed at frequencies from 100 Hz down to 10 mHz at each voltage level. The series were always preformed twice at the same voltage level in order to detect any changes in the test object caused by the measurement itself. Both measurement series from 100 Hz to 0.1 Hz where preformed the same day. The 10 mHz measurements were performed during the night because of the long measuring time. Measuring times were chosen so that a minimum of 600 cycles were recorded each time. PD being a stochastic variable must always be measured over time to get statistically valid results.

Table 4. Measurement times and cycles at different frequencies used in experiment.

Duration [min]	Duration [hr]	Frequency [Hz]	Cycles [#]
1000	16,7	0,01	600
100	1,7	0,1	600
10	0,2	1	600
5	0,1	10	3000
5	0,1	50	15000
5	0,1	100	30000

3.2.6 Finding inception/extinction voltage

A decreasing inception/extinction voltage level was expected as aging progressed. PD inception and extinction voltage could reveal deterioration in test objects when measured between the aging cycles. The values were found using the variable frequency PD measurement setup. A 50 Hz voltage was increased across the test object with small increments every 2-5 minutes until inception voltage was reached. The level was determined by detecting PD occurring above the noise level. The

voltage was then reduced until extinction voltage was reached, determined by all PD disappearing above noise level.

An inception/extinction voltage measurement with frequencies between 100 and 0.1 Hz was performed on all joints after aging was complete.

3.2.7 Dissection

After aging and electrical characterization of the joints was completed, dissection and visual inspection of joint parts was carried out. The aim was to be able to find and visually observe the degradation of the different joint materials and, if possible, see the actual discharge locations.

An acoustic PD measurement was done to pinpoint the most severe discharges before the dissection took place. This was done by subjecting the joints to $2 \times U_0$ ($17\text{Kv}_{\text{peak}}$) 50 Hz with microphones placed directly on the joint. Microphones were connected to preamps that feed a voltage signal to an oscilloscope. The amplitude of the signal represents the amplitude of the sound detected in the joint. The preamps were powered by a 27 V_{DC} power source. The oscilloscope was set to accumulate the discharges over a period of 2 minutes to find the average sound level. The equipment used is listed in appendix F.

Six different positions along the joint were measured. Thereafter the position with the most PD was measured again to determine which quarter of the cable circumference had the most PD. The hypothesis was that most PD would occur in the center of the joint where the materials had experienced the most heat.

3.3 Aging procedure

The hypothesis was that high temperatures would cause oxidation and embrittlement in the cable materials. Constant heating and cooling cycles would strain the materials mechanically leaving voids and cracks between the different joint layers. A heat cycling setup was built to conduct the experiment.

3.3.1 Heat cycling setup

A ring transformer was used to induce current in a loop containing the test objects and a dummy cable. The test objects were bolted together for easy demounting and PD-testing. Current was measured by an ammeter placed in the loop. Thermocouple elements were placed at strategic places in the loop to maintain control of the temperature cycle. A Labview program was created to control the current cycles by controlling the variac voltage. It was necessary to use an automatic controller with current level feedback since changing temperature in the loop also changed the resistance and the resulting induced current. Alarms were programmed to trip the current if temperatures rose above certain threshold. The whole rig would be shut down by a smoke detector in case of fire.

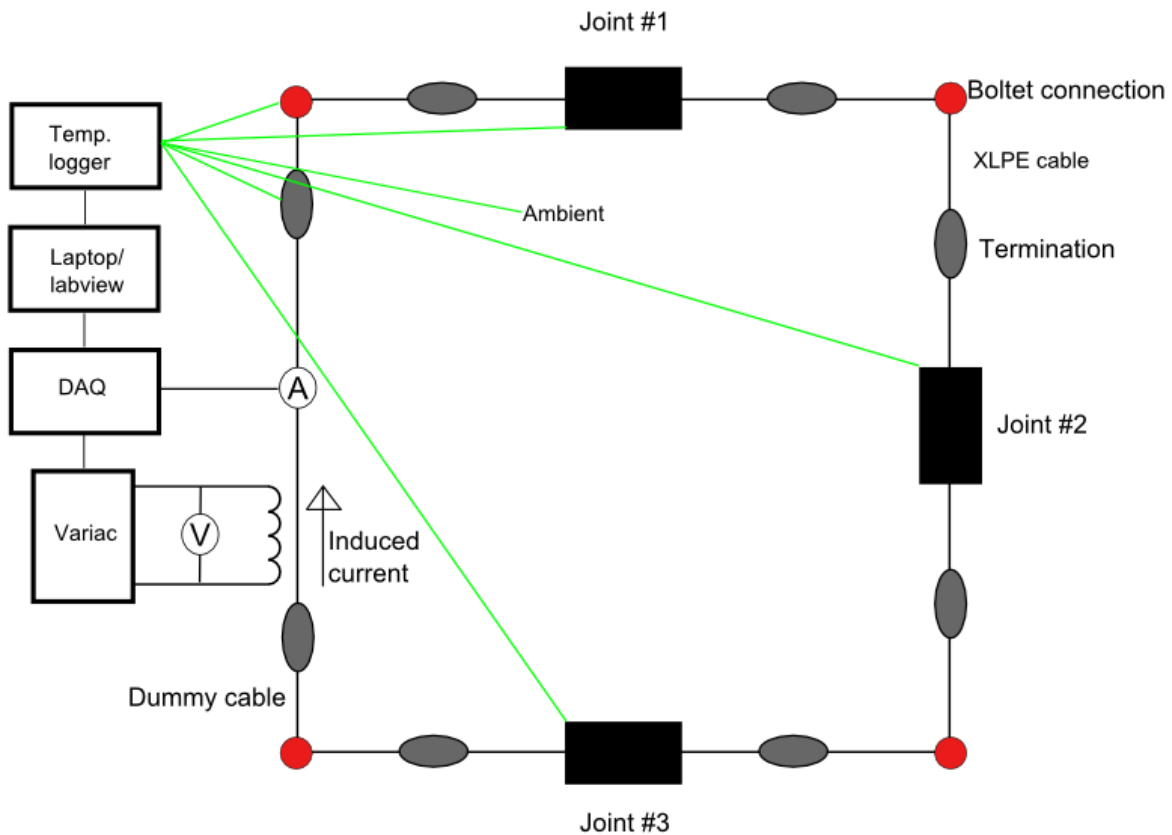


Figure 30. Heat cycling setup for aging of test objects. Thermocouples placed in each joint, on bolted connection, on cable termination and ambient air.

4. Results and observations

4.1 Test objects

4.1.1 Finding physical properties (joint # 4)

Joint # 4 was tested with 7 different current cycles to establish the physical properties of the test object. Altogether the joint experienced approximately 12-15 hours above 175 °C. The following information was gathered:

- 225-230 A gave a stable 180 °C temperature in the metal of the joint
- With 180 °C in the core, the temperature dropped to approximately:
 - 170 °C ($\Delta T_S = 10$ °C) over stresstube
 - 150 °C ($\Delta T_J = 20$ °C) over joint body
 - 140 °C ($\Delta T_W = 10$ °C) over wraparound
- The temperature difference between the joint metal and the joint body (metal screen) was 30 °C ($\Delta T_S + \Delta T_J$)
- The time delay between inner and outer joint reaching stable temperature was over 1 hr.
- The minimum heat up time from ambient to 180 °C was 3.5 hr.
- The cool down time from 180 °C to ambient was about 13 hr.

Based on results from experiments on joint # 4, the following current cycle was found to be optimal for quickly increasing the core temperature to 180 °C. The cycle also maintained stable temperature without overheating the cable or cable lugs.

Table 5. 48 hour current cycle for aging of test objects

Time int. [s]	Acc. Time [s]	Current [A]
10	10	0
1 800	1 810	330
10 800	12 610	270
5 400	18 010	240
10 800	28 810	227
48 600	77 410	226
48 600	126 010	226
46 800	172 810	0

Dissection of joint # 4 revealed no apparent severe damage to the different materials other than some discoloring and deformation of the XLPE. It seemed as if the joint had slightly squeezed and deformed the XLPE under the high temperatures. Yellow mastic in immediate contact with the metal ferrule was in some places dried out and discolored. No further investigations were done to joint # 4.

4.1.2 Simulation of contact failure and electrothermal aging

Figure 31 shows three of the fourteen 48 h heat cycles performed on the test objects. It was not possible to achieve a 100 % equal temperature progression between the test objects despite trying to insulate all test objects equally. The temperature difference between the coldest and hottest joint was within 10 °C during heating and 3 °C during stable heat.

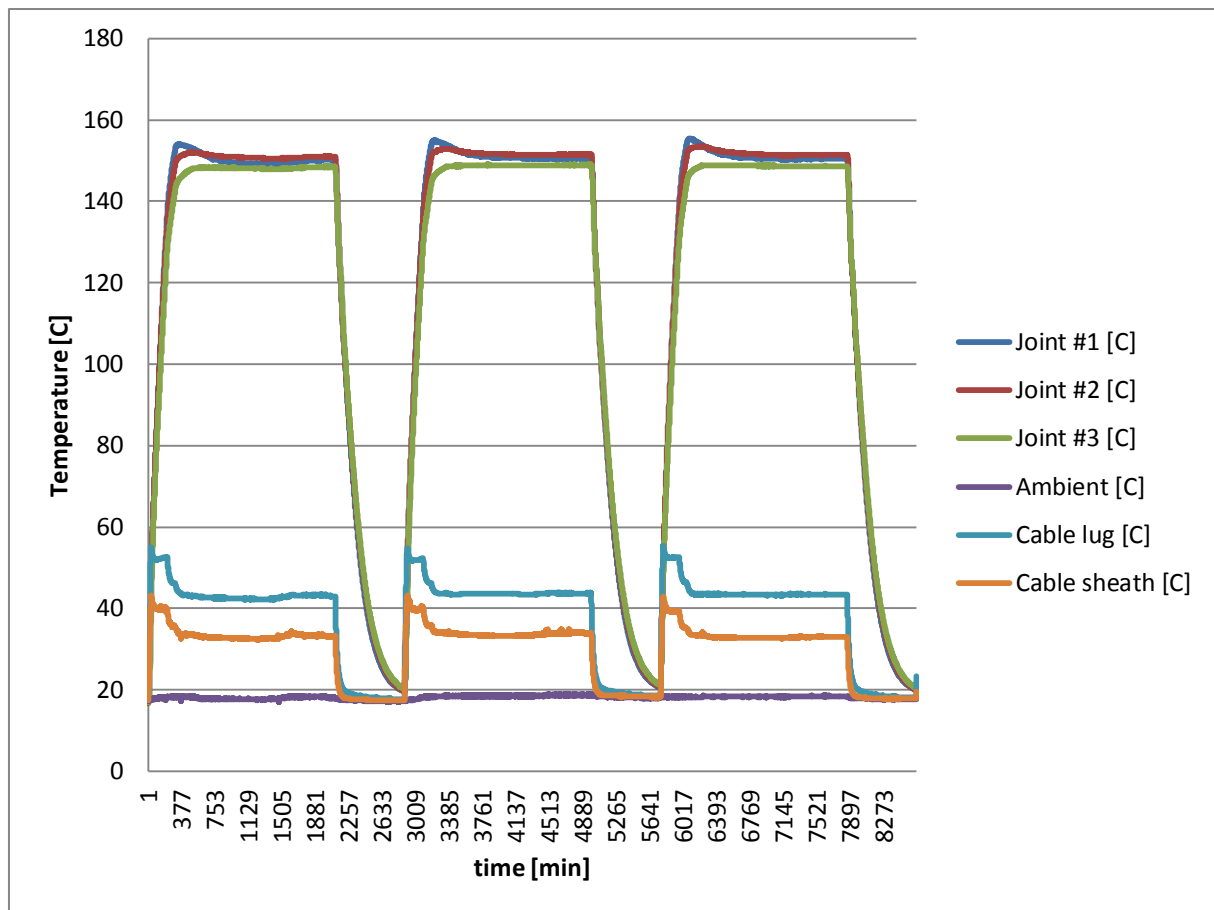


Figure 31. Typical 48 h heat cycle subjected to the test objects. The temperature of the joint ferrule is 30°C higher than the temperature measured on the joint body and plotted in the graph.

Table 6 shows the complete aging program for joints # 1, 2 and 3. The test objects were subjected to 14 temperature cycles. The table shows when PD was registered for the first time and the corresponding inception voltage. The hours reported show

the accumulated time during which the joint core was above 175 °C. The results seem to fit quite well with the anticipated aging time calculated with activation energy.

Table 6. Aging program and inception /extinction voltage for test objects

		Joint #1	Joint #2	Joint #3
Aging time [hr]	Aging Cycles [#]	U_i/U_e 50Hz [kV_{peak}]	U_i/U_e 50Hz [kV_{peak}]	U_i/U_e 50Hz [kV_{peak}]
0	0	>17 / >17	>17 / >17	>17 / >17
7	1			
31	5	>17 / >17		
32	6			
46,5	7			
76,5	8			
136,5	10	>17 / >17	14 / 13	16 / 15
256,5	14	10 / 9	8 / 7	10 / 9

As a result of these test one can see a clear trend. The simulated contact failure causes PD to occur in the joint after a relatively short time. The 50 Hz inception voltage (U_i) declines as the test objects ages. Continuing the cycles would most probably lead to total failure in the insulating capabilities of the joint and cable within a short time.

4.2 Characterization of test objects

Table 7 shows the complete characterization program for joints # 1, 2 and 3. For increased readability, all PD plots, histograms and statistic results are gathered in the appendix. Some results are included in this chapter as illustrations.

Table 7. Characterization program.

PD = tested with results. no PD = tested without results. Blank = not tested

0 h of aging							
		50 Hz					
Joint #1	2xU ₀		no PD				
Joint #2	2xU ₀		no PD				
Joint #3	2xU ₀		no PD				
136 h of aging							
		100 Hz	50 Hz	10 Hz	1 Hz	0,1 Hz	0,01 Hz
Joint #1	2xU ₀	no PD					
Joint #2	2xU ₀	PD	PD	no PD	no PD	no PD	
Joint #3	2xU ₀	PD	PD	no PD	no PD	no PD	
256 h of aging							
		100 Hz	50 Hz	10 Hz	1 Hz	0,1 Hz	0,01 Hz
Joint #1	2xU ₀	PD	PD	PD	PD	PD	PD
Joint #1	1.5xU ₀	PD	PD	PD	PD	PD	PD
Joint #2	2xU ₀	PD	PD	PD	PD	PD	PD
Joint #2	1xU ₀	PD	PD	PD	PD	PD	PD
Joint #3	2xU ₀	PD	PD	PD	PD	PD	PD
Joint #3	1.75xU ₀	PD	PD	no PD			

All tests were performed two times. The results from the first and second run were in most cases very close. If there was any difference, there was a tendency for the second PD measurement to be slightly less than the first. The two measurements were done right after each other. The heat developed by the first measurement could cause the PD reduction by increasing the conductivity of void surfaces.

Some of the measurements at early aging and below 2 x U₀ revealed very few (hundreds) PD. These measurements are included, but are not weighed as much as the measurements revealing thousands and millions of PD. The measurements with few PD are especially visible in the Weibull and histogram plots.

4.2.1 PRPDA plots

With the possibility of studying each PD in detail through MATLAB, less emphasis has been put into analyzing the PRPDA plots. The plots taken after each measurement gave a good first indication of the test objects status. Potential contact problems in the low-pass filter would be revealed as well as the general noise level from the voltage source. The PRPDA plots are presented in appendix C.

4.2.2 Inception/extinction voltage as a function of frequency

Aging was found to reduce the inception voltage significantly, as expected. Also the inception voltage was recorded to be higher than extinction voltage for all joints at all frequencies. However, it was not possible to find data suggesting consistent frequency dependency. For two of the joints the trend was that decreasing frequency increased inception voltage. For joint # 2, which was the joint with the most PD, decreasing frequency gave decreasing inception voltage. This may be because the different test objects have aged in a slightly different way. All the inception/extinction voltage measurements are presented in appendix B.

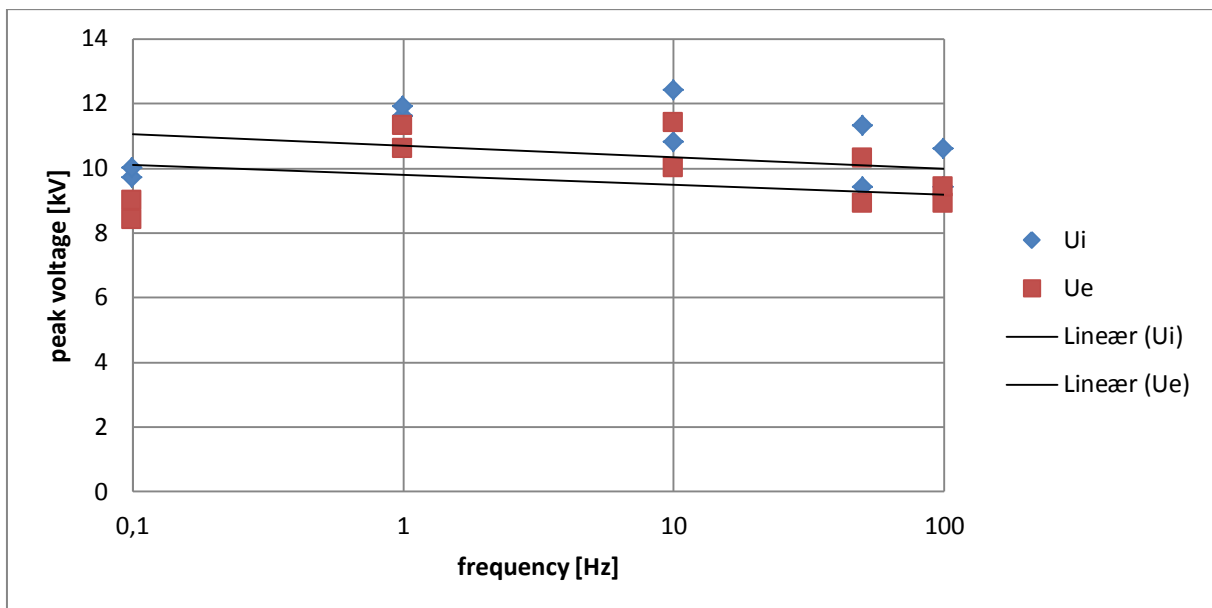


Figure 32. Joint #1. Inception and extinction voltage after 256 hours of aging. Increasing inception voltage with decreasing frequency.

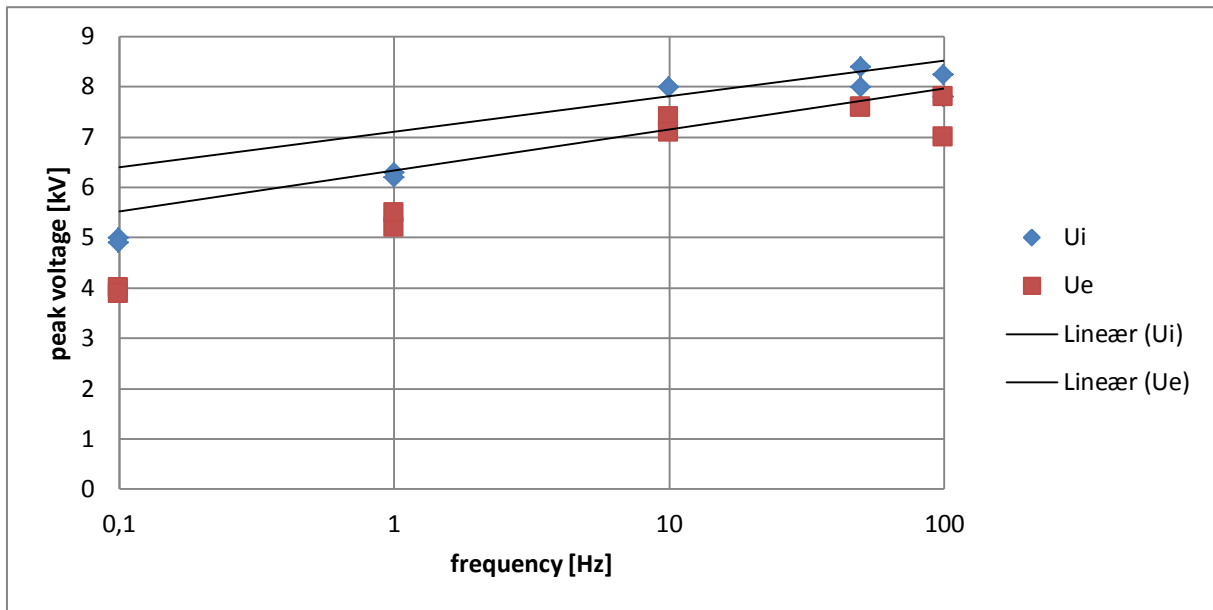


Figure 33. Joint # 2. Inception and extinction voltage after 256 hours of aging. Decreasing inception voltage with decreasing frequency.

4.2.3 PD count and charge per cycle as a function of frequency and voltage

The PD count per cycle and the charge per cycle seem to follow the same trends. This is as expected since the charge per cycle is a product of the PD count per cycle. Two different trends were found when counting PD at different frequencies. At early stages of aging or if the voltage was not sufficiently high, the amount of PD went to zero for low frequencies. At later stages of aging and at sufficiently high voltage, the amount of PD seemed to increase at lower frequencies. Decreasing PD activity can be explained by a shielding effect in cavities due to surface conductivity. Increasing PD activity can be explained by field concentration in cavities due to increased conductivity or strong dispersion.

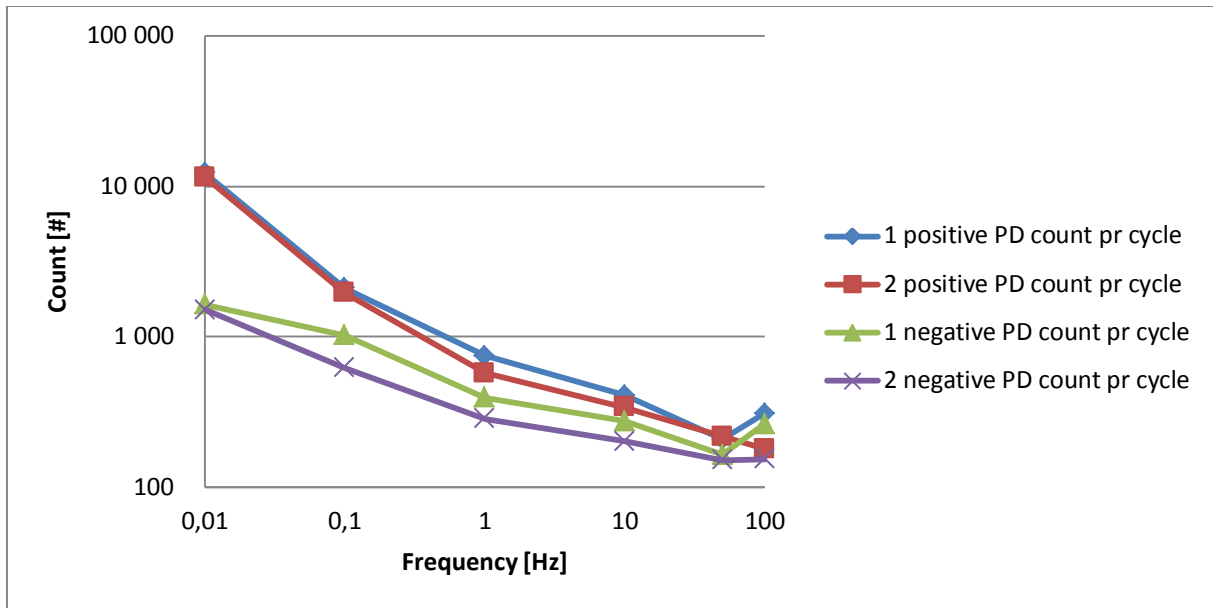


Figure 34. Joint # 2. 256 h of aging. $2xU_0$. Increasing number of positive/negative PD per cycle with decreasing frequency. Measured twice.

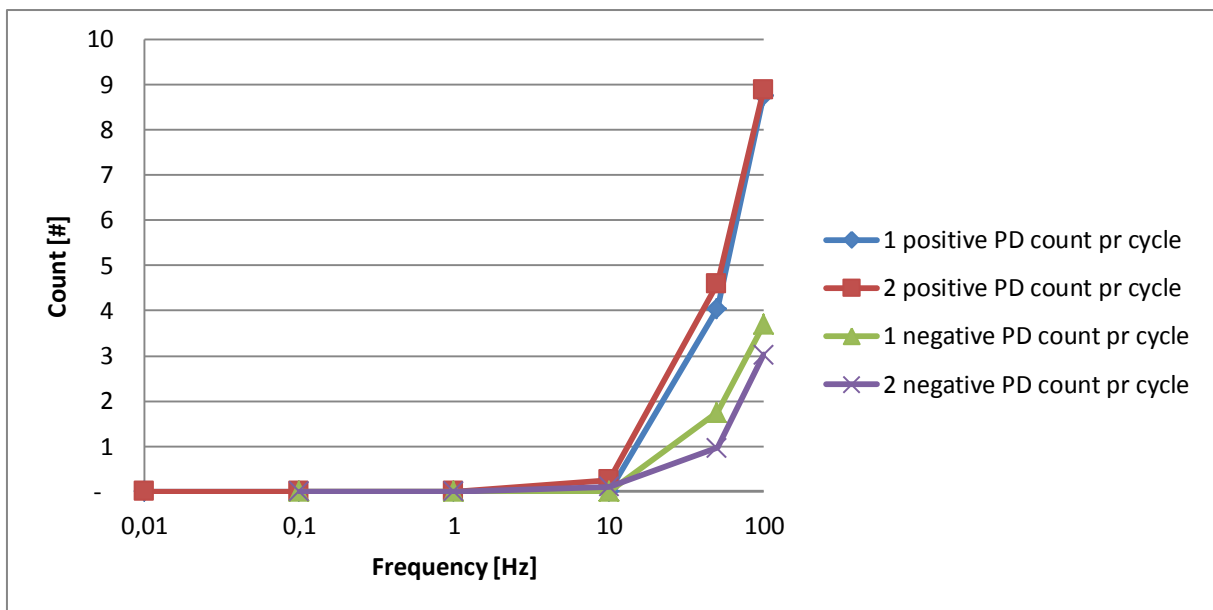


Figure 35. Joint # 2. 136 h of aging. $2xU_0$. Decreasing number of positive/negative PD per cycle with decreasing frequency. Measured twice.

Voltage level has great impact on the PD count per cycle and charge per cycle. Lowering the voltage reduces the amount of PD occurring in the test objects and also the charge per cycle. This seems to be the case for both positive and negative charges.

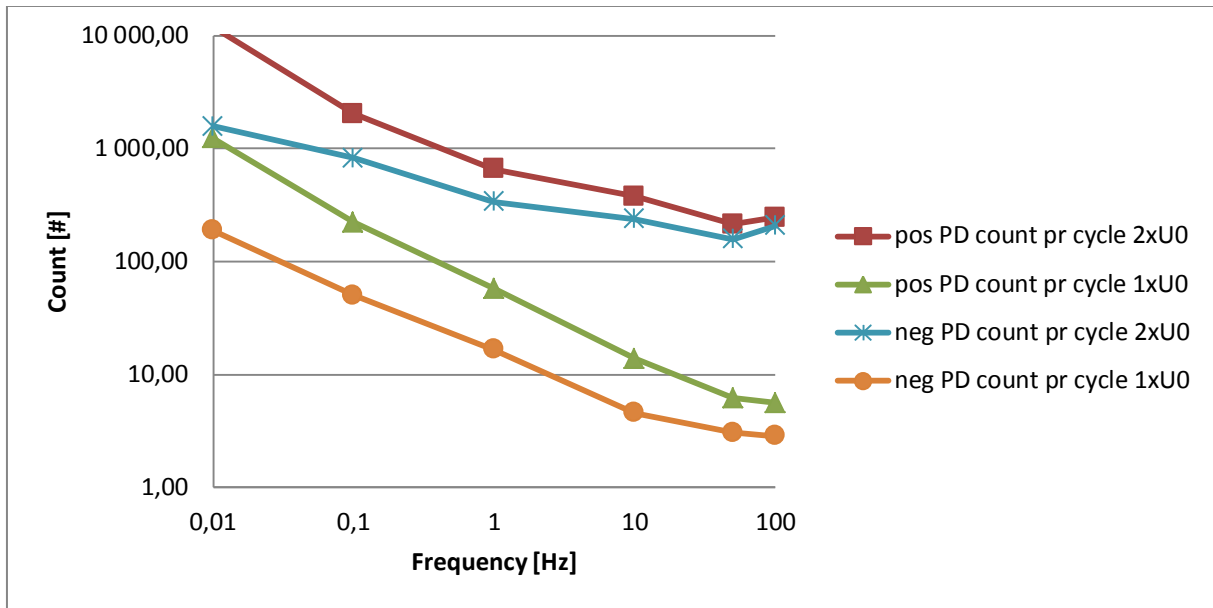


Figure 36. Joint # 2. 256 h of aging. Decreasing number of positive/negative PD when reducing voltage.

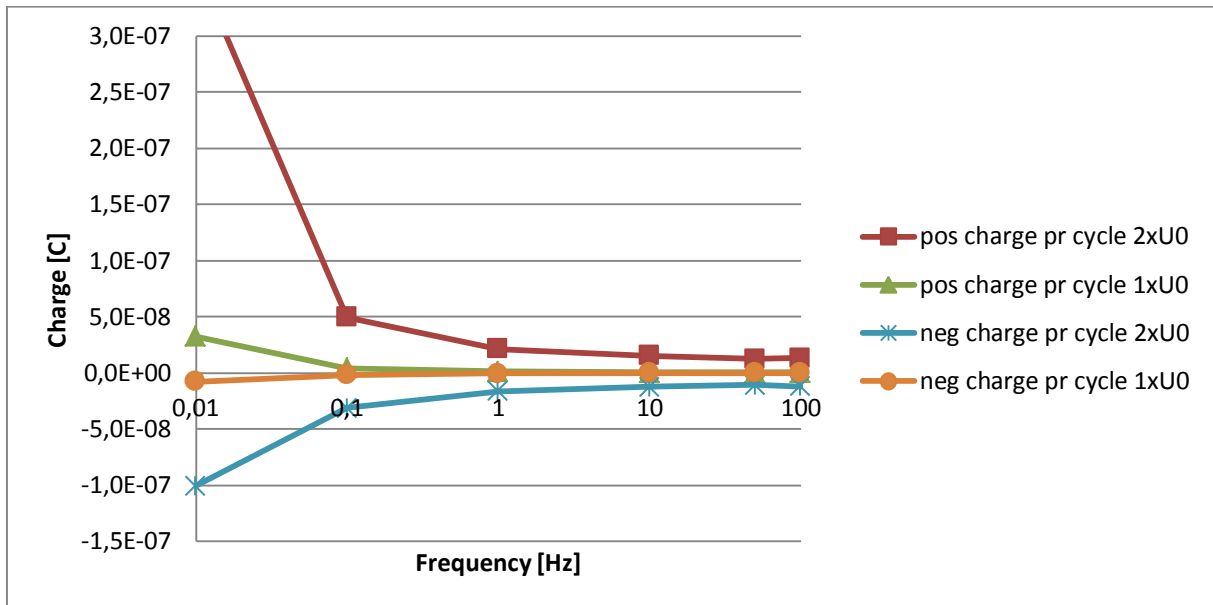


Figure 37. Joint # 2. 256 h of aging. Decreasing charge per cycle when reducing voltage.

4.2.4 Mean charge as a function of frequency and voltage.

The mean charge amplitude seems to change less as a function of frequency. This shows that the frequency does not influence the PD amplitude as much compared to the PD count and charge per cycle. This can be explained by the void geometry which determines the charge amplitude. When a voltage collapse finally occurs, it collapses across the same geometric distance regardless of the frequency.

Therefore, changing the frequency will not have as big an impact on the mean charge as on the PD count and charge per cycle.

The exception to this is at early aging or low voltage, when PD dies out at low frequency. Mean charge drops to zero when reducing the frequency. This reduction can be explained by far less PD activity from which to calculate.

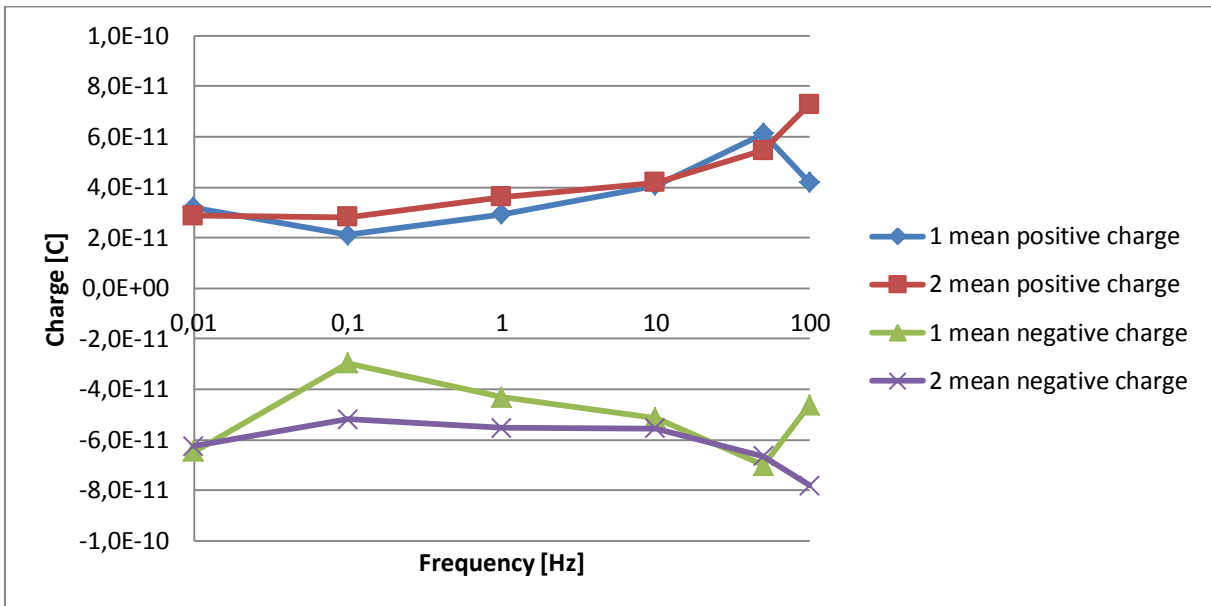


Figure 38. Joint # 2. 256 h of aging. $2xU_0$. Stable mean charge regardless of frequency.

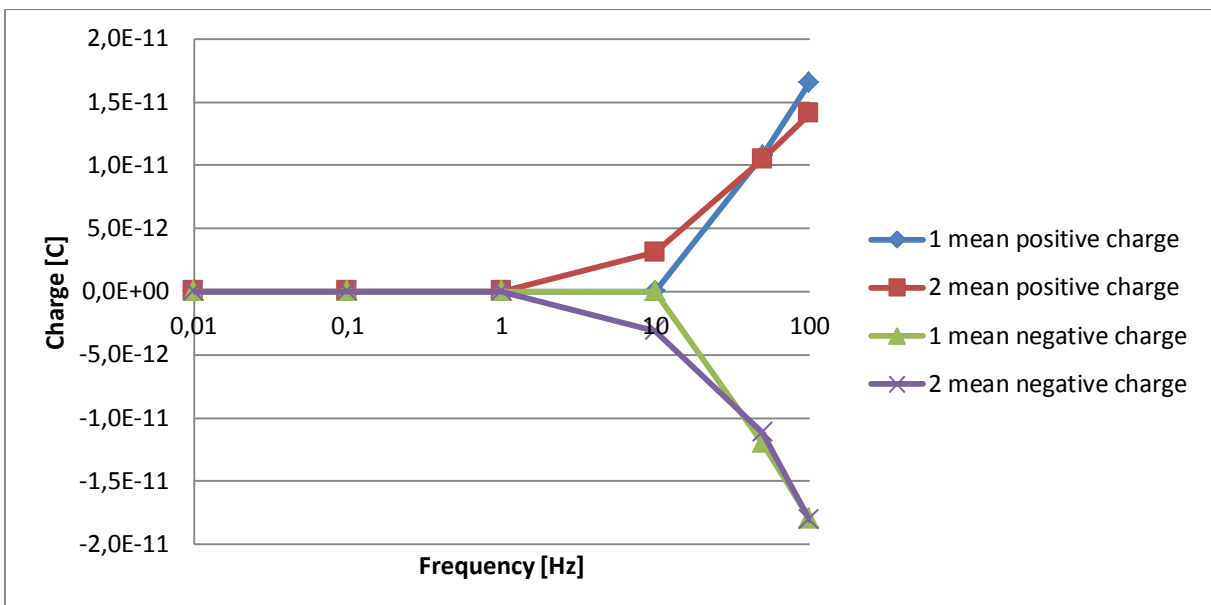


Figure 39. Joint # 2. 256 h of aging. $2xU_0$. Reduced mean charge because of disappearing PD.

The voltage level also has minimal influence on the mean discharge. This makes sense in the same way as mentioned earlier; the void geometry is unchanged. Voltage level only influences the PD count and charge per cycle.

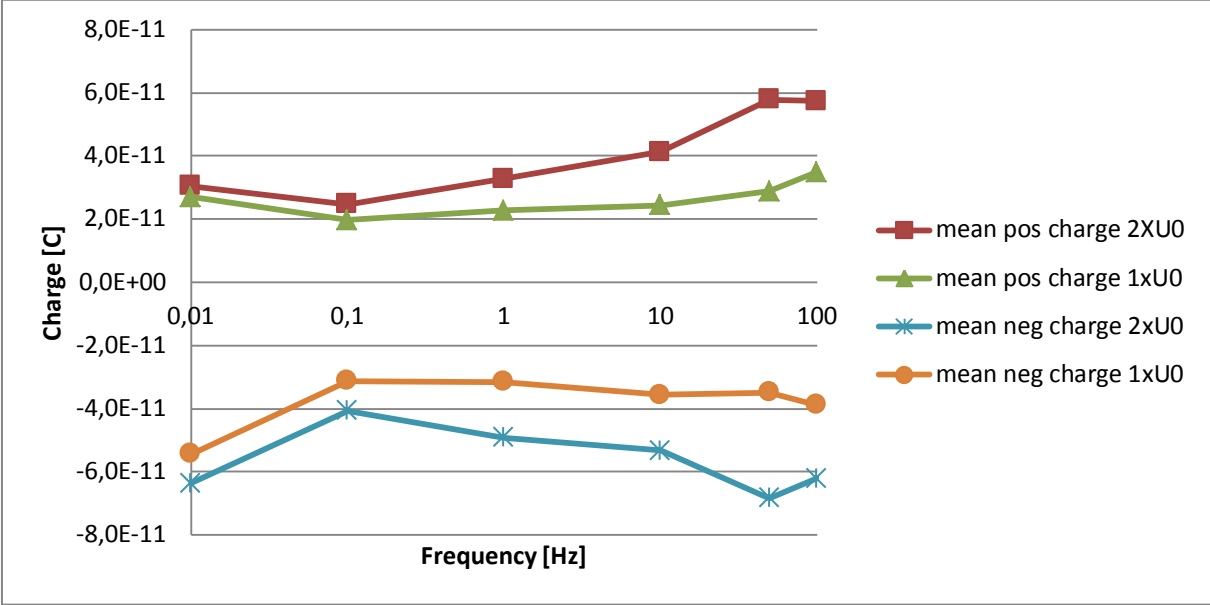


Figure 40. Joint # 2. 256 h of aging. Mean charge almost unchanged by voltage change.

4.2.5 Charge amplitude distribution

Separating the negative and positive discharges in histograms clearly shows that certain PD amplitude levels are more represented than others in the measurements. The histograms presented in this thesis contain one bar for each discharge level found. The main trend is that the low amplitude discharges are more numerous than high amplitude discharges. It is also possible to distinguish an increase in PD activity at certain amplitude levels. This can be seen in the saw tooth form in the histogram. The fact that the different amplitude levels each represent a different failure/void in the test object may explain this. The trend is most visible at high frequency and high voltage.

The histograms also clearly show a reduction in negative discharges compared to positive discharges at lower frequencies. For steady state this should not occur between two insulated surfaces. The asymmetry between positive and negative discharges can be explained by the existence of conductive paths between the surfaces that are activated by low frequency fields. It is the same shielding effect that reduces the PD counts per cycle with lower frequencies.

The distinctive saw-tooth form is also visible at low frequency. However, the teeth are not at the same place as when measured with higher frequency. This shows that equal faults are represented differently in histograms when measured at different frequencies.

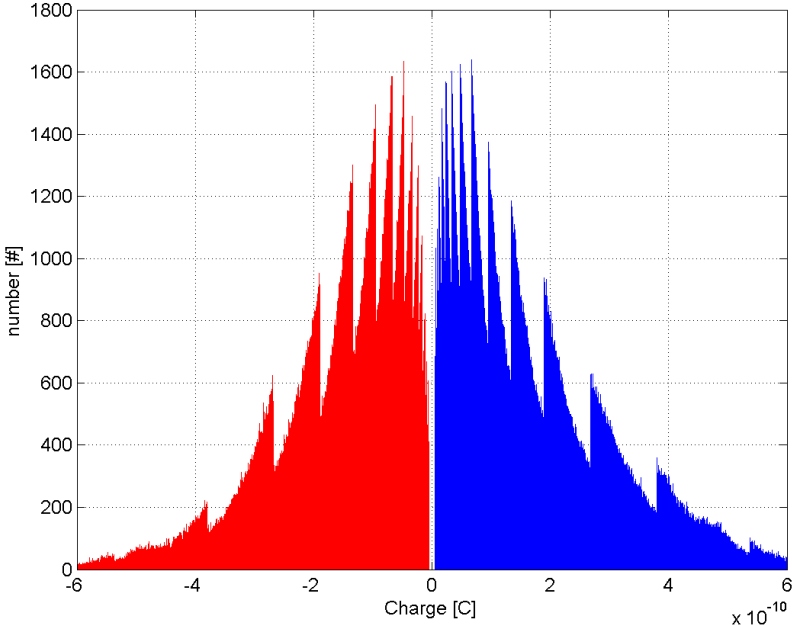


Figure 41. Joint # 2. 100Hz 2xU₀. 256 h aging. Symmetry between negative and positive discharge levels when measuring at high frequency. There are more low-amplitude discharges than high amplitude.

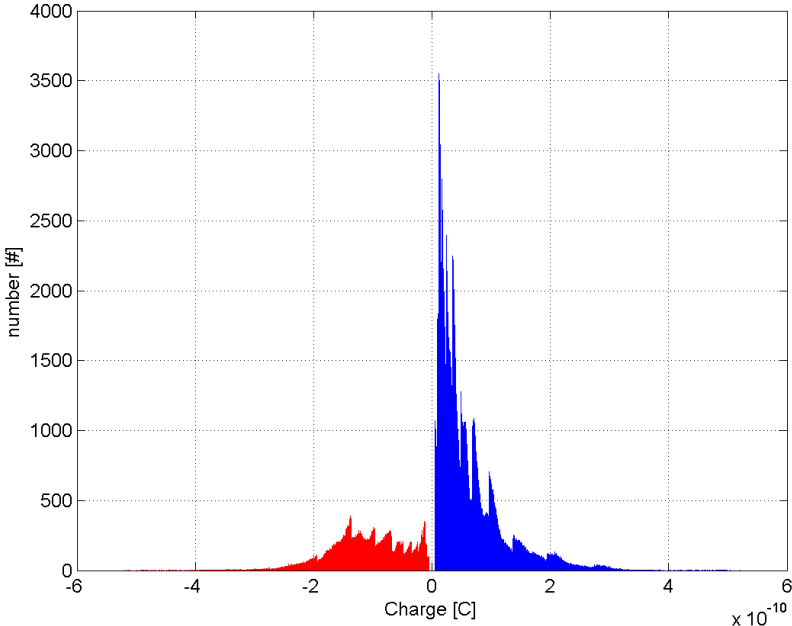
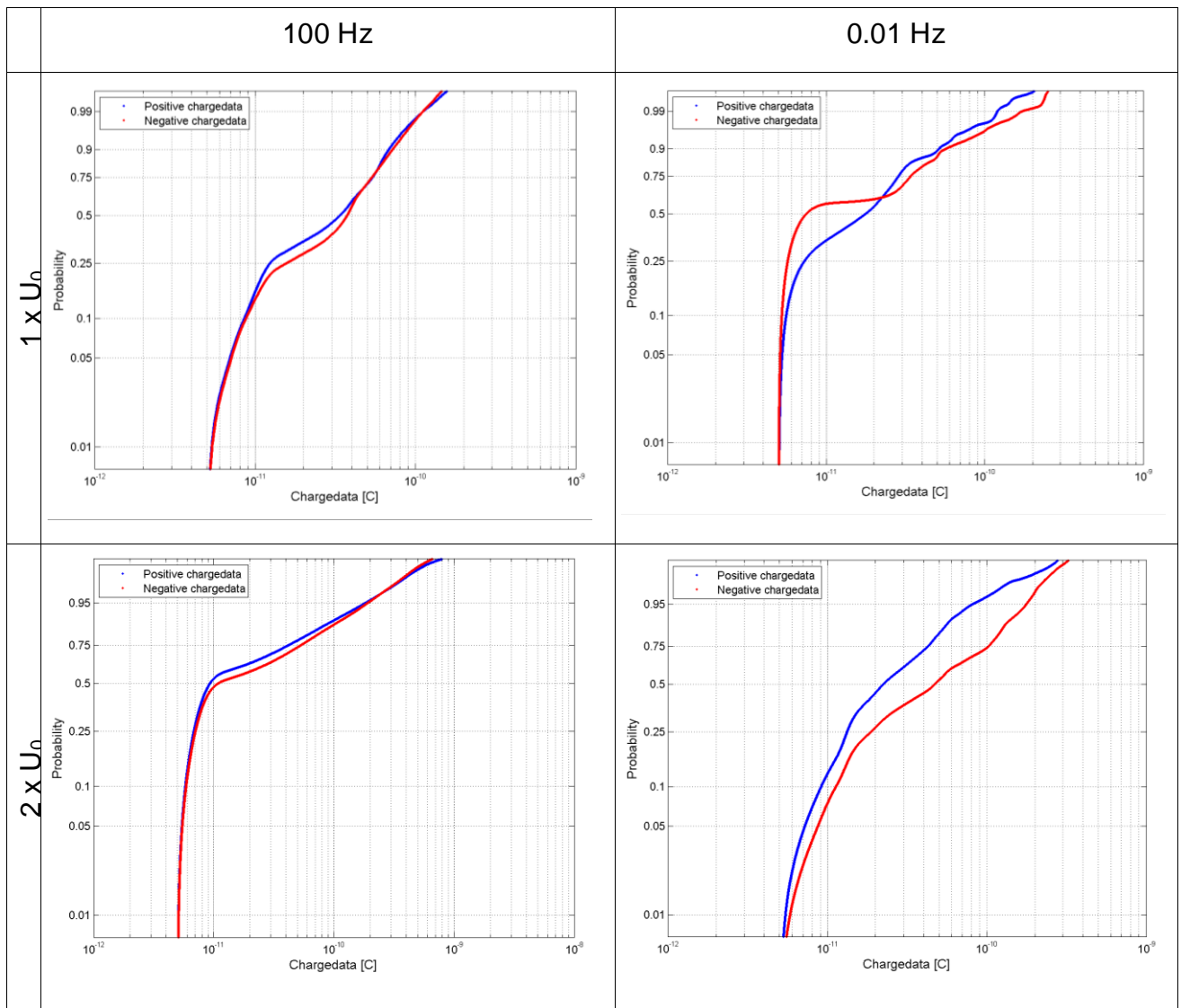


Figure 42. Joint # 2. 10 mHz 2xU₀. 256h aging. Asymmetry between positive and negative discharges when measuring at low frequency. There are more positive charges than negative.

4.2.6 Weibull distributions

The Weibull distributions of the charge data reveal that fault signatures (β -values) detected at high frequencies are not necessarily equal to fault signatures detected at low frequencies. Most of the test objects show at least two β -values at 100 Hz, but the same test object may have three or more β -values at lower frequencies. Also the voltage affects the form of the Weibull curve. This shows that Weibull distributions may not tell the truth about the test objects condition when only measuring at one frequency or voltage.

Table 8. Weibull plots for Joint # 2 after 256 hours of aging. Clear differences can be seen when studying the same test object at different frequency and voltage.



Another trend in the Weibull plots (see appendix E) is that the negative discharge probability becomes lower than positive when frequency drops. The probability for both positive and negative discharge levels is most often close when measured at high frequencies.

4.2.7 Acoustic analysis of test objects

Prior to dissecting the joints, acoustic PD measurements were performed. The joints were divided into six areas which were measured individually. The measurement pointed to where the loudest discharges took place in the joint. The joint ferrule was found to emit the most sound within joints # 1 and 2. For joint # 3, there were not loud enough discharges to pinpoint the location. The PD signals correlated nicely with the applied voltage showing that the signals did come from within the joint.

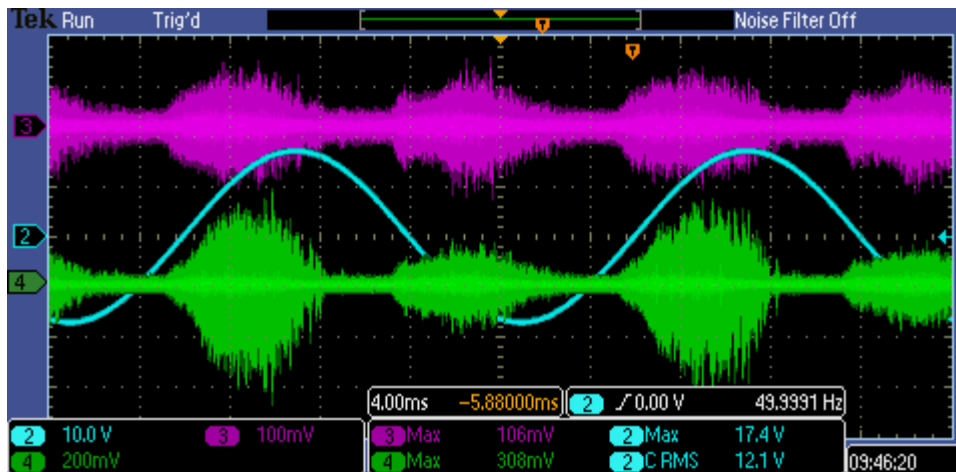


Figure 43. Acoustic PD measurement on joint # 2. Two microphones placed on top and bottom of center joint. The results are equivalent to 500-700 pC average measured with Omicron.

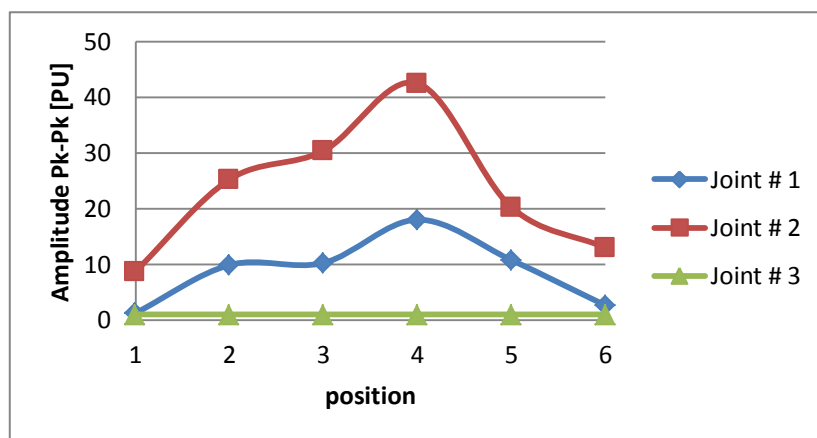


Figure 44. Acoustic PD measurement on joints. The joint was measured at 6 positions along the joint. Position 4 was found to emit the most sound for two joints. This is where the joint ferrule is located. Joint # 3 did not emit any sound. PU base = ambient noise = joint # 3 values

4.2.8 Dissection of joints

All the joints were cut into 6 pieces, approx. 10 cm long. A selection of the pieces was dissected, mostly the parts containing the joint ferrule. These areas were most likely to be the PD source based on the acoustic measurements.

The external thermal insulation had become dried out and brittle in the area which was in contact with the joint. Much of the glue from inside the laminated outer sheath had been pressed out and had accumulated inside the thermal insulation. The outer sheet was quite easy to open as remaining glue had dried out. The insulating tubing had patterns from the curled up aluminum laminate on the outside and from the Cu-mesh on the inside. No serious deformations were detected. The Cu-mesh was more or less incorporated into the insulating tubing. The insulating tubing was also quite easy to detach from the joint body. A noticeable difference was observed between the middle and the end part of the joint. In the middle most of the glue had dried out and the different materials were easy to rip apart. Close to the end the glue was still sticky, making the dissection harder.

The outer screen of the joint body had patterns from the Cu-mesh. This was probably caused by the heat and compression. No punctures penetrated through to the red insulating body. The joint body had not become brittle. Its continued elasticity could be observed by a bulging of the material in the cut area. The joint body seemed to be able to squeeze the material out through the incision. The inner layer had a slight discoloring compared to the fresh materials. A discoloring in the narrow area between the two joint body materials was also clear. This was not visible prior to aging. The discoloring was not as significant towards the ends of the joint.

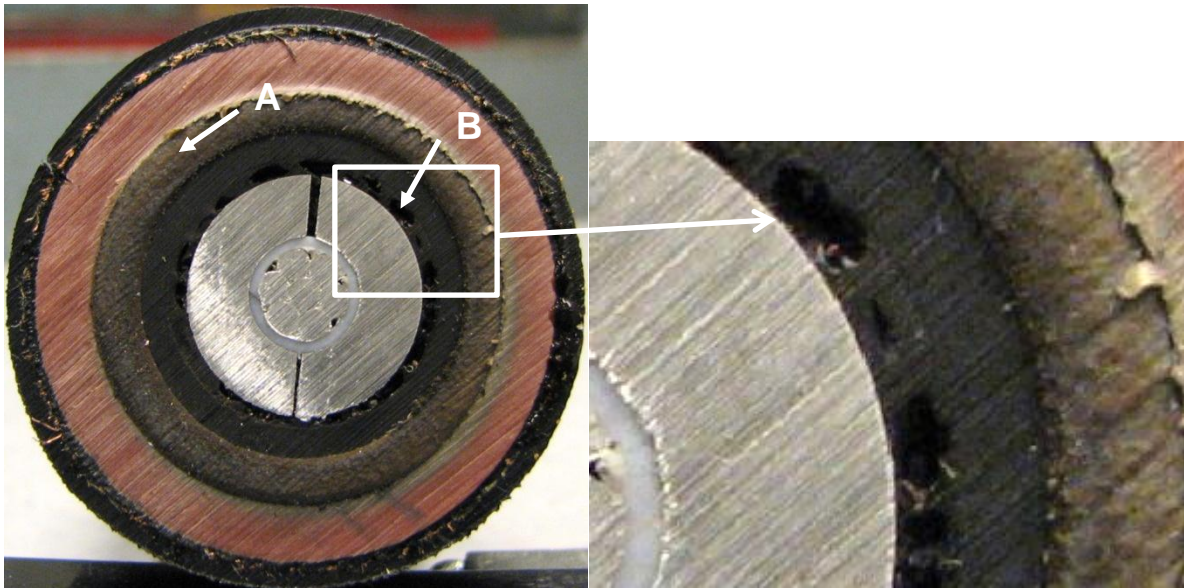


Figure 45. Cross section of joint (center piece). A: Discolored joint body material. B: Voids and cavities in brittle mastic over joint ferrule.

The contact strength was quite high between the joint body and the stress-control tube. River-like marks could be observed on the interface between the materials. These were created when the two materials were pulled apart. The joint body material was stretched and changed color as it was pulled apart from the stress-control tube. The materials were so attached that the writing on the stress-control tube had been “printed” on the inside of the joint body. Both the joint body and the outside of the stress control tube seemed to be physically intact. An exception was joint # 2, where the two materials were fused together along a narrow line.



Figure 46. Stress control tube pulled apart from the joint body leaving marks in the joint body material.

The stress control tube over the joint ferrule had become brittle. In some parts it was possible to extract large pieces and in other parts the tube was so brittle that it broke easily when bent. It was less brittle nearer to the ends of the joint. The mastic on the inside of the stress-control tube was severely damaged, discolored and burnt in the mid-area of the joint. Pits and cavities of different size and shape were found all over the mastic covering the joint ferrule. In the bottom of some of the pits towards the stress control tube a white/yellow residue could be seen. Although it was difficult to see if the pits extended into the stress-control material, they did reach it. The mastic had become brittle and the material volume was clearly reduced.



Figure 47. Pits and cavities in mastic between joint ferrule and stress-control tube. Comparison between joints # 1, 2 and 3 (from left to right). A clear difference in the amount of pits in the mastic can be seen between the different joints.

Throughout the dissection procedure it became clear that the joints had significant gradients of aging from the middle to the sides. The materials close to the joint ferrule (heat source) was more brittle and easier to take apart. The materials close to the end of the joint were aged, but not as severely as in the middle. Mastic used at the cable screen cutoff was still yellow, but not as bright as before installation. More uniform aging could be attained by better thermal insulation of the joint and lower core temperature. A strong odor was emitted from the joints as they were dissected. The materials were being naturally degassed after being exposed to free air.

No obvious PD locations were found in the high stress areas between earth potential and the stress-control tube. All materials seemed intact and in contact with each other. The voids and cavities in the mastic were left as a possibility. Micro-cracks in the stress-control tube may also be the source. PD must have a sufficiently high

electric field to initiate. In theory there is no such electric field between the stress-control tube and the joint ferule. However, the heavy aging and oxidation of the material may have altered the electrical properties causing the field-control to stop working. The material has also most likely been contaminated with gases from the melted mastic and other surrounding metals and materials. This may also influence the electrical properties.

A collection of photos and comments are placed in appendix F.

5. Conclusions and further work

A variable frequency PD measurement setup has been utilized to detect PD in test objects up to 17 kV_{peak} with frequencies between 10 mHz and 100 Hz. A three stage RLC low-pass filter between the high voltage source and test object gave measurement accuracy at 5 pC.

The results found in the project suggest that electrothermal aging of cable joints is an effective way of deteriorating the cable materials causing PD and faults. Already after 10 cycles and 136 hours at 180 °C significant discharges could be measured in the joints. Arrhenius models and activation energy calculations have given a good estimation of lifetime for the polymers at hand when subjected to high temperatures.

PD measurement results will vary significantly with regards to measuring technique. The voltage and frequency has a great impact on the PD results found in the aged test objects. At early stages of aging the PD signals totally disappeared at frequencies below 10 Hz. A relatively low voltage level would also cause PD signals to totally disappear. This means that signs of aging are not visible at lower frequencies unless sufficiently high voltage is used. This could lead to a wrong diagnosis of cable systems tested only with VLF methods or with online voltage levels.

The number of PD and charge per cycle increased with decreasing frequency after a certain period of aging. Also voltage levels have a big impact on the amount of PD and charge. This suggests that deterioration of the cable materials will be higher if they are subjected to elevated voltages at low frequency. This supports the reported faster tree growth rate at VLF compared to power frequency. It must be mentioned that most offline PD tests are not exposing the test objects to these stresses for long periods of time compared to their normal operation.

Weibull analyses show that two or more fault locations are active in the joints. The results varied so much that it was not possible to find any consistent patterns.

Further investigations into joint materials, when aging and oxidation progress, could be an interesting topic. The electric capabilities of the materials, especially the field-control material, should be studied. This material is very close to the heat source, with only a thin layer of mastic in between. There are many ways to characterize materials in order to establish a correlation between condition and oxidation. Oxidation Induction Time (OIT), Melting Temperature and Crystallinity Index are all methods which are performed by a Differential Scanning Calorimeter (DSC). These are only three of several methods used in Ontario Hydro Technologies study [29]. In this project only electrothermal aging has been used. Adding voltage to the test object during electrothermal aging would imitate the real life wear in a better way.

Test objects with premade faults could aid our understanding and interpreting PD results. When the void geometry is known, simulations can be made and compared to the measurements. Some work has been done on this subject already. Studying the effect of frequency could contribute to a broader understanding of the factors influencing PD phenomenon.

6. References

- [1] http://www.pesicc.org/iccWebSite/subcommittees/subcom_b/Presentations/2011Fall/B1-WindfarmDesignandCableAccessories.pdf, IEEE/ICC, 21.05.2012.
- [2] http://www.pesicc.org/iccwebsite/subcommittees/subcom_f/F05/Presentations/2009Fall/F12-ExperienceswithPDmeasurementsonMVCablesinwindfarmsintheNetherlands.pdf, IEEE/ICC, 21.05.2012.
- [3] ICC Newsletter, IEEE/ICC, Spring 2012-Vol1-Issue1.
- [4] DeVries, Smit og Sebregts, Experience with joint failures in new smart-grid MV cable circuits, Versailles: Jicable, 2011.
- [5] J. Benjaminsen og H. Faremo, «Oversikt over problemer med ulike kabeltyper og kabelutstyr,» Sintef, Trondheim, 2008.
- [6] Energi Norge, «Tilstandskontroll av Kraftnett. Håndbok Massekabelanlegg,» Energi Norge, 2011.
- [7] Energi Norge, «Tilstandskontroll av Kraftnett. Håndbok PEX Kabelanlegg,» Energi Norge.
- [8] E. Ildstad, «Condition Assessment of Power Apparatus,» The 1998 International Conference on Communication, Computer & Power, 1998.
- [9] J. Benjaminsen og H. Faremo, «Feil på PEX-kabel og kabelutstyr for 2001 og 2002 (12 og 24 kV),» Sintef, Trondheim, 2006.
- [10] K. D. Hammervoll, Ikke-destruktiv tilstandskontroll av kabelskjøter i distribusjonsnett, Trondheim: NTNU, 2010.
- [11] IEC, 60270 - High-voltage test techniques - Partial discharge measurements (third edition), IEC, 2000-12.
- [12] IEEE/ICC, IEEE P400.D15 Draft Guide for Field Testing and Evaluation of the Insulation of Shielded Power Cable Systems Rated 5 kV and Above, New York: IEEE, 2011.
- [13] IEEE/ICC, IEEE P400.4.D3 Draft Guide for Field-Testing of Shielded Power Cable Systems Rated 5kV and Above with Damped Alternating Current Voltage (DAC), New York: IEEE, 2011.

- [14] E. Ildstad, TET 4160 High Voltage Insulating Materials, Trondheim: NTNU, 2010.
- [15] IEEE/ICC, IEEE P400.2.D11 Draft Guide for Field Testing of Shielded Power Cable Systems Using Very Low Frequency (VLF) less than 1Hz, New York: IEEE, 2011.
- [16] IEEE/ICC, IEEE 400.3 Draft Guide for Partial Discharge Testing of Shielded Power Cable Systems in a Field Environment, New York: IEEE, 2005.
- [17] Baur, Mohaupt og Schlick, New results in medium voltage cable assessment using very low frequency with partial discharge and dissipation factor measurement, Barcelona: CIRED, 2003.
- [18] H. Edin, Partial Discharges Studied with Variable Frequency of the Applied Voltage, Stockholm: Kungl Tekniska Högskolan, 2001.
- [19] H. Edin, Variable Frequency Partial Discharge Analysis of In-Service Aged Machine Insulation, Stockholm: Nordic Insulation Symposium, 2003.
- [20] Wester, Bodega, Cavallini og Morshuis, «The effect of Voltage Frequency on Partial Discharge Activity,» Annual Report Conference on Electrical Insulation and Dielectric Phenomena, Delft/Bologna, 2002.
- [21] T. I. Information, No. 21, partial discharge measurement techniques, Tettex Instruments.
- [22] V. Larsen, H.O.Kristiansen og K.Lien, Field experience from acoustic diagnosis of power cable accessories, Trondheim: Doble/TransiNor, 2008.
- [23] Cigré Task Force 15.11/33.03.02, 226 - Knowledge rules for partial discharge diagnosis in service, vol. April 2003, Cigré, 2003.
- [24] L. Lundgaard, TR A4403 - Partielle utladninger. Begreper, måleteknikk og mulige anvendelser for tilstandskontroll, Trondheim: EFI, 1996.
- [25] Nilsson og Riedel, Electric Circuits, Sixth Edition, New Jersey: Prentice-Hall Inc., 2001.
- [26] Contin, Gulski, Cacciari og Montanari, «A Weibull Approach to the Investigation of Partial Discharges in Aged Insulation Systems,» IEEE, Quebec, 1996.
- [27] Contin, Montanari, Conti og Cacciari, «An Invariant Diagnostic Marker for the Identification of Partial Discharge Sources in Electrical Apparatus,» IEEE, Eindhoven, 2001.

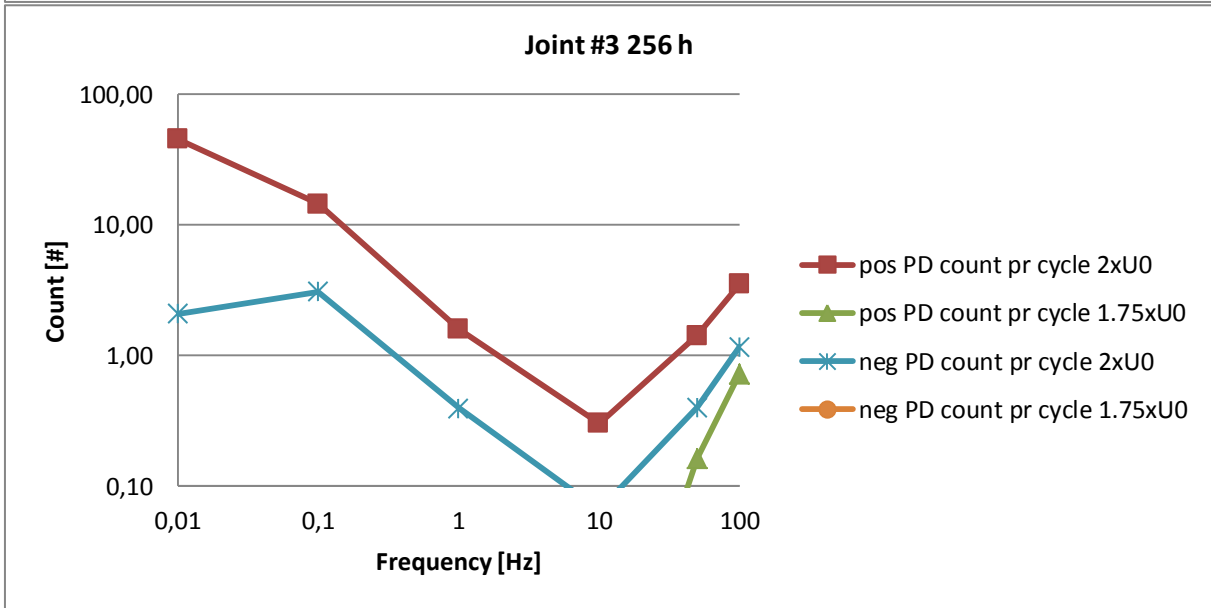
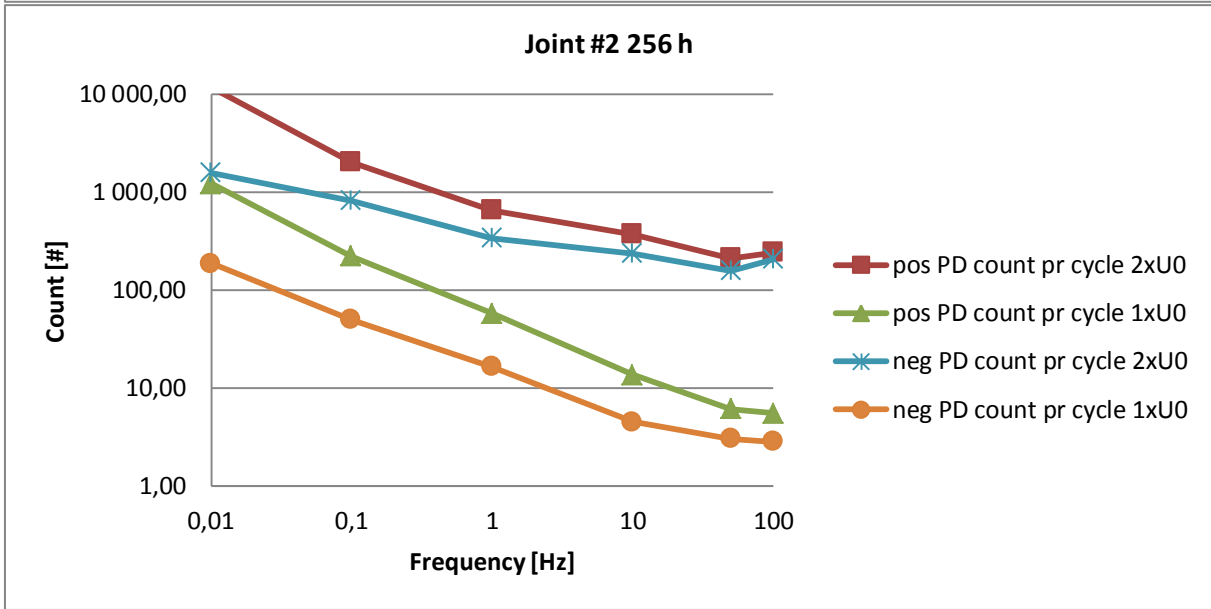
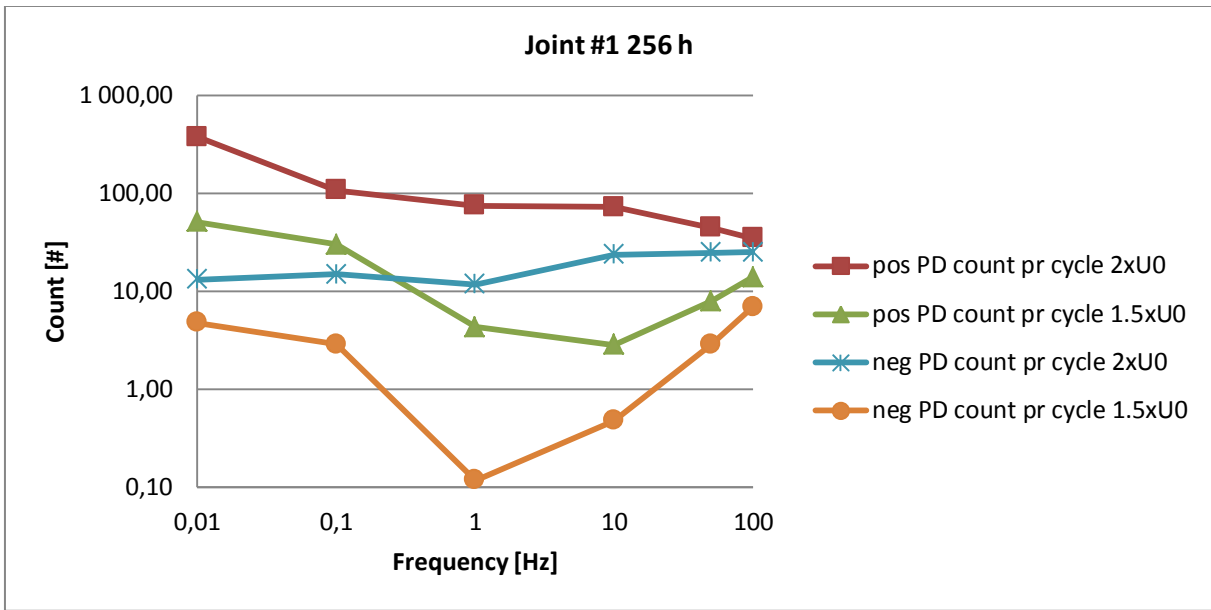
- [28] Cacciari, Contin og Montanari, «Use of a Mixed-Weibull Distribution for the Identification of PD Phenomena,» IEEE, Trieste/Bologna, 1995.
- [29] O. H. Technologies, «Long Term Reliability of Polymer Cables at High Temperatures,» Canadian Electricity Association, Toronto, Ontario, 1997.
- [30] F. Foss, frode.foss@ensto.com, Oslo: Ensto Norge, 2012.
- [31] H. L. Halvorson, «Condition Assessment of Medium Voltage Cable Joints,» NTNU, Trondheim, 2011.
- [32] Omicron, Manual MPD 600 Partial Discharge Measurement System, Austria: Omicron mtronix technology, October 2007.
- [33] TREK inc, Operator's manual High Voltage Power Amplifier model P0622B, New York.
- [34] PSCAD X4, Help File, Manitoba HVDC Research Centre, 2011.

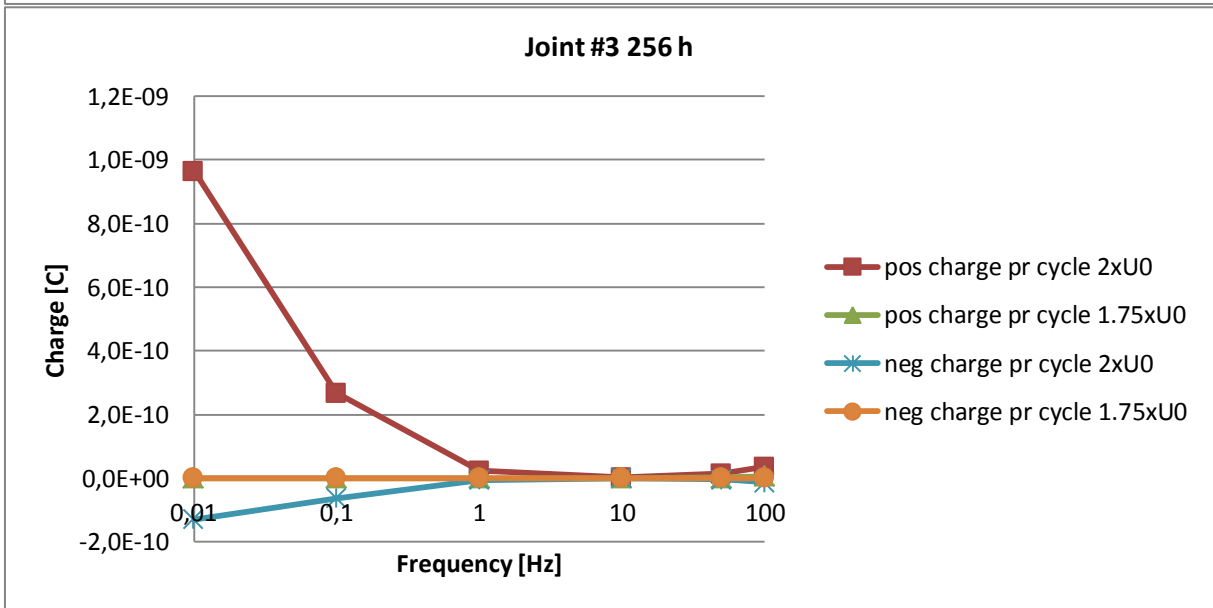
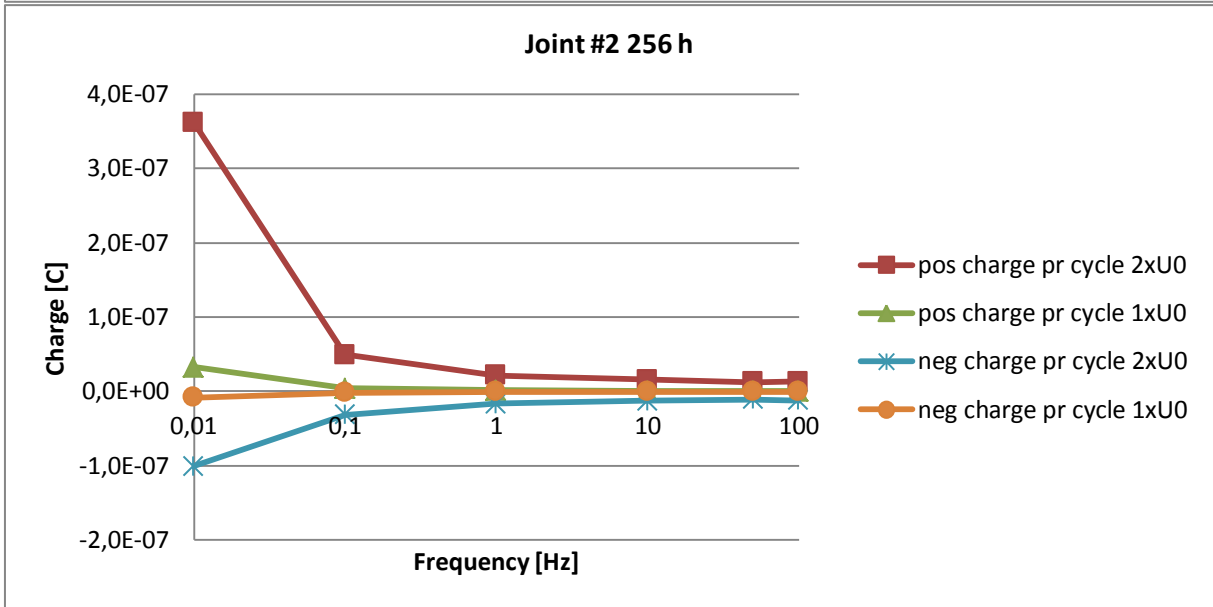
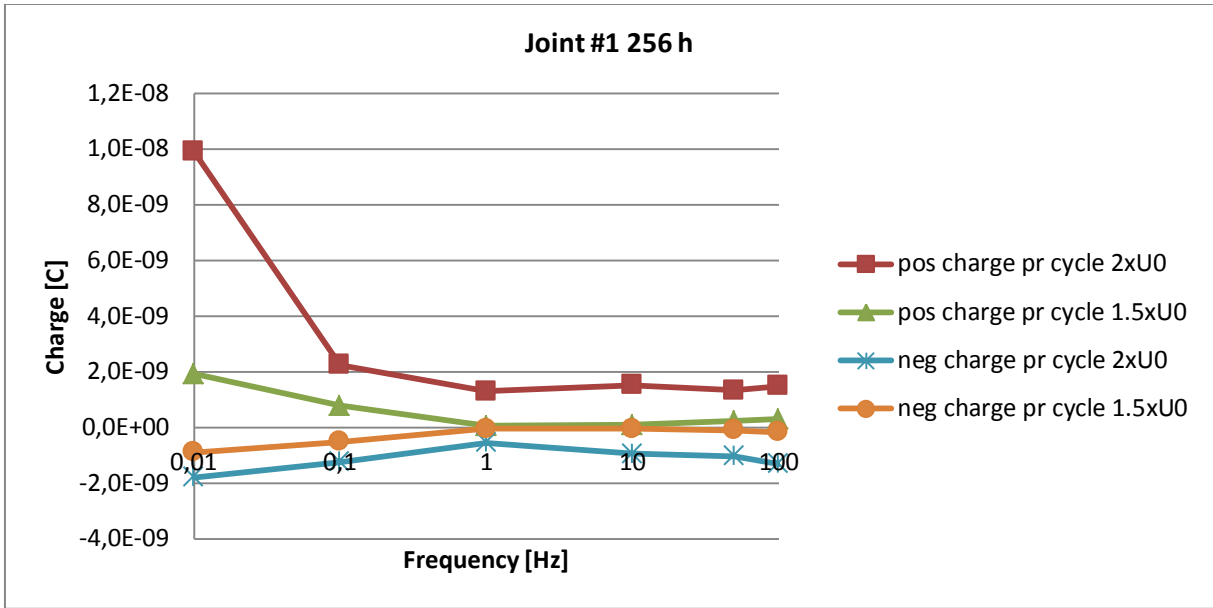
7. Appendices

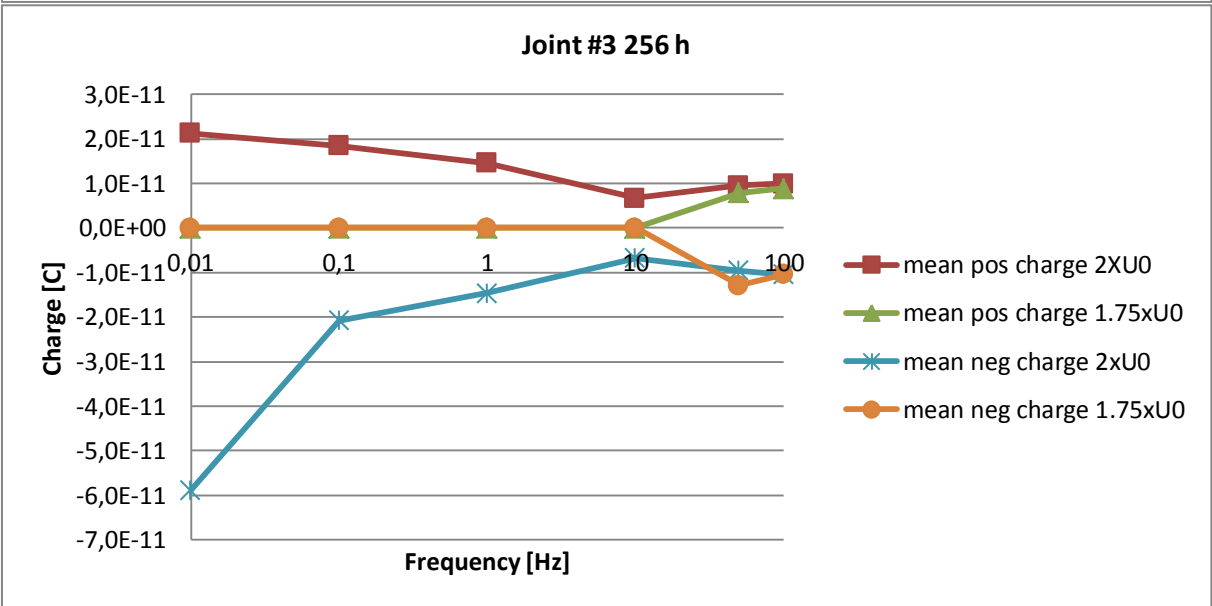
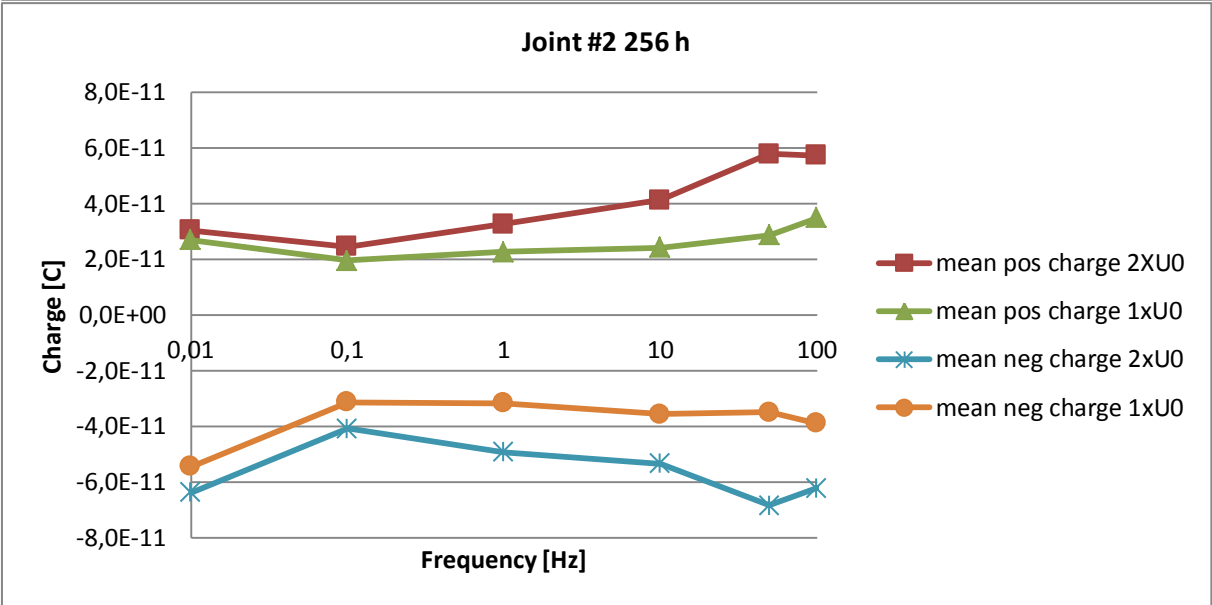
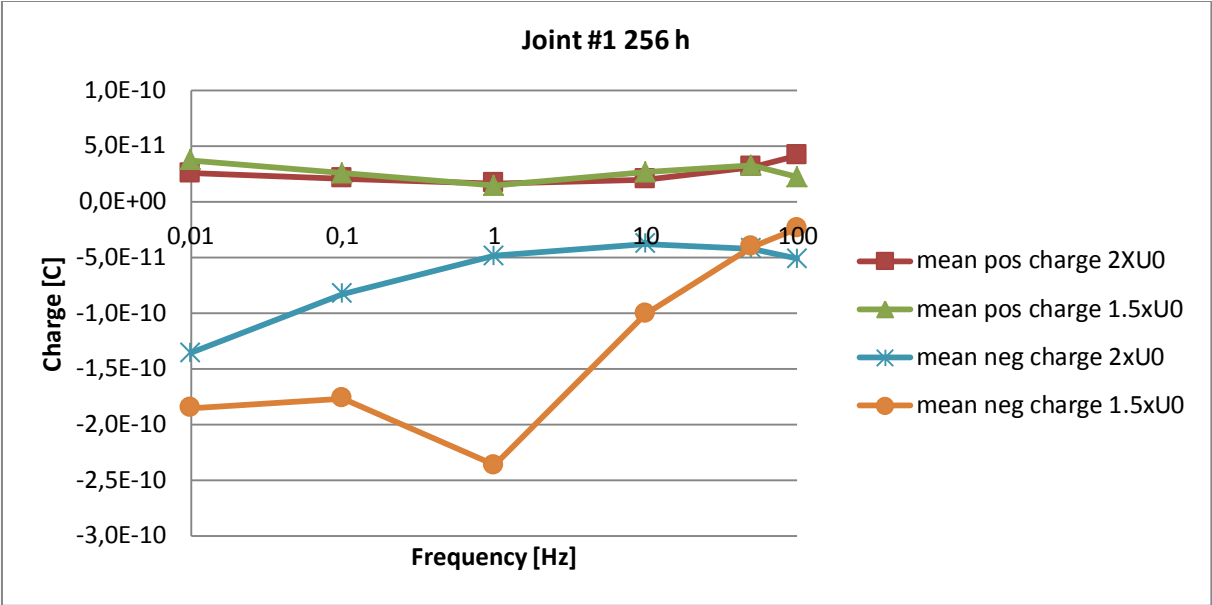
A. Statistical results

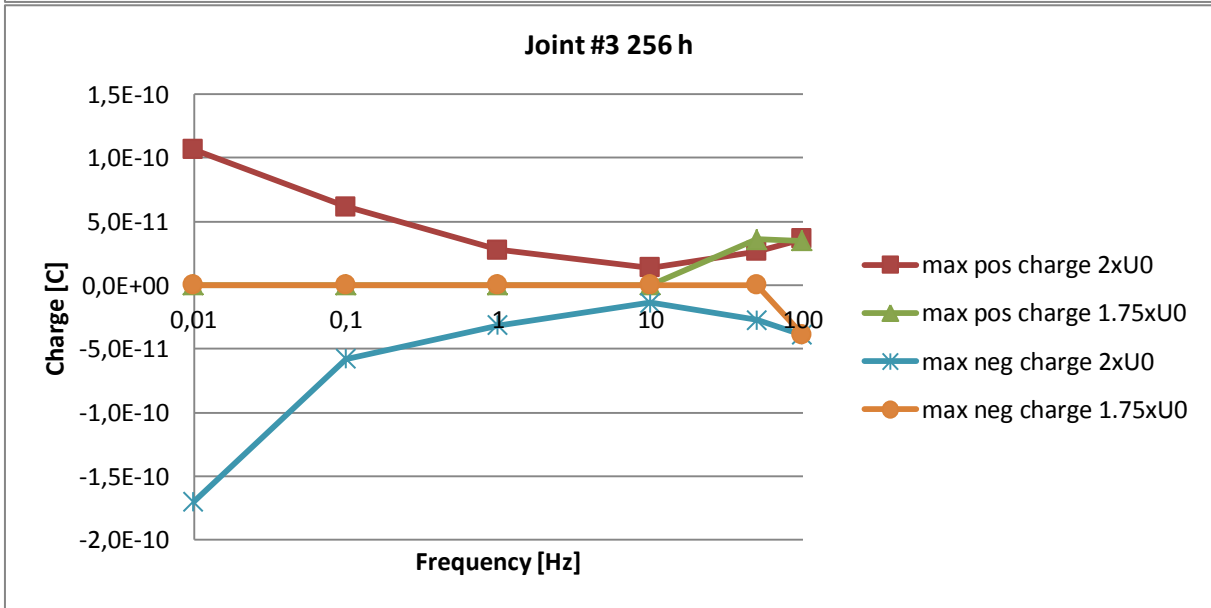
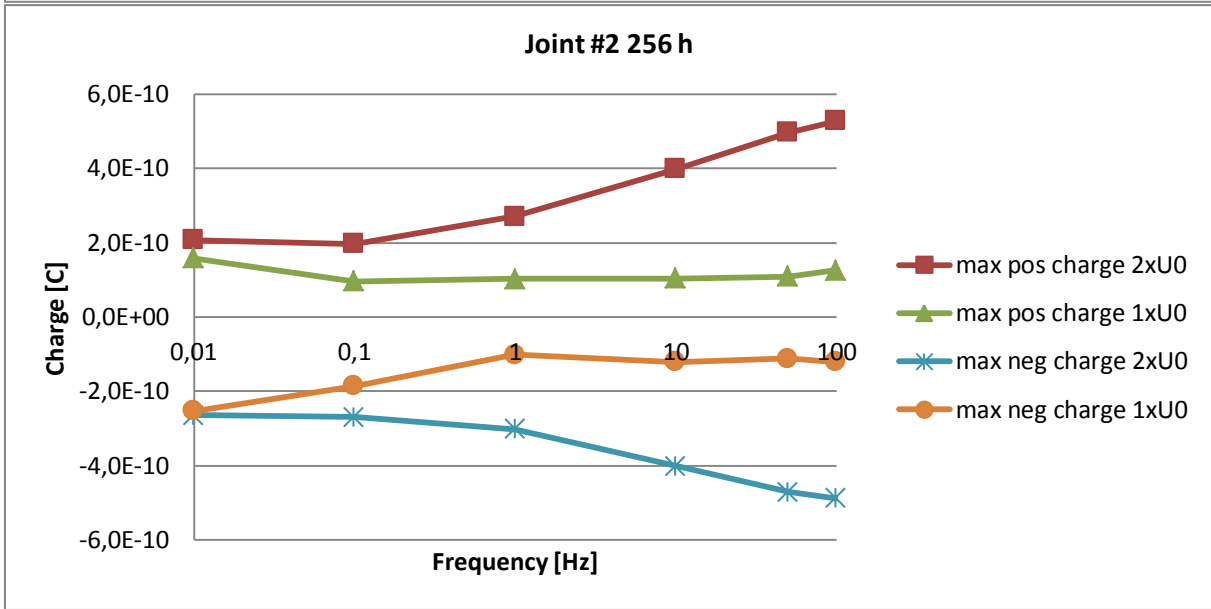
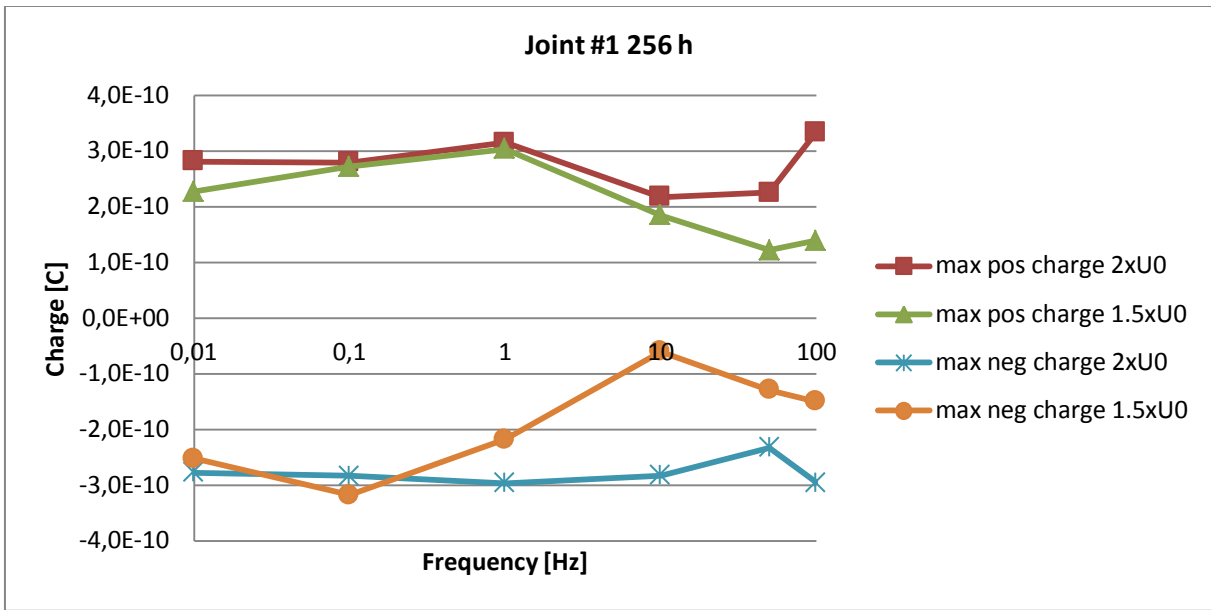
The following pages contain statistical results from PD measurements

- PD count per cycle
- Charge per cycle
- Mean charge
- Max/min charge



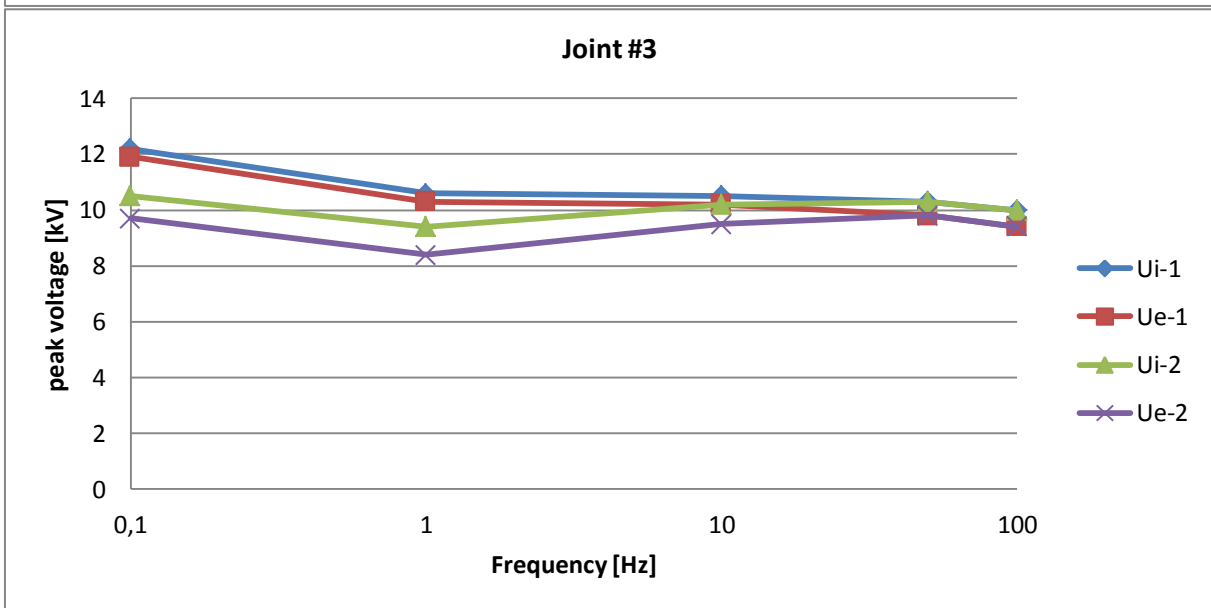
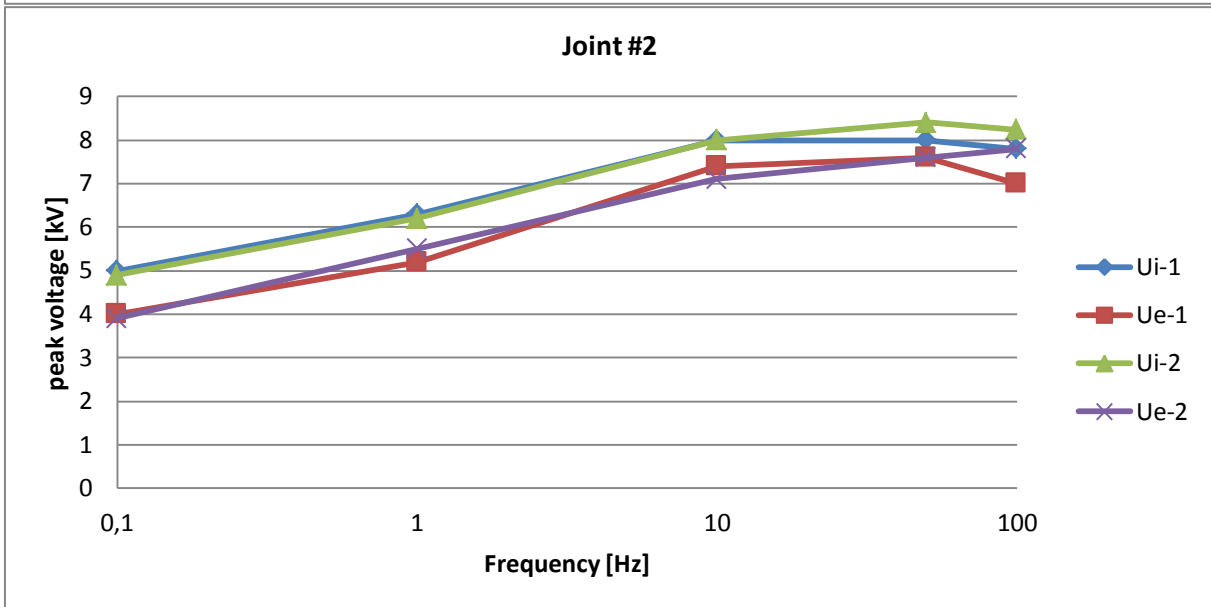
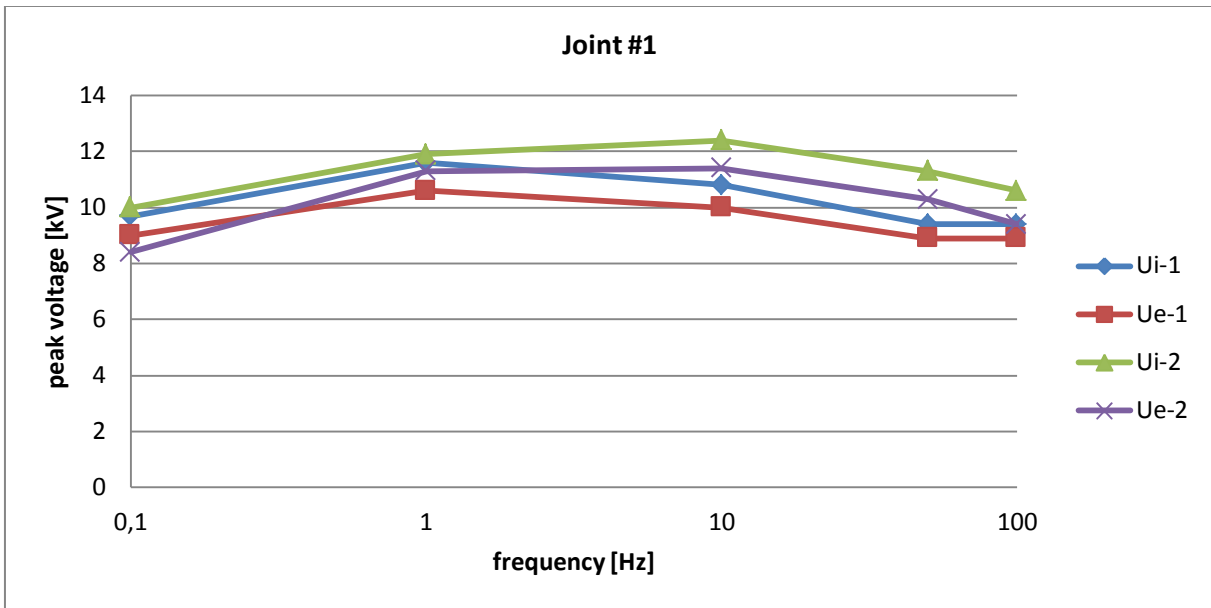






B. Inception voltage results

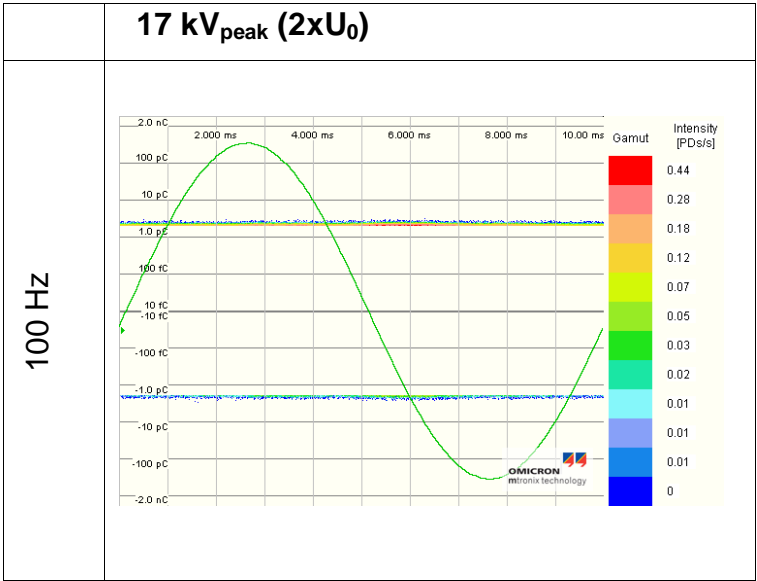
The following pages contain the results from inception and extinction voltage measurements performed on the test objects. The measurements were performed twice.



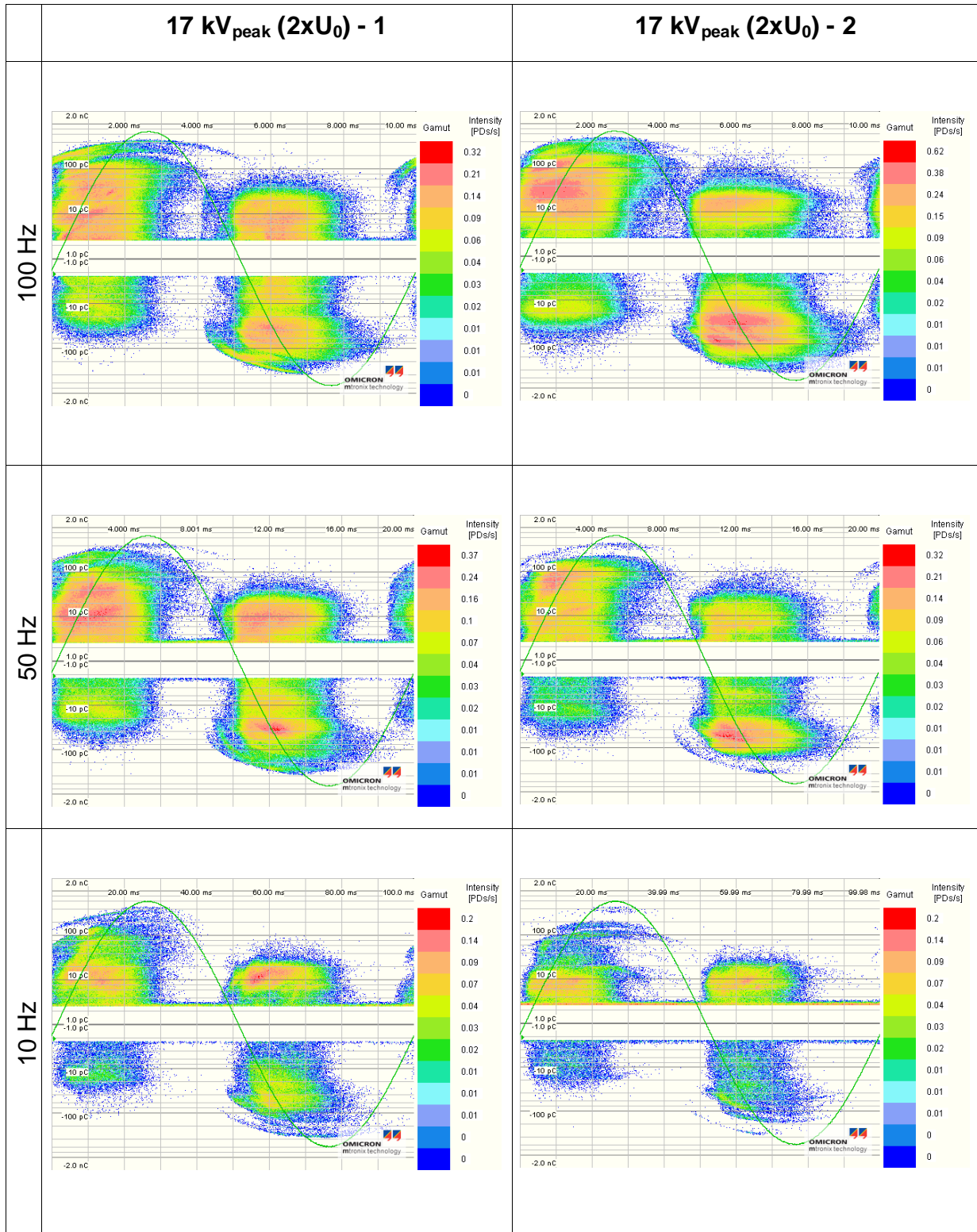
C. PRPDA plots

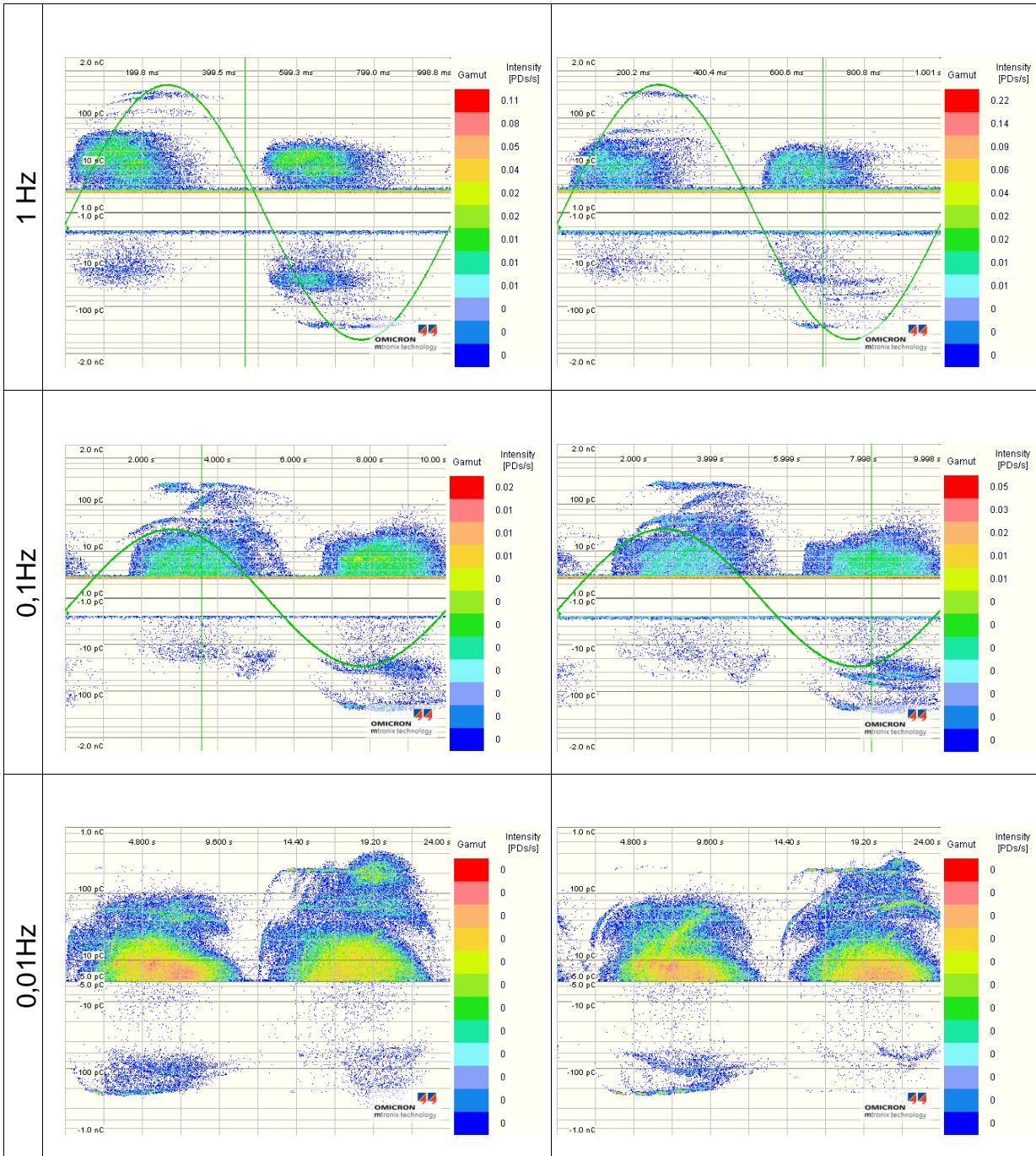
The following pages contain PRPDA plots from all PD measurements performed on the test objects. All measurements were performed twice.

Joint #1 Aging: 136 h / 10 cycles

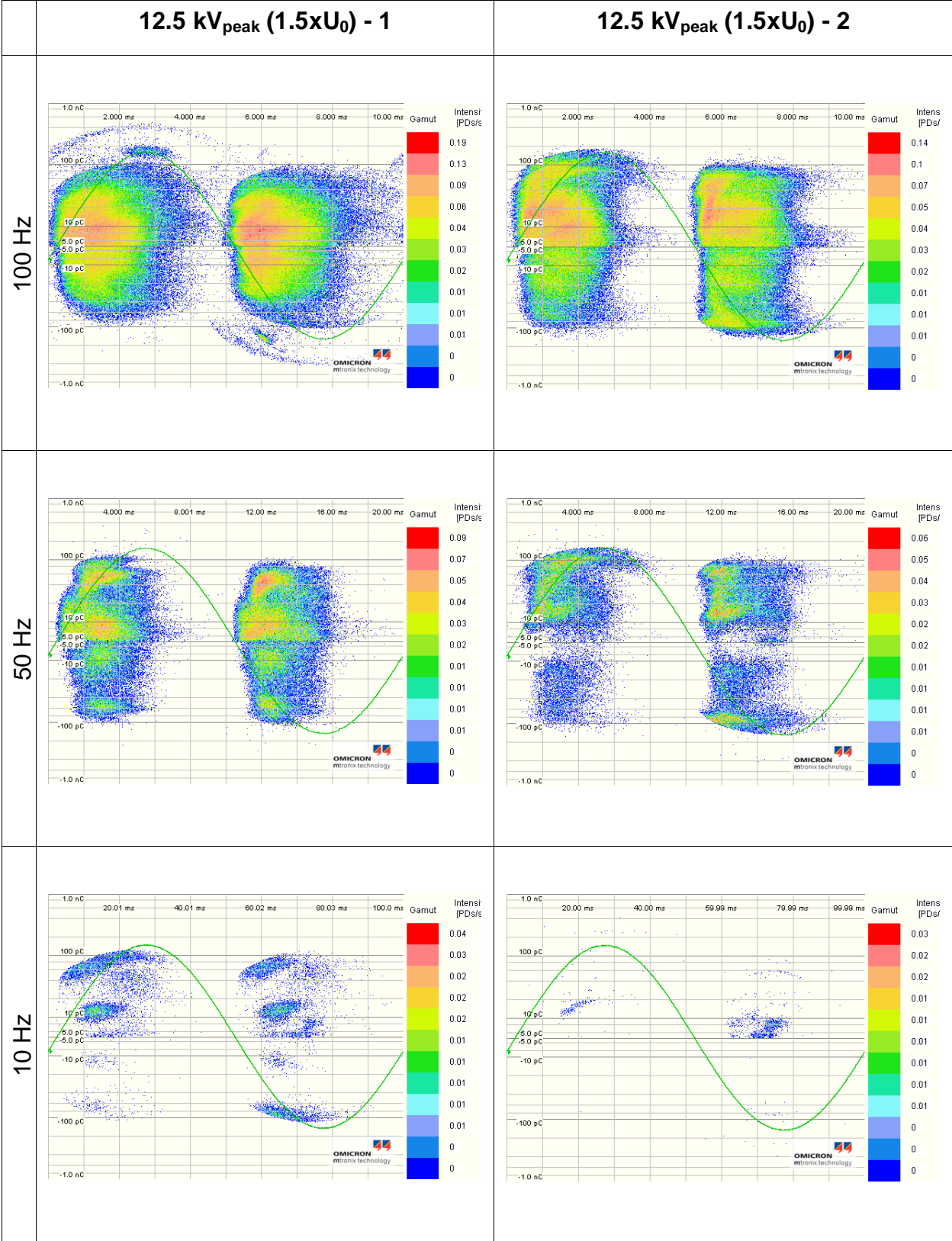


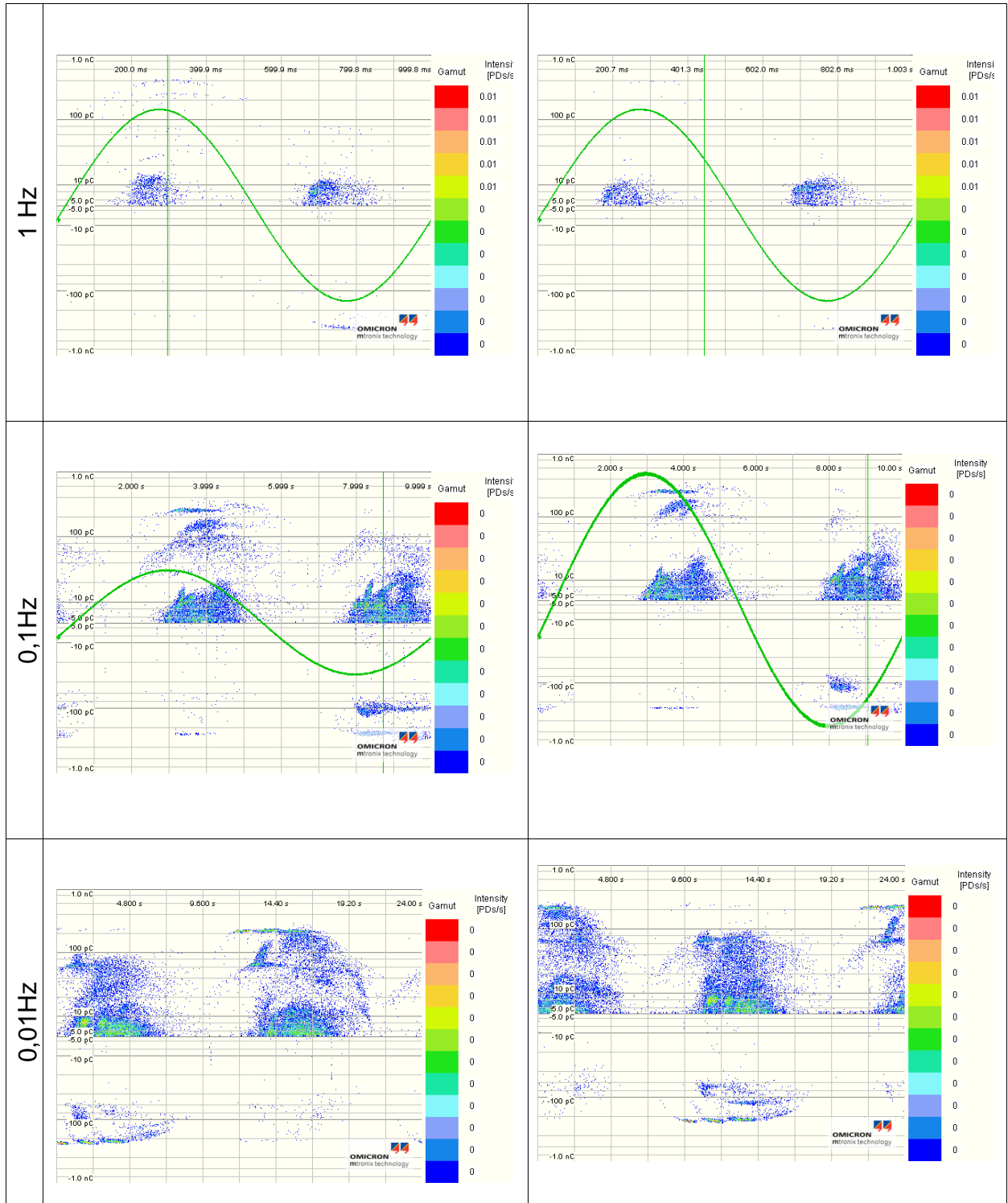
Joint #1 Aging: 256h / 14 cycles



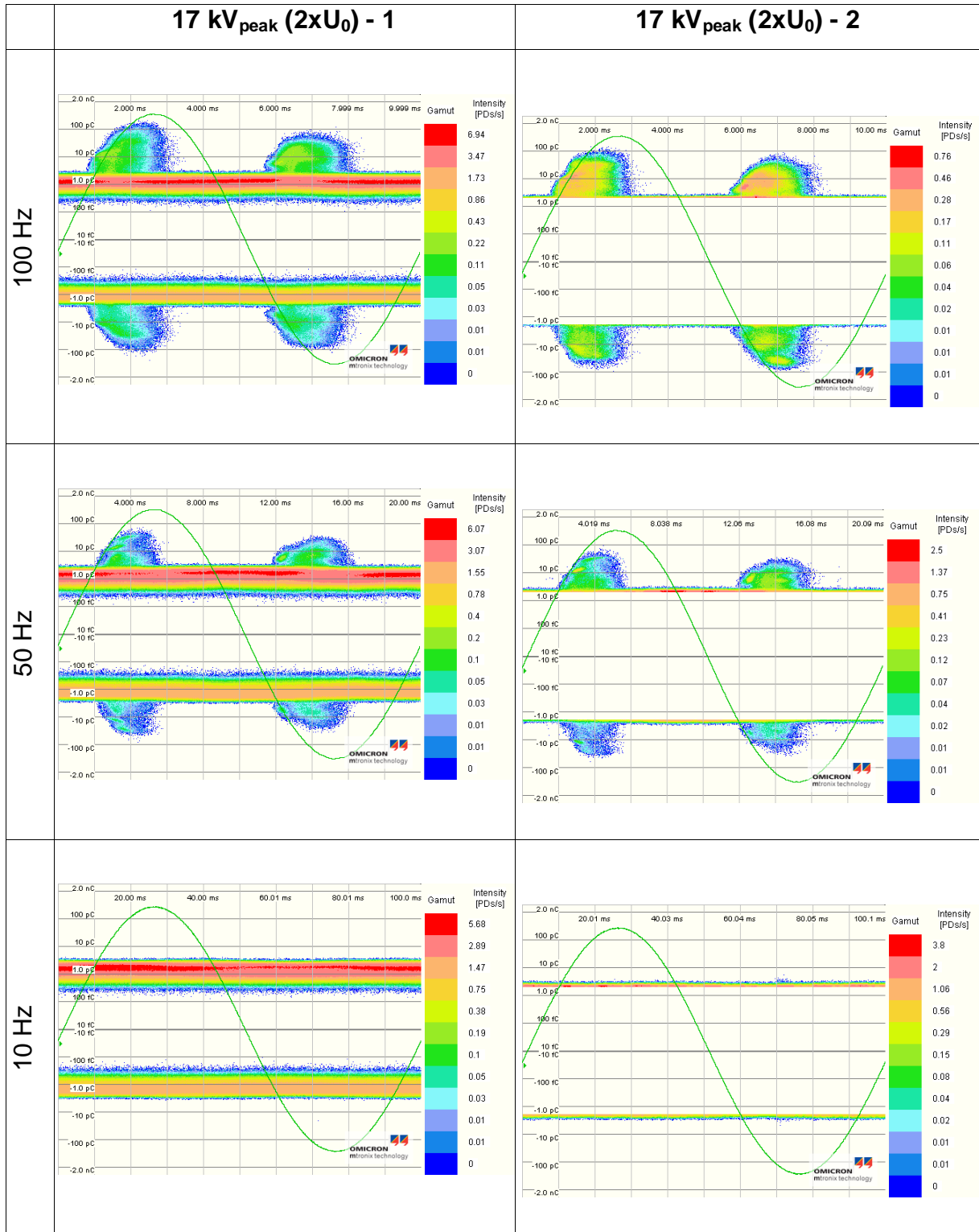


Joint #1 Aging: 256h / 14 cycles

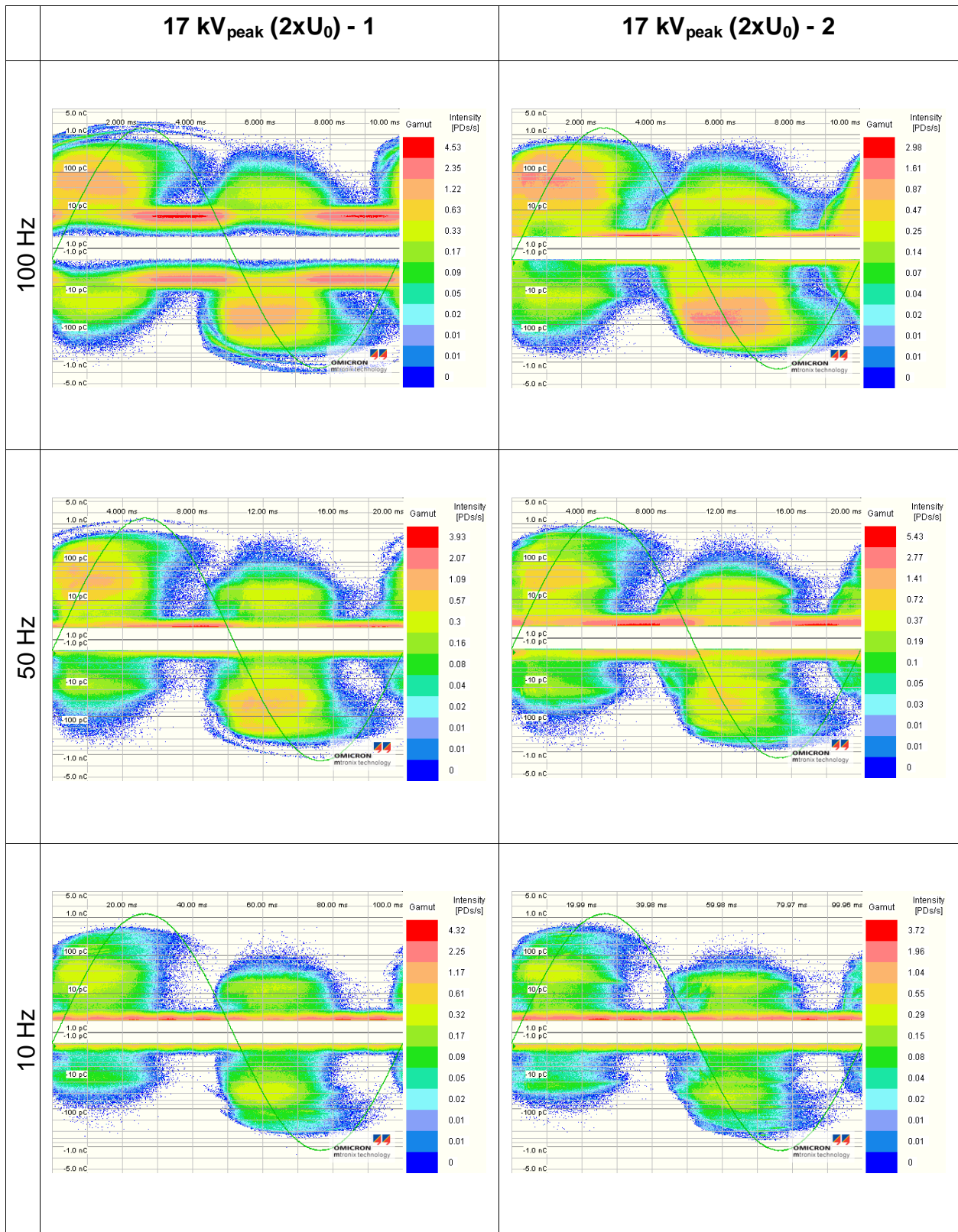


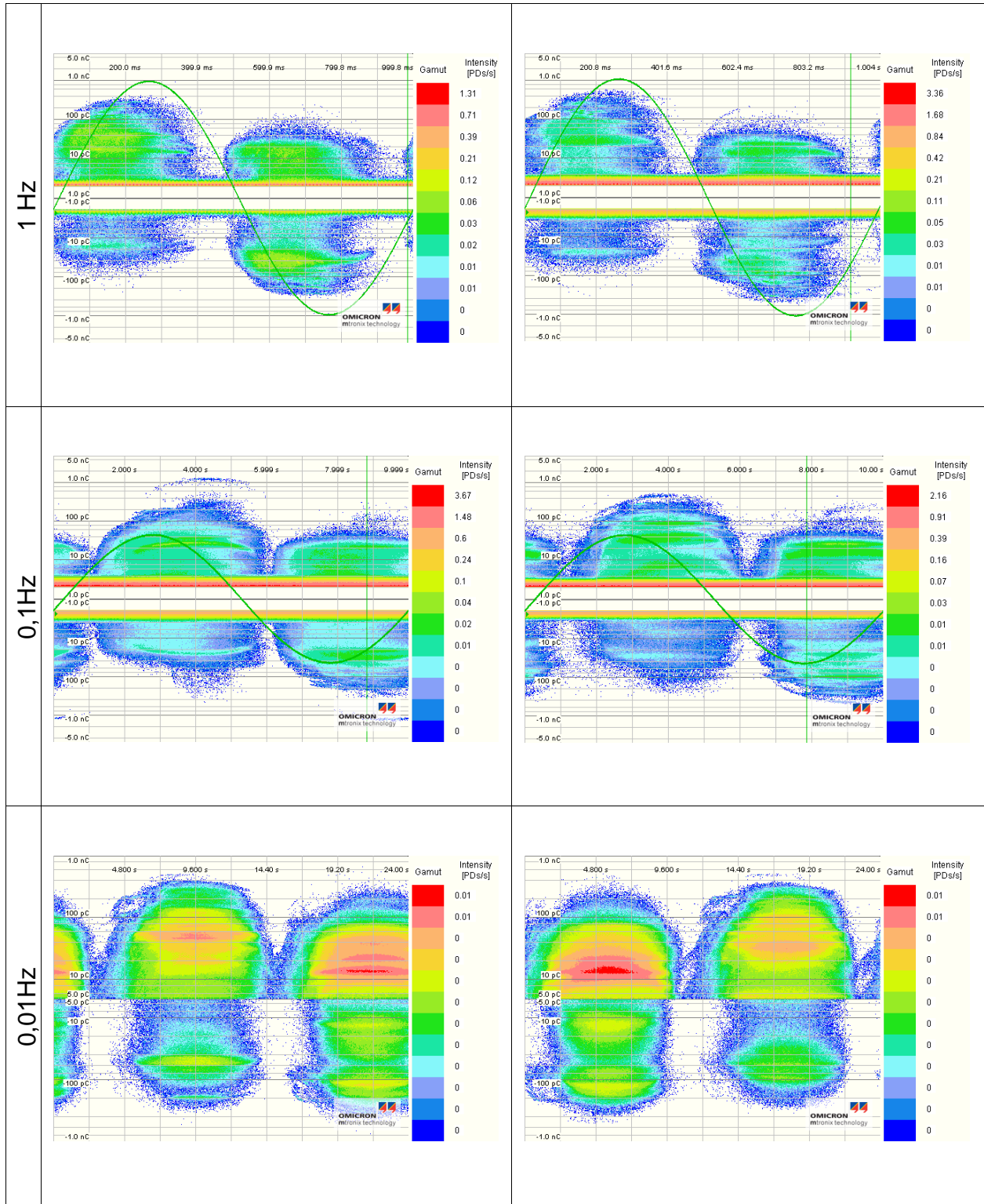


Joint #2 Aging: 136 h / 10 cycles

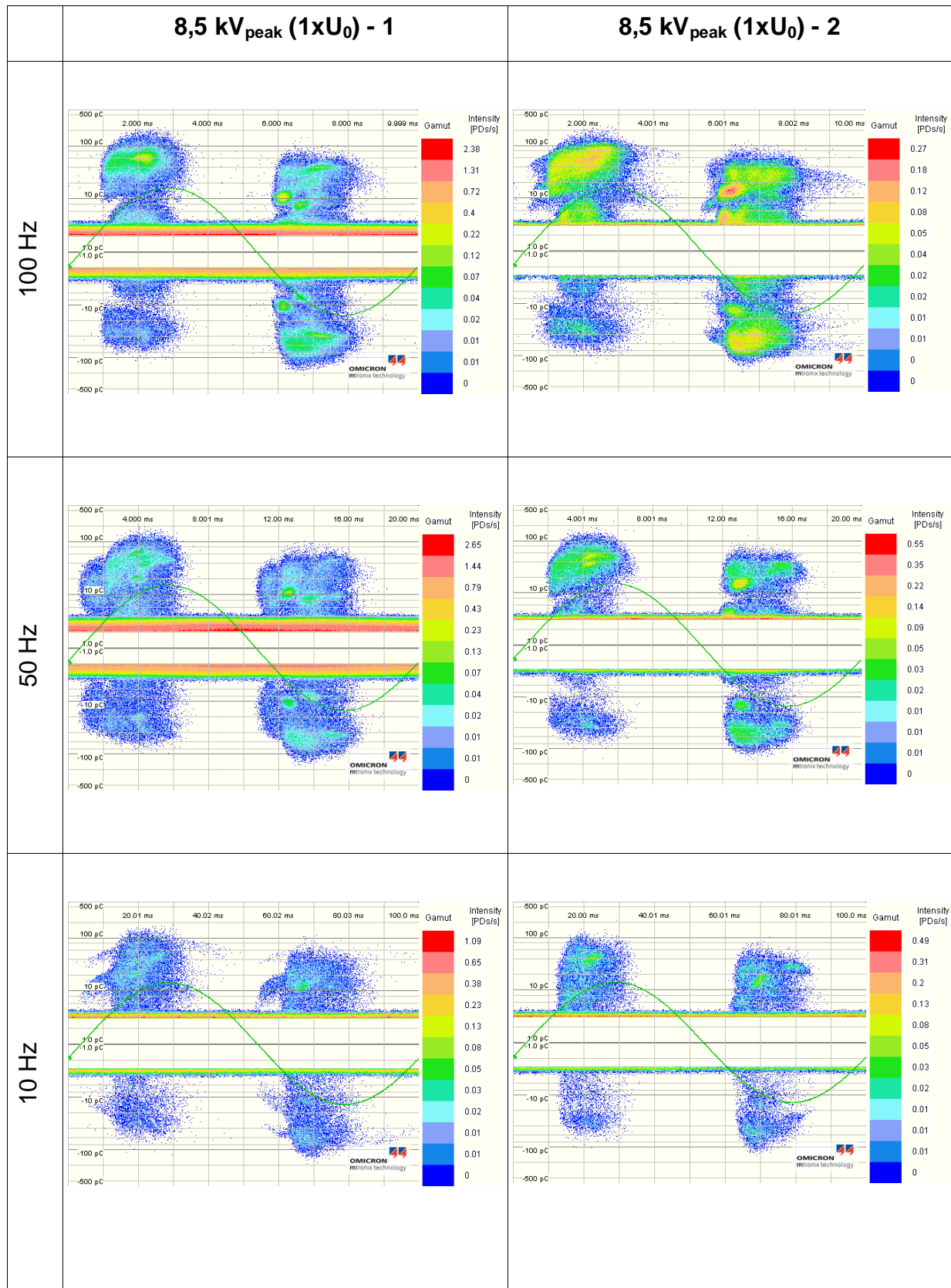


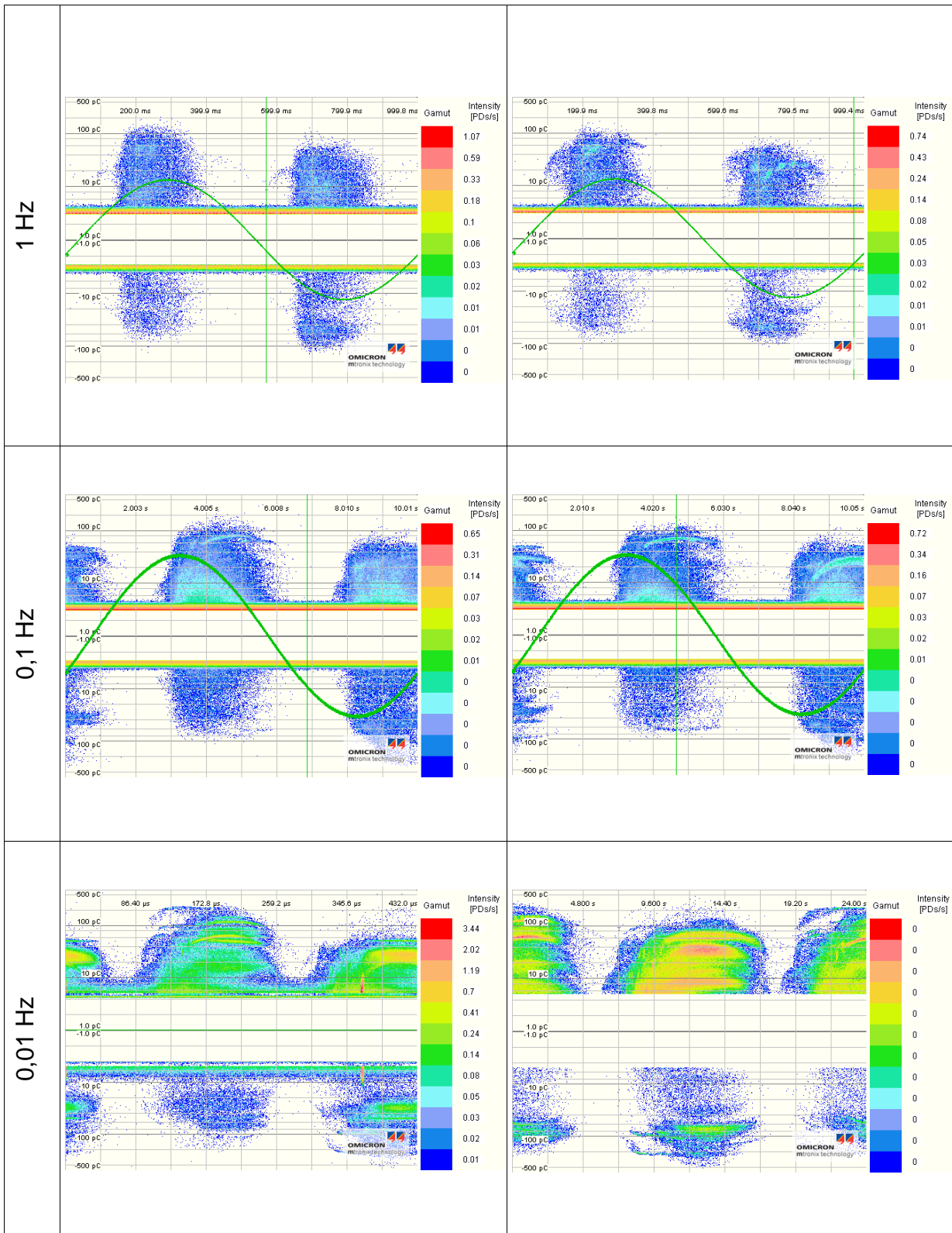
Joint #2 Aging: 256h / 14 cycles



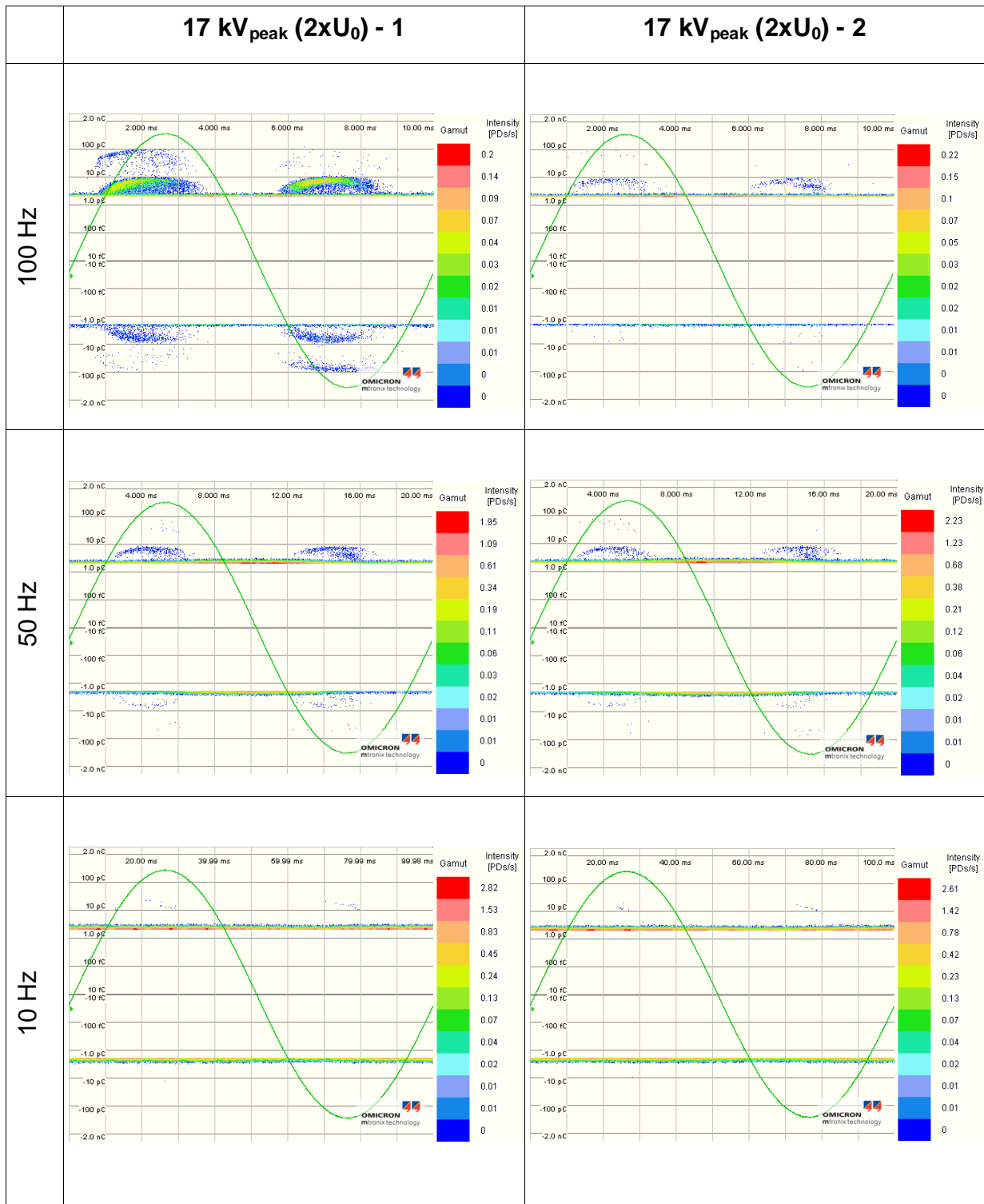


Joint #2 Aging: 256 h / 14 cycles

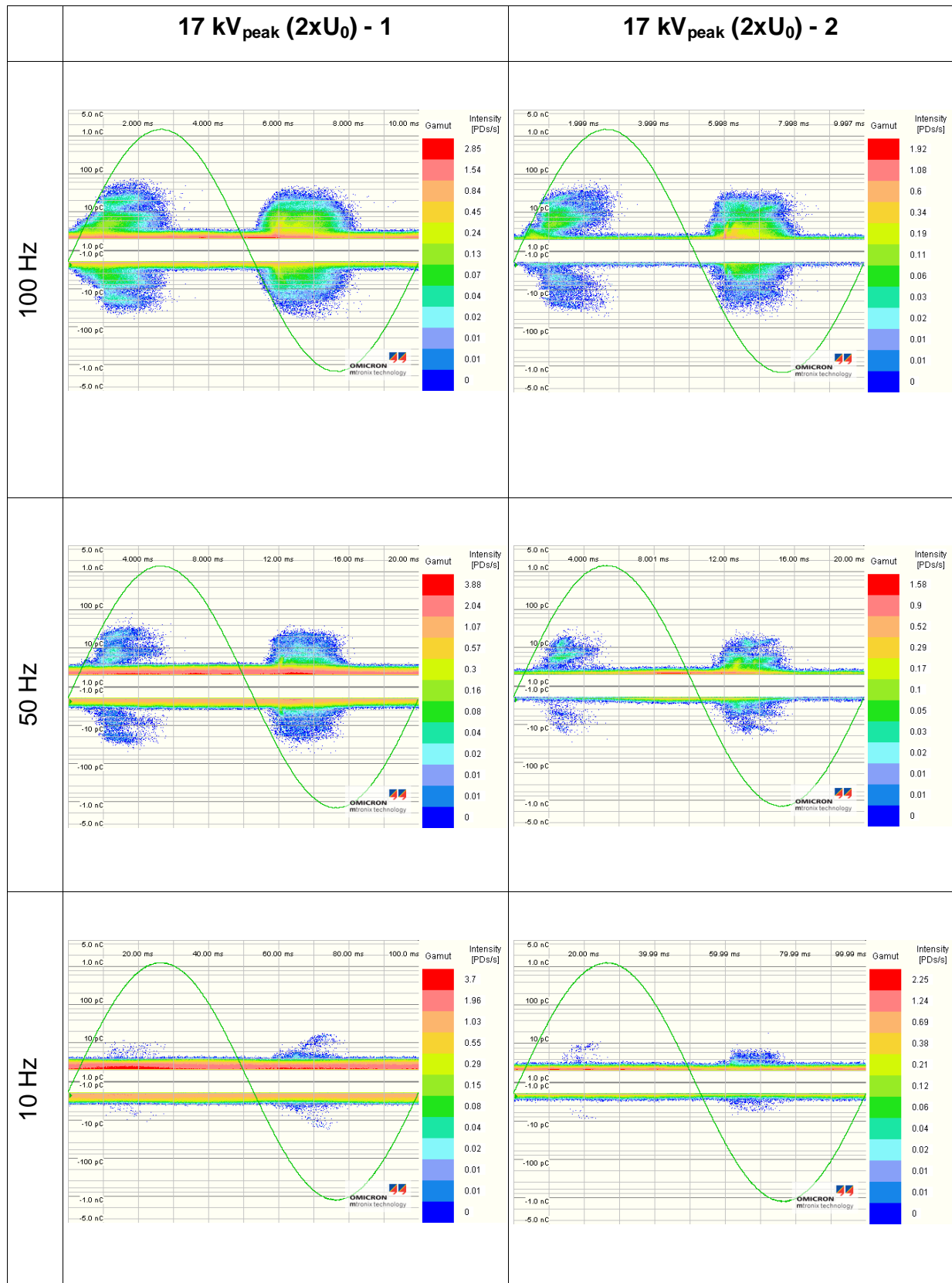


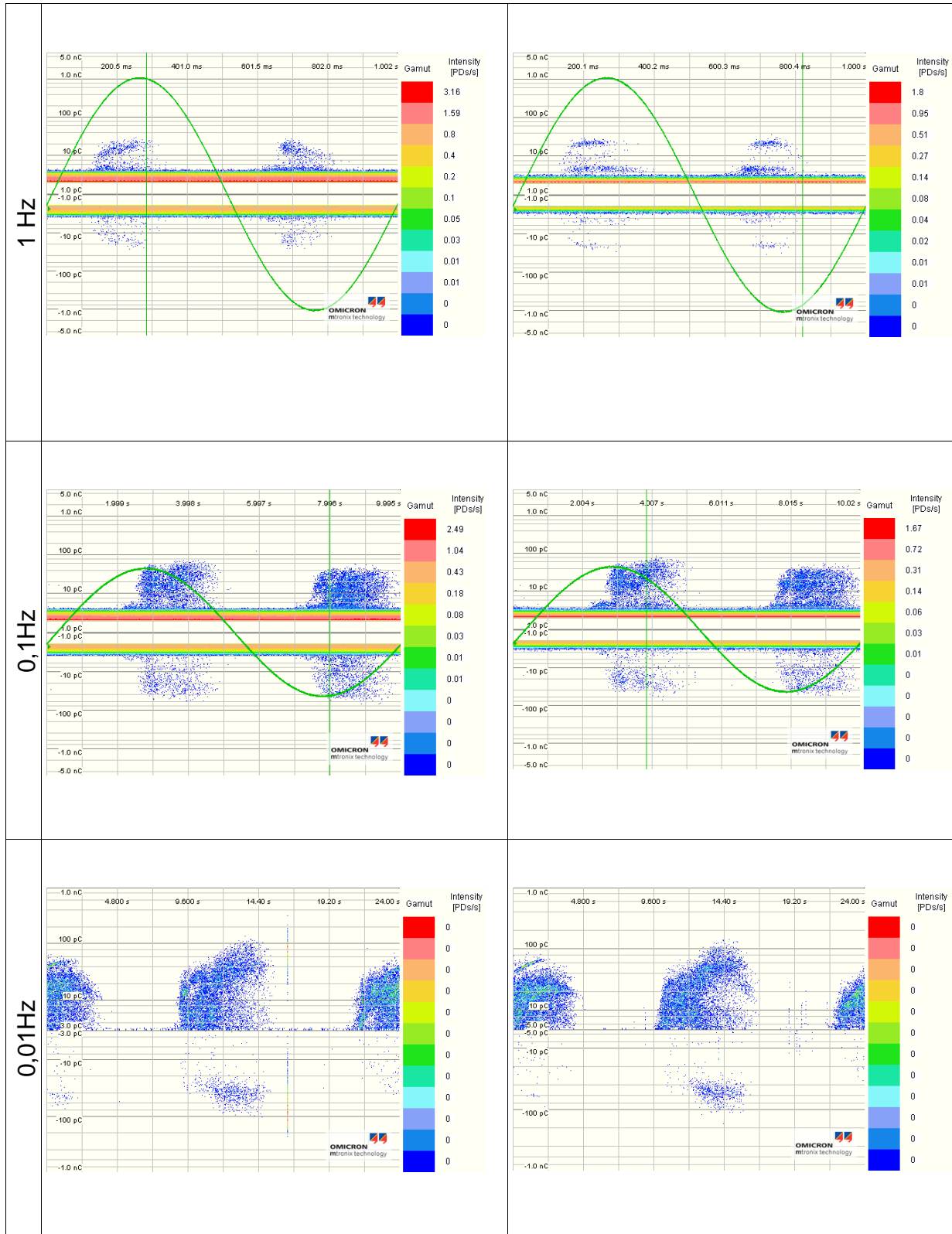


Joint #3 Aging: 136 h / 10 cycles

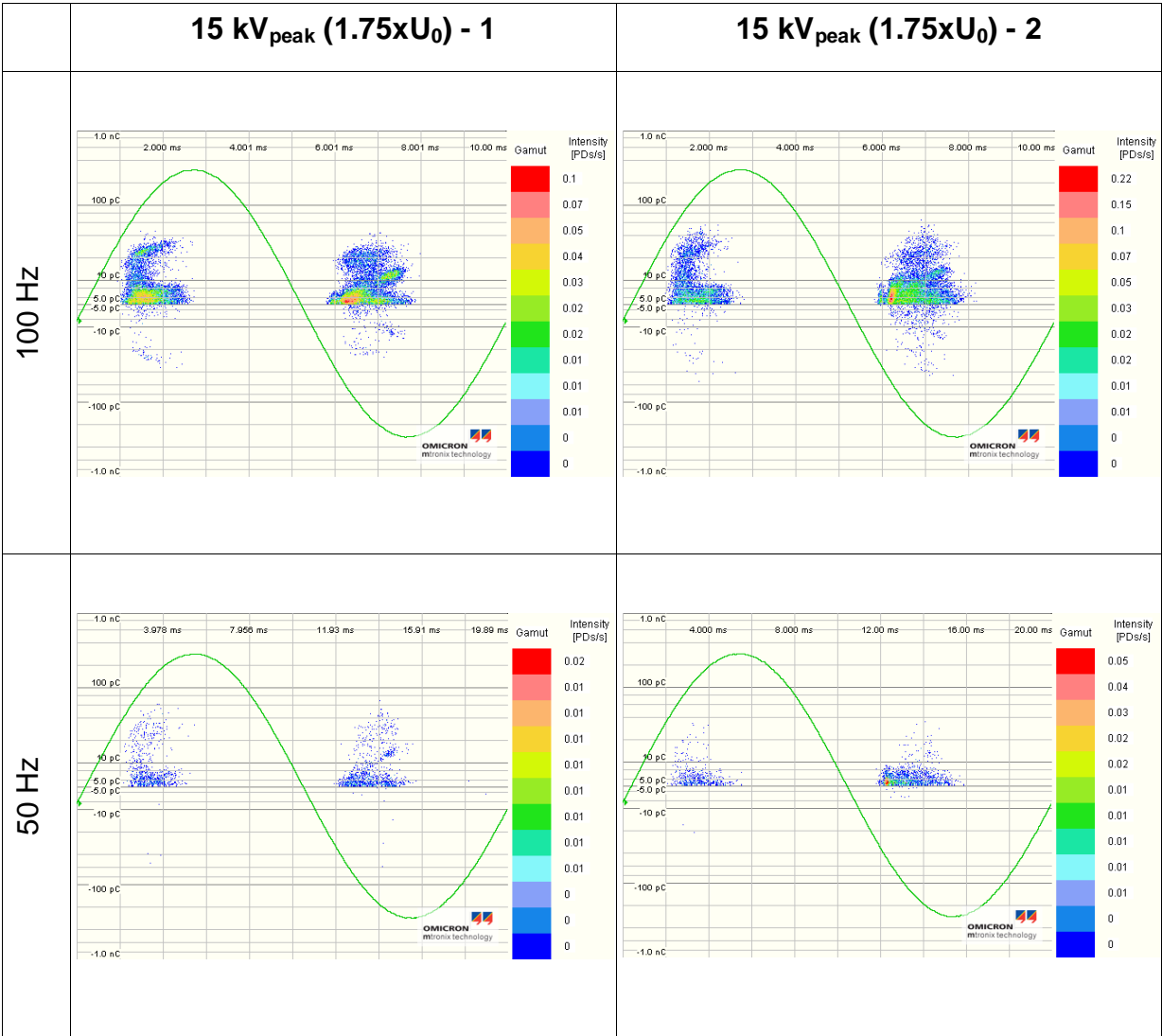


Joint #3 Aging: 256h / 14 cycles





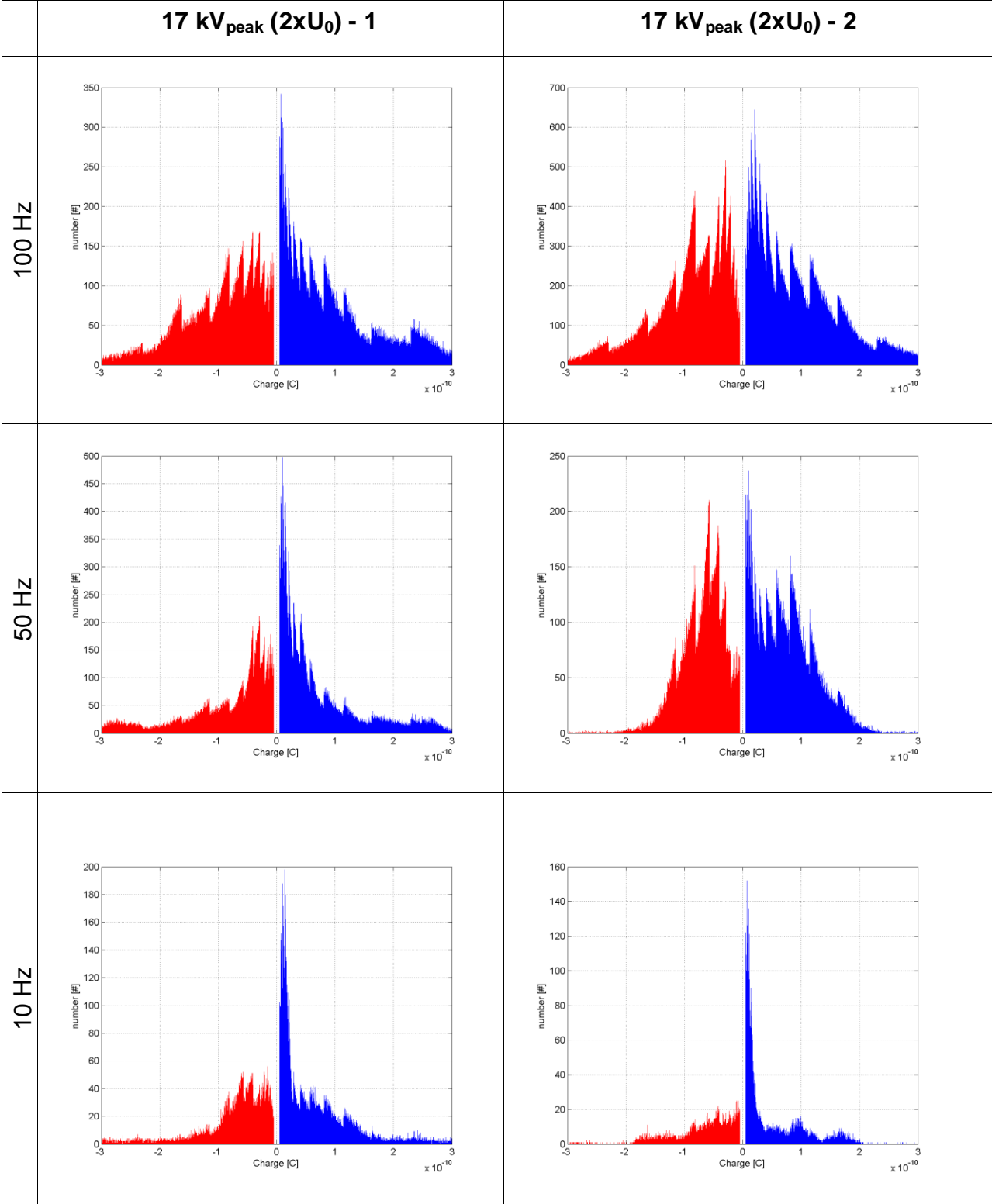
Joint #3 Aging: 256h / 14 cycles

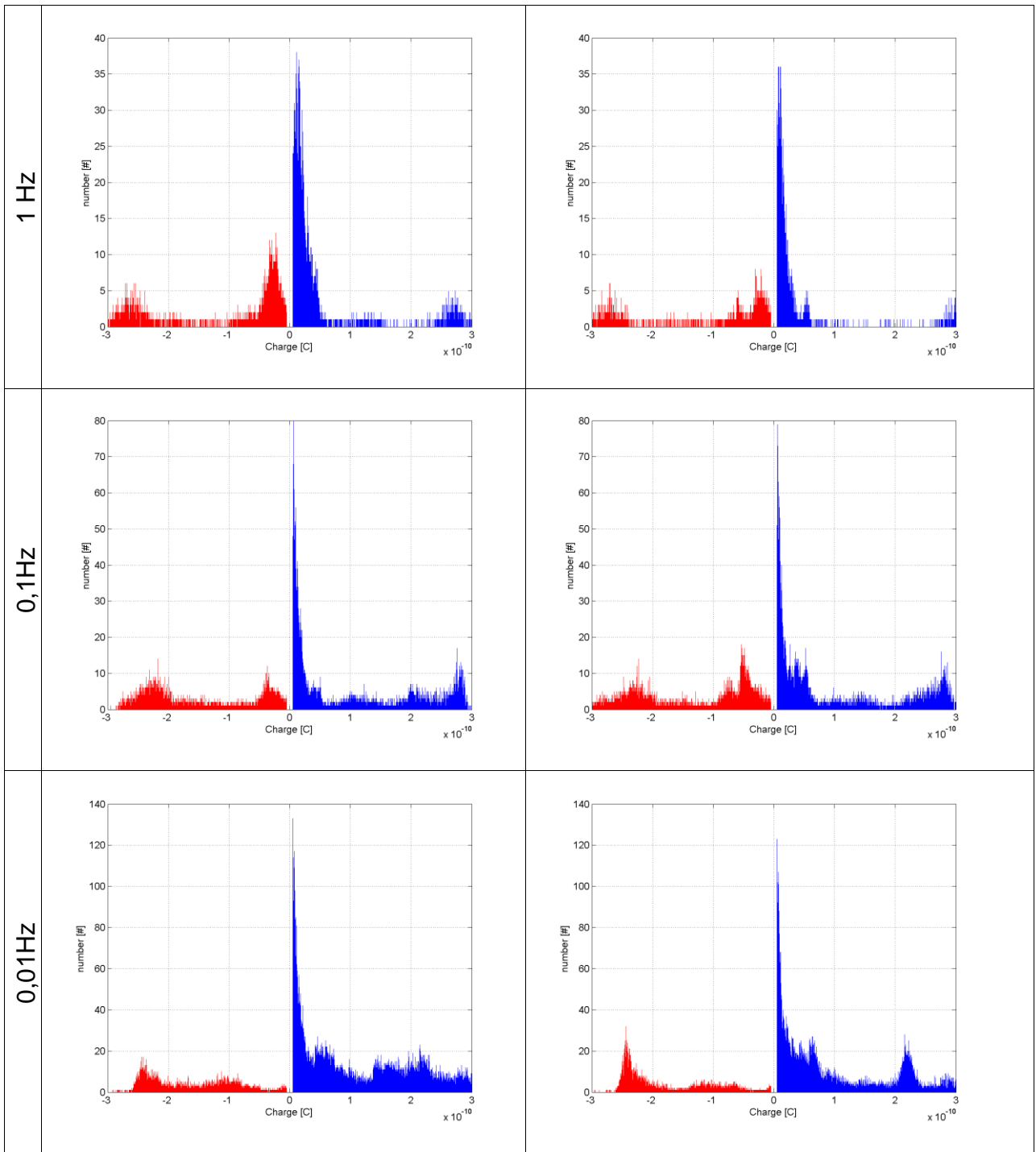


D. Histogram plots

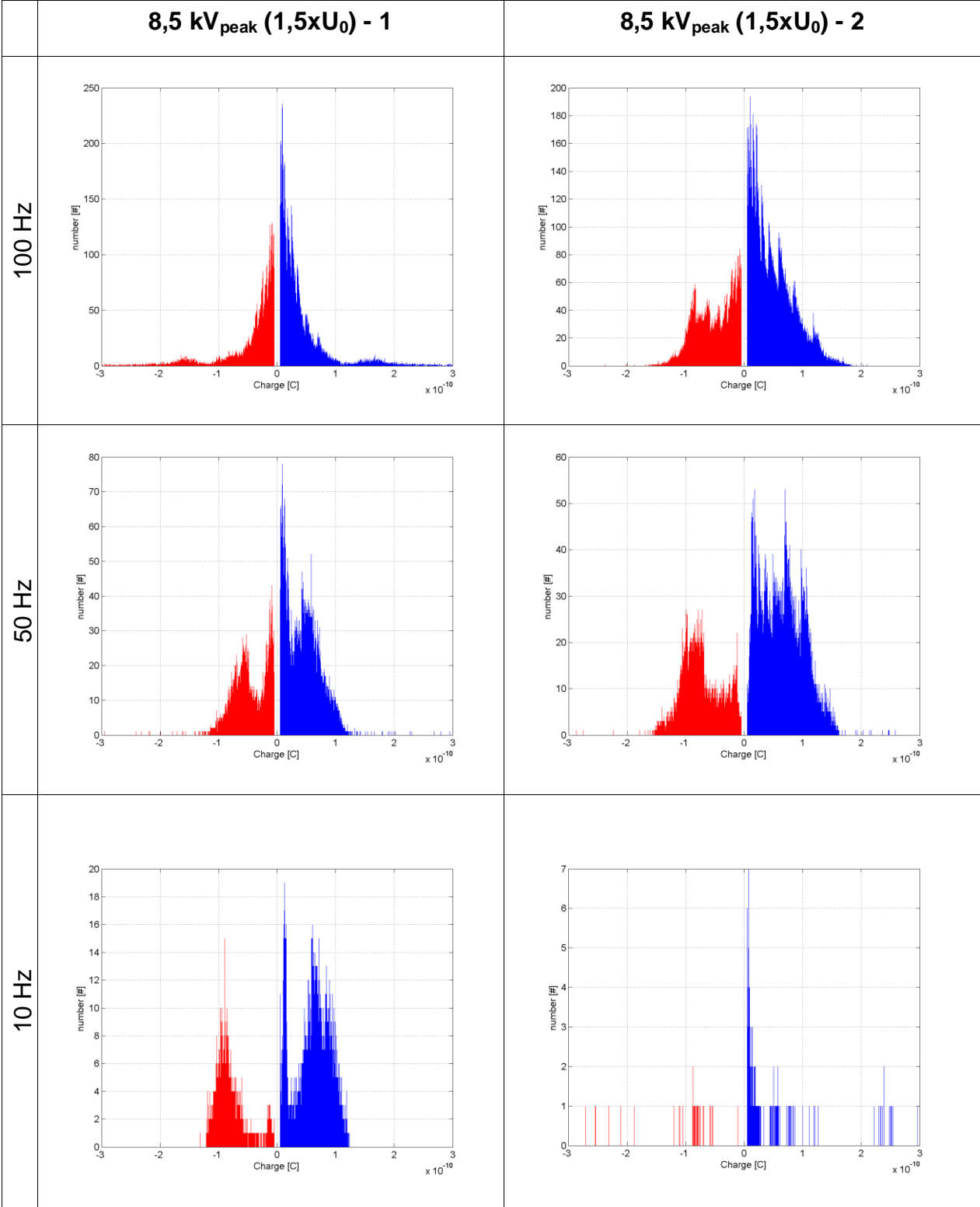
The following pages contain histogram plots from all PD measurements performed on the test objects. All measurements were performed twice.

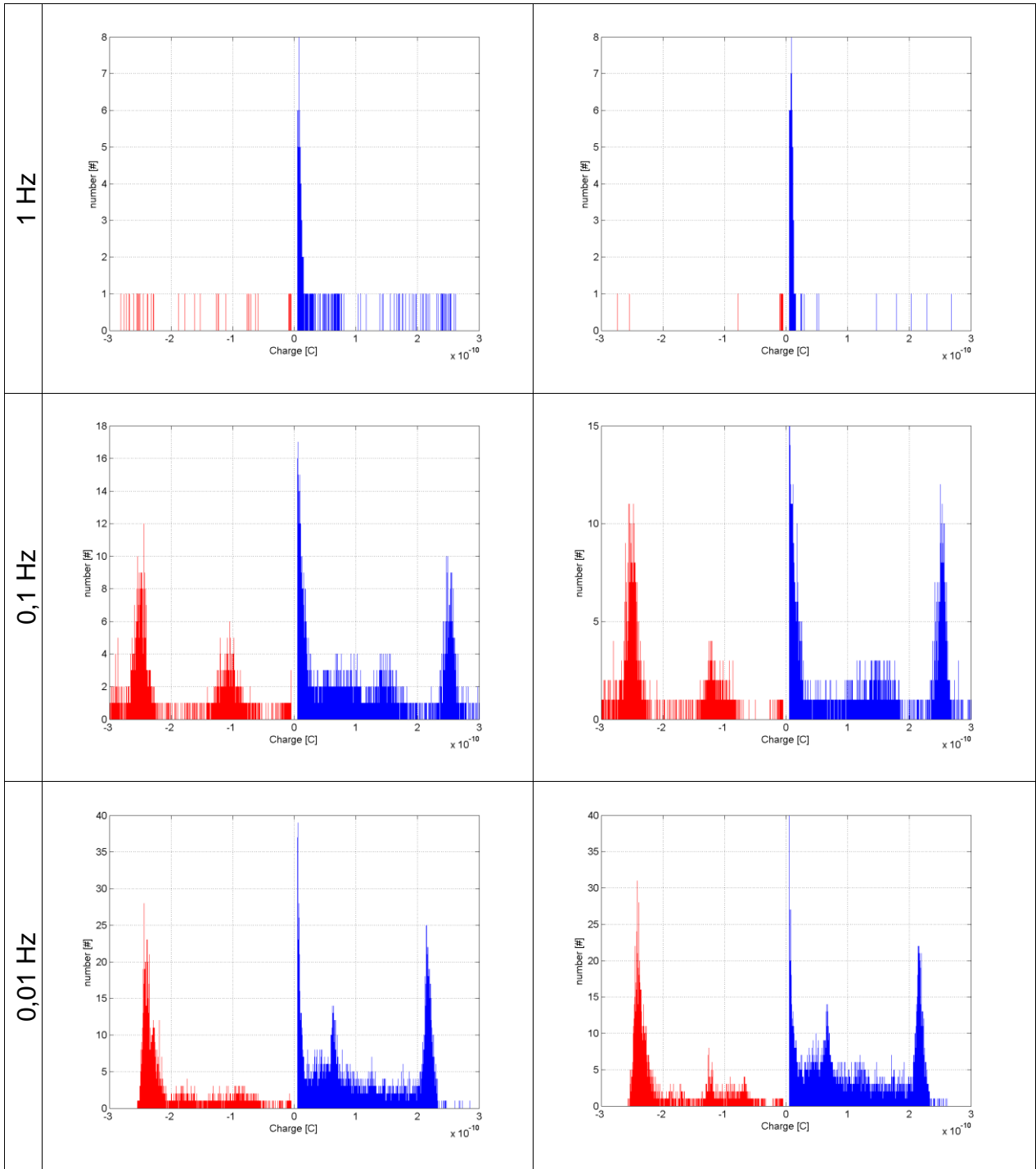
Joint #1 Aging: 256h / 14 cycles



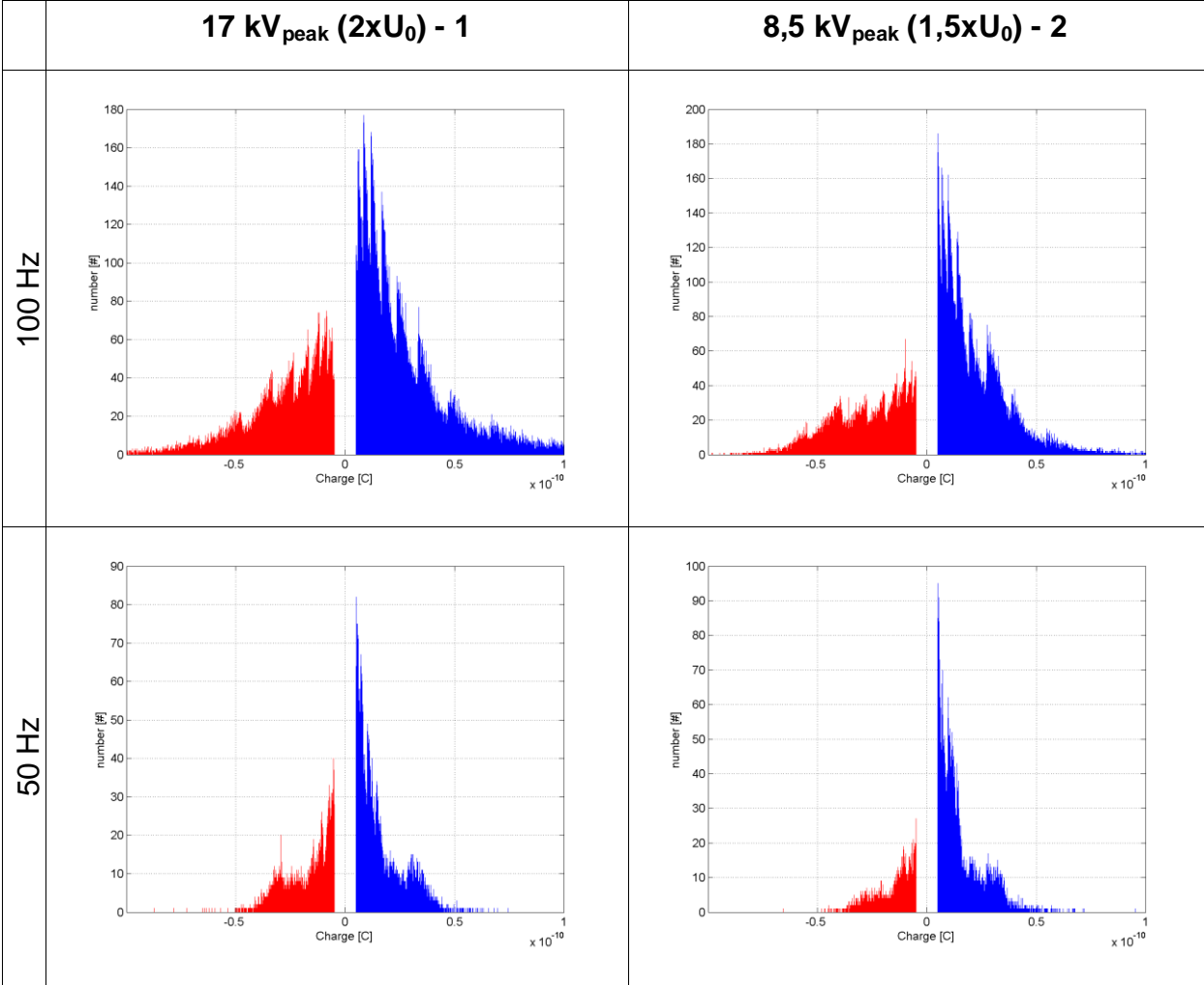


Joint #1 Aging: 256h / 14 cycles

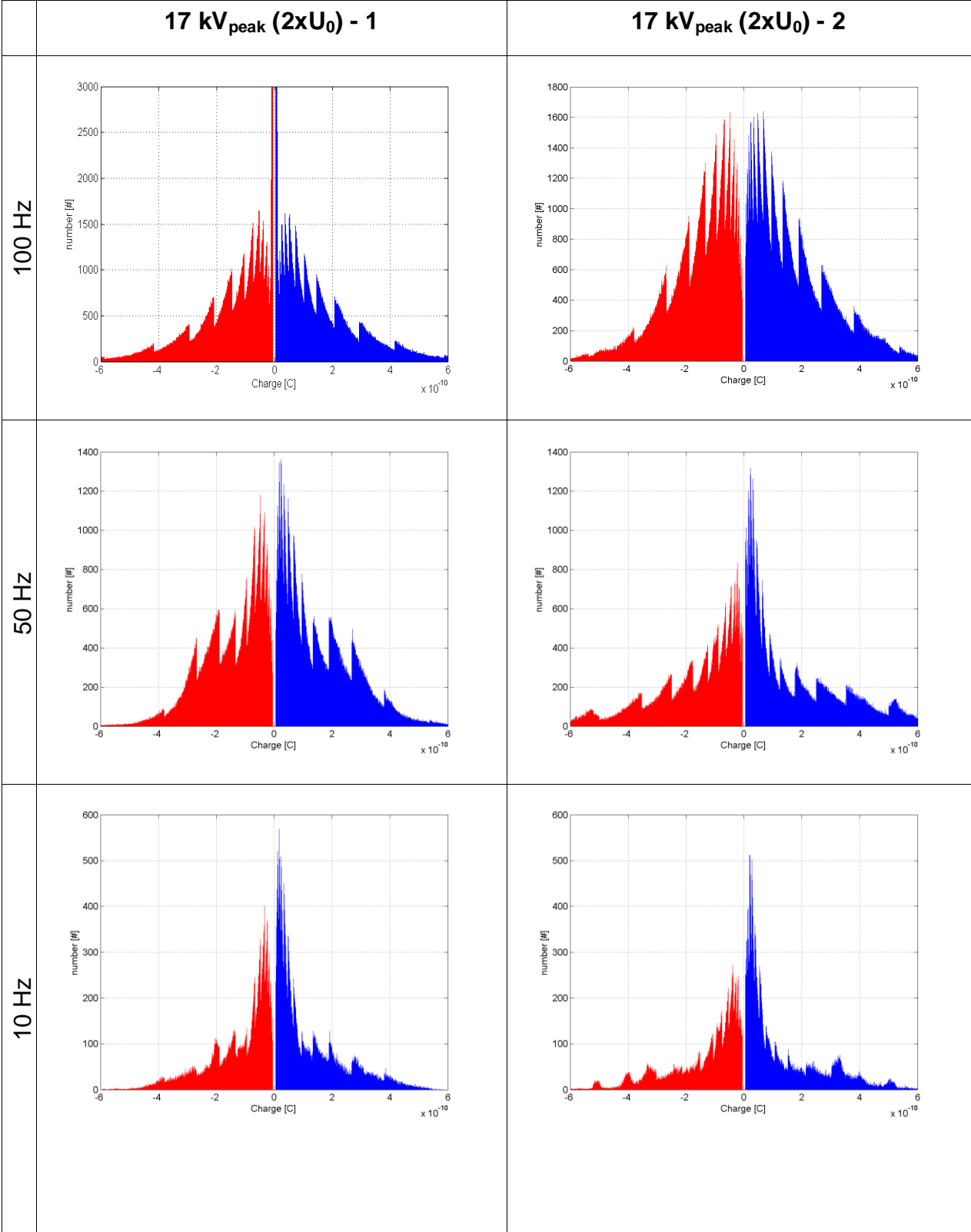


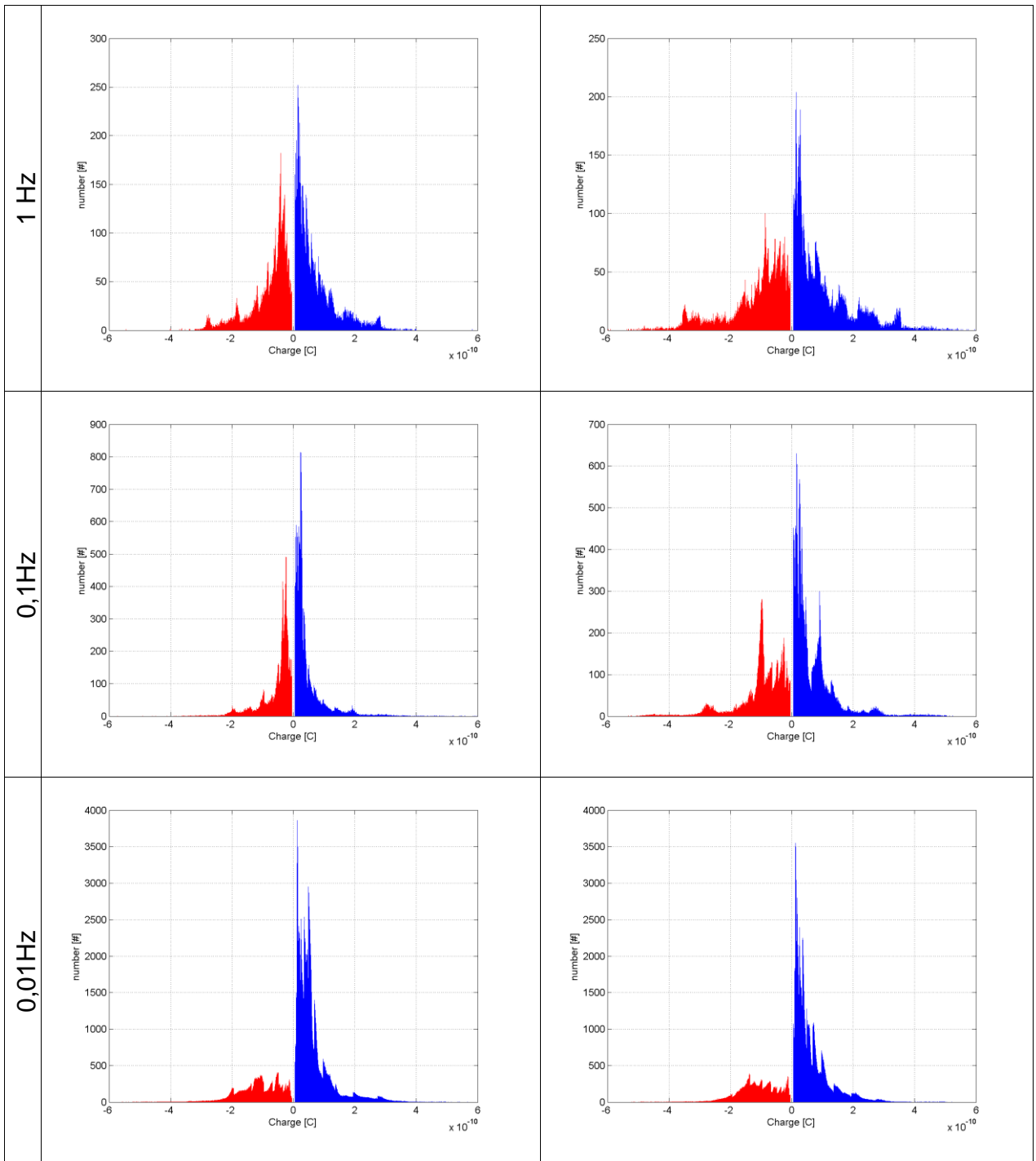


Joint #2 Aging: 136 h / 10 cycles.

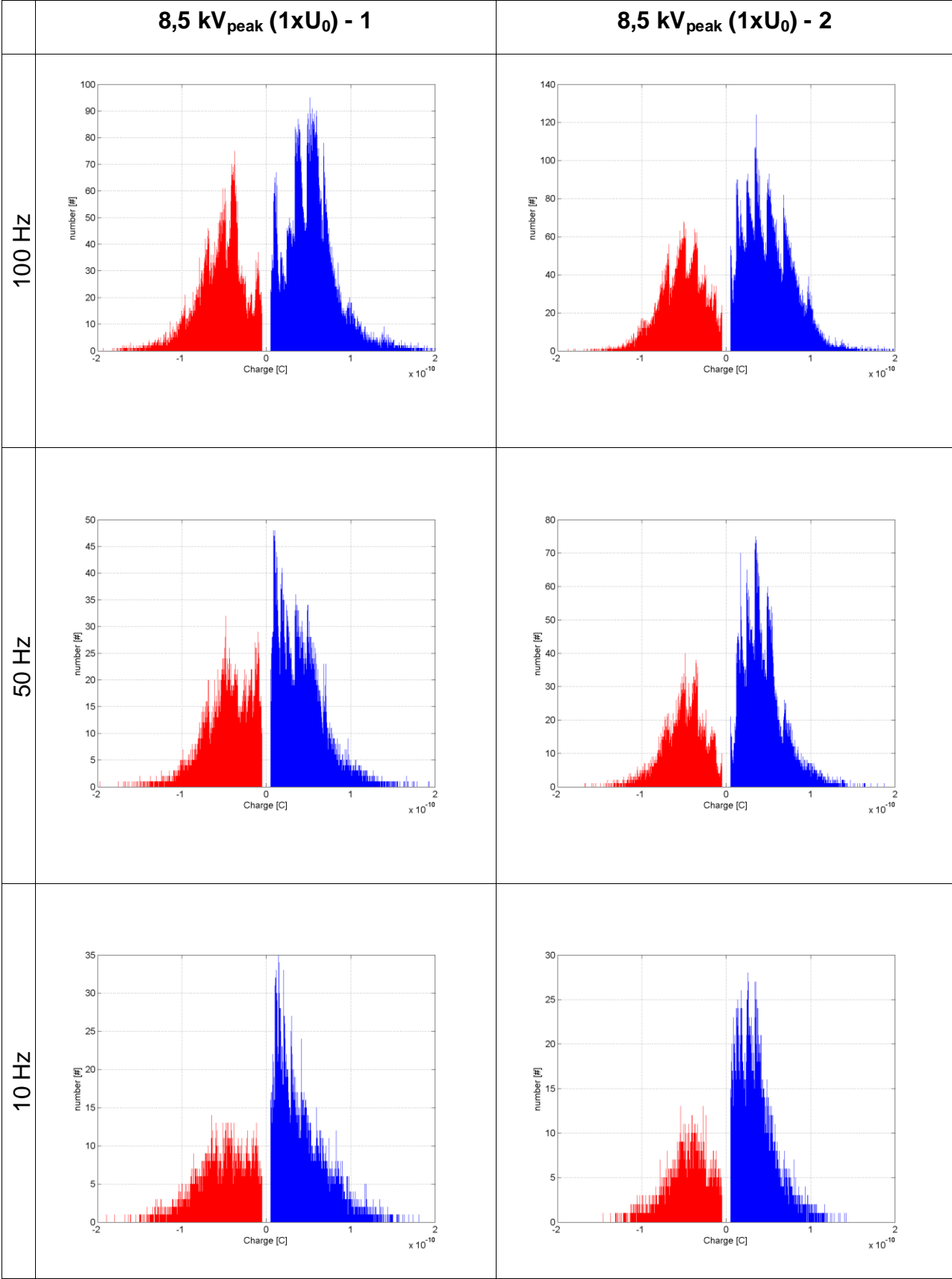


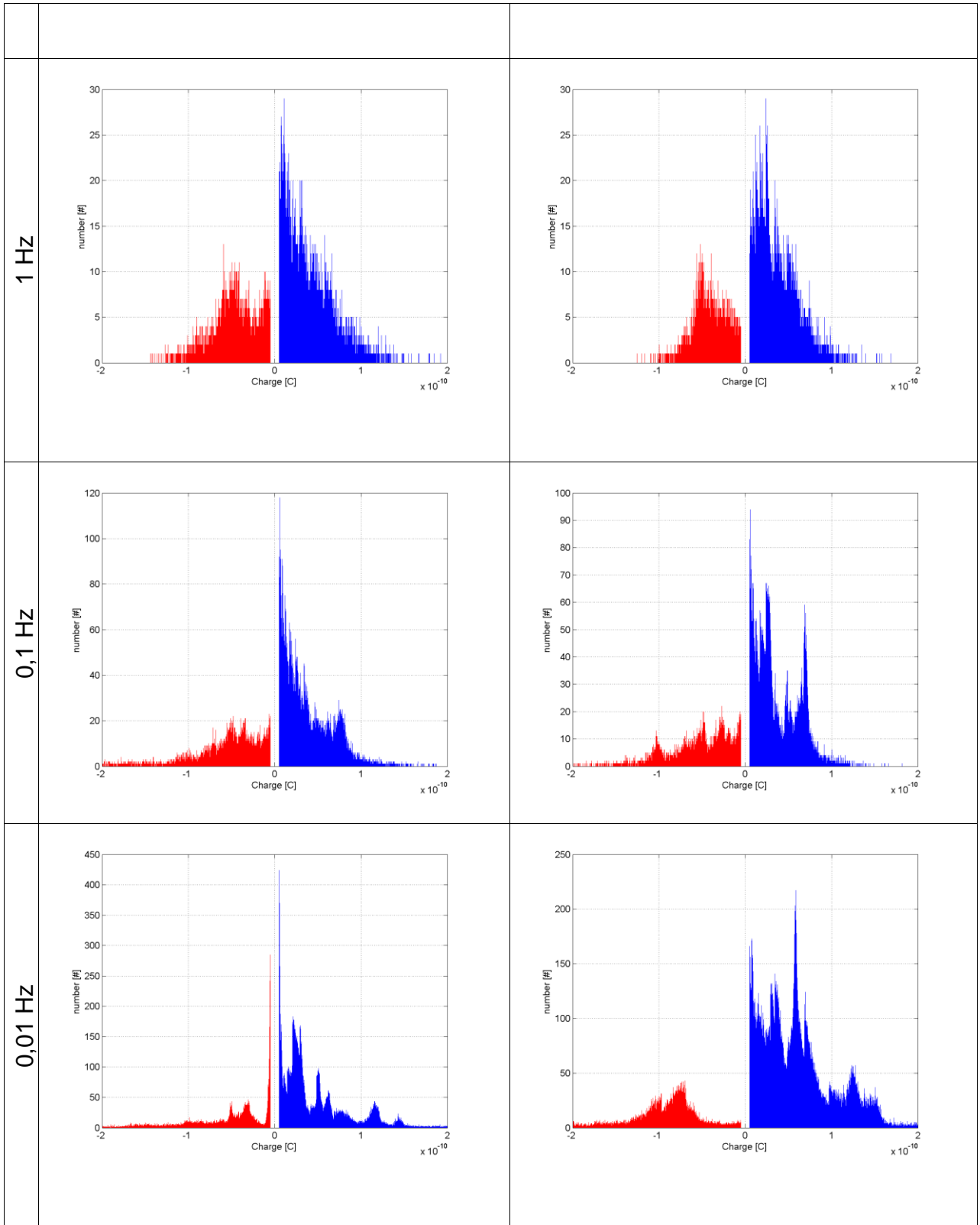
Joint #2 Aging: 256h / 14 cycles



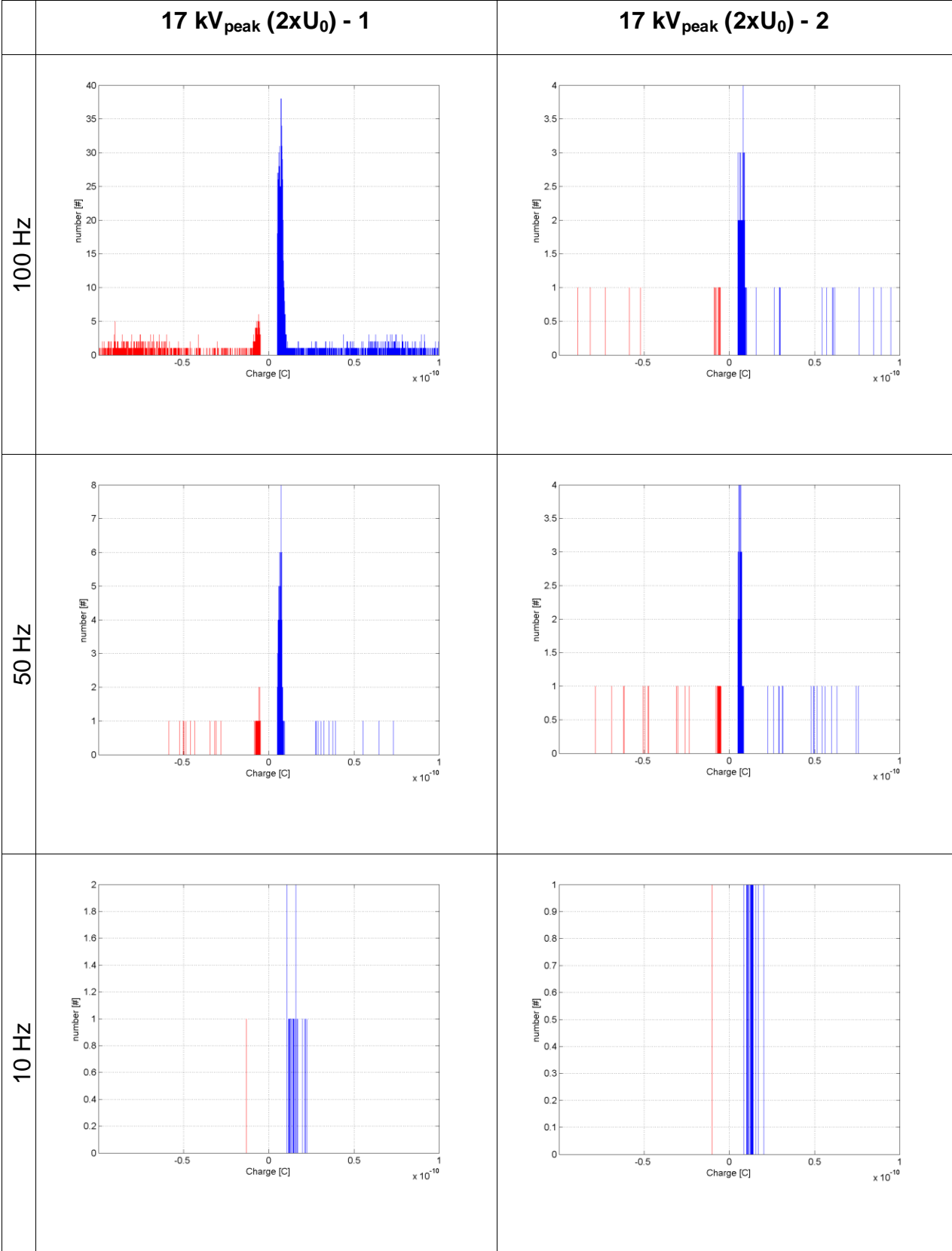


Joint #2 Aging: 256 h / 14 cycles

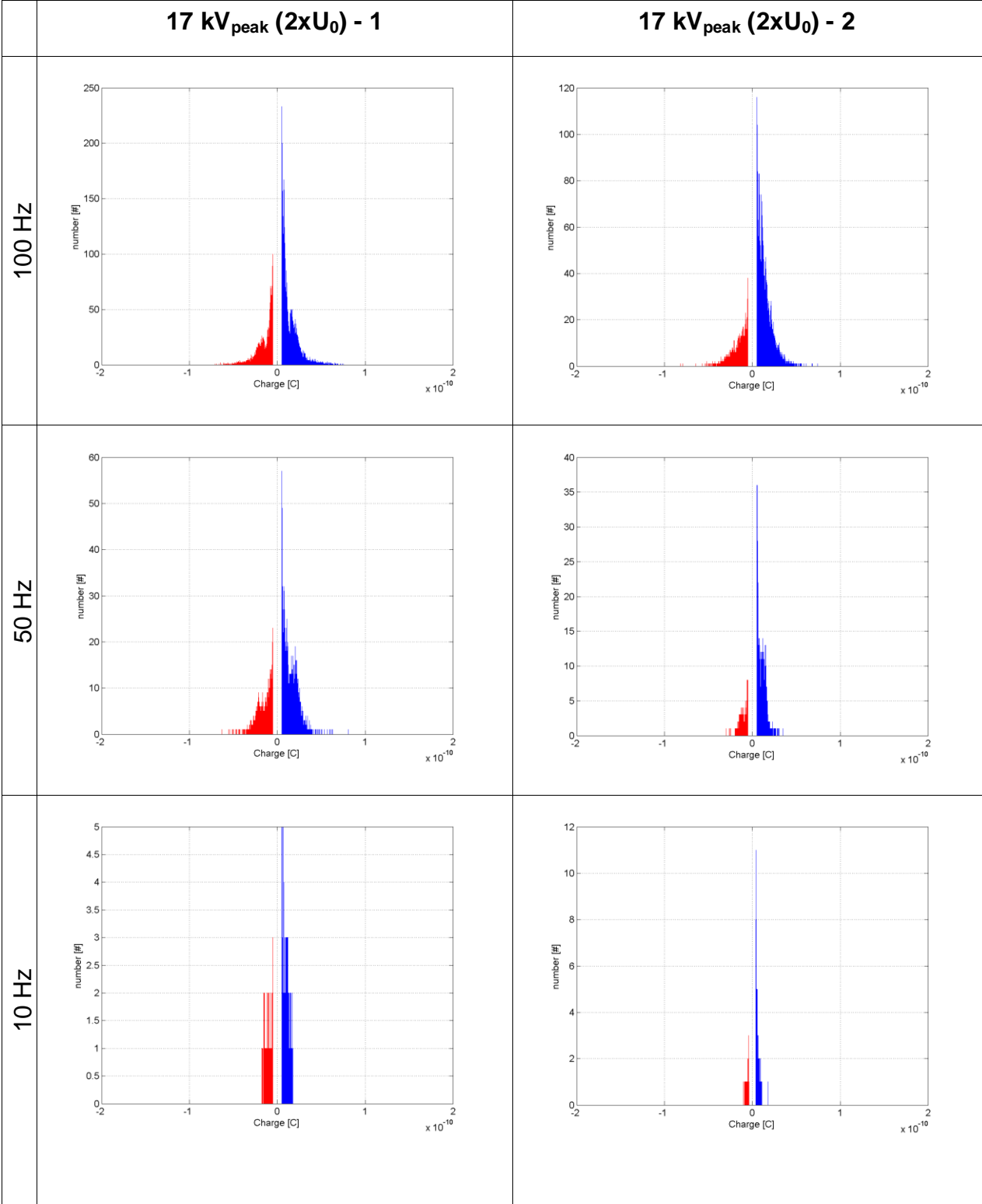


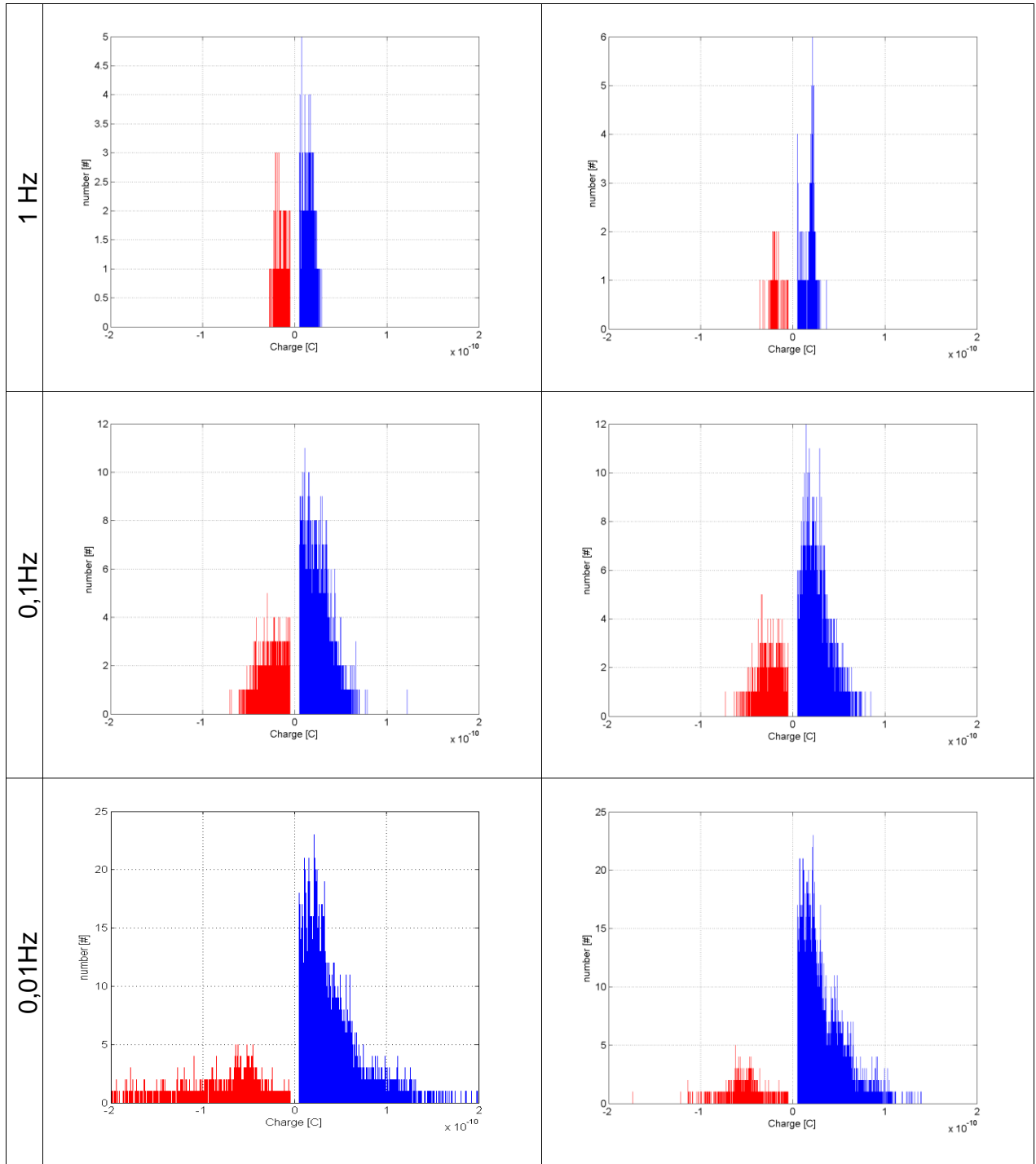


Joint #3 Aging: 136 h / 10 cycles

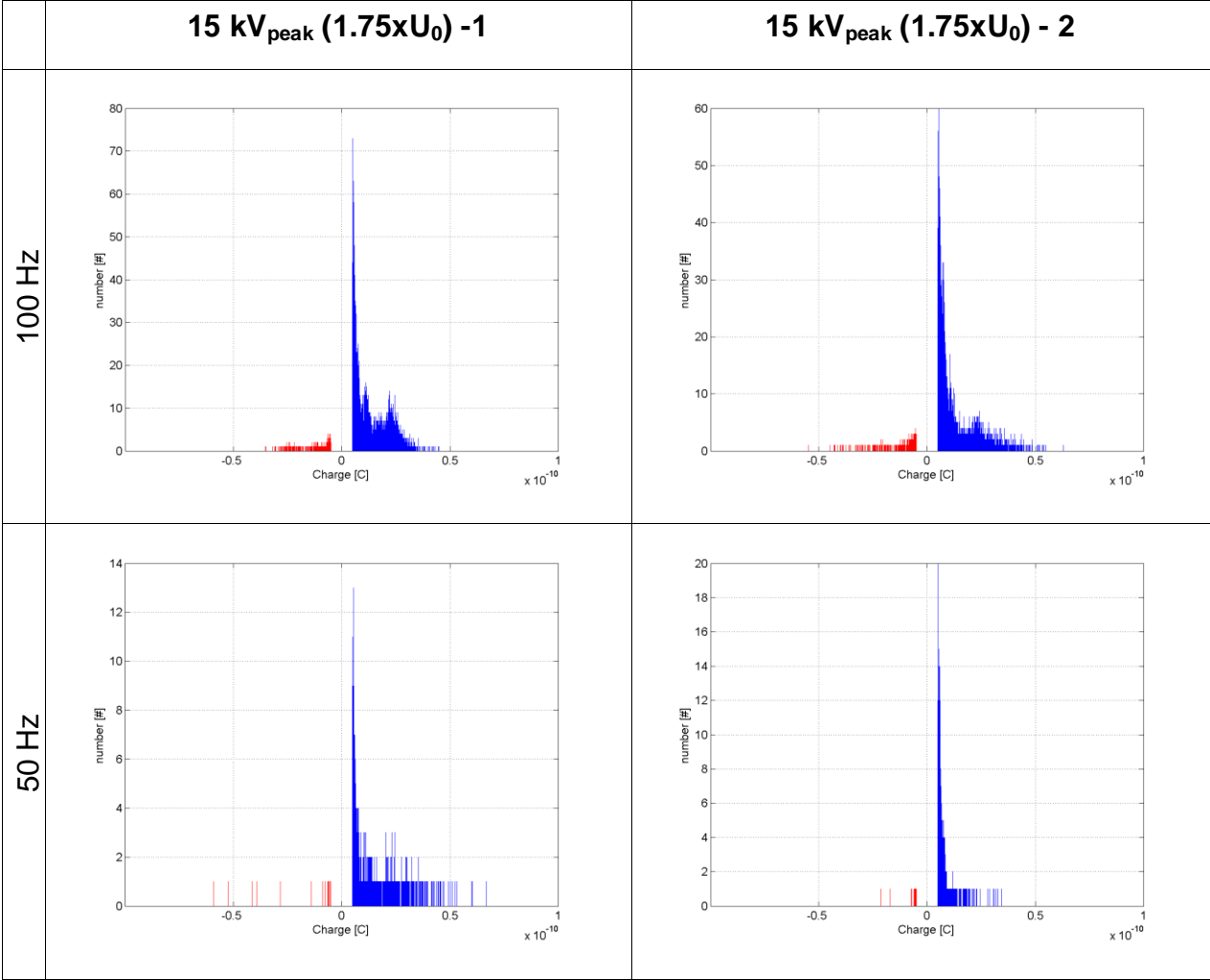


Joint # 3 Aging: 256h / 14 cycles.





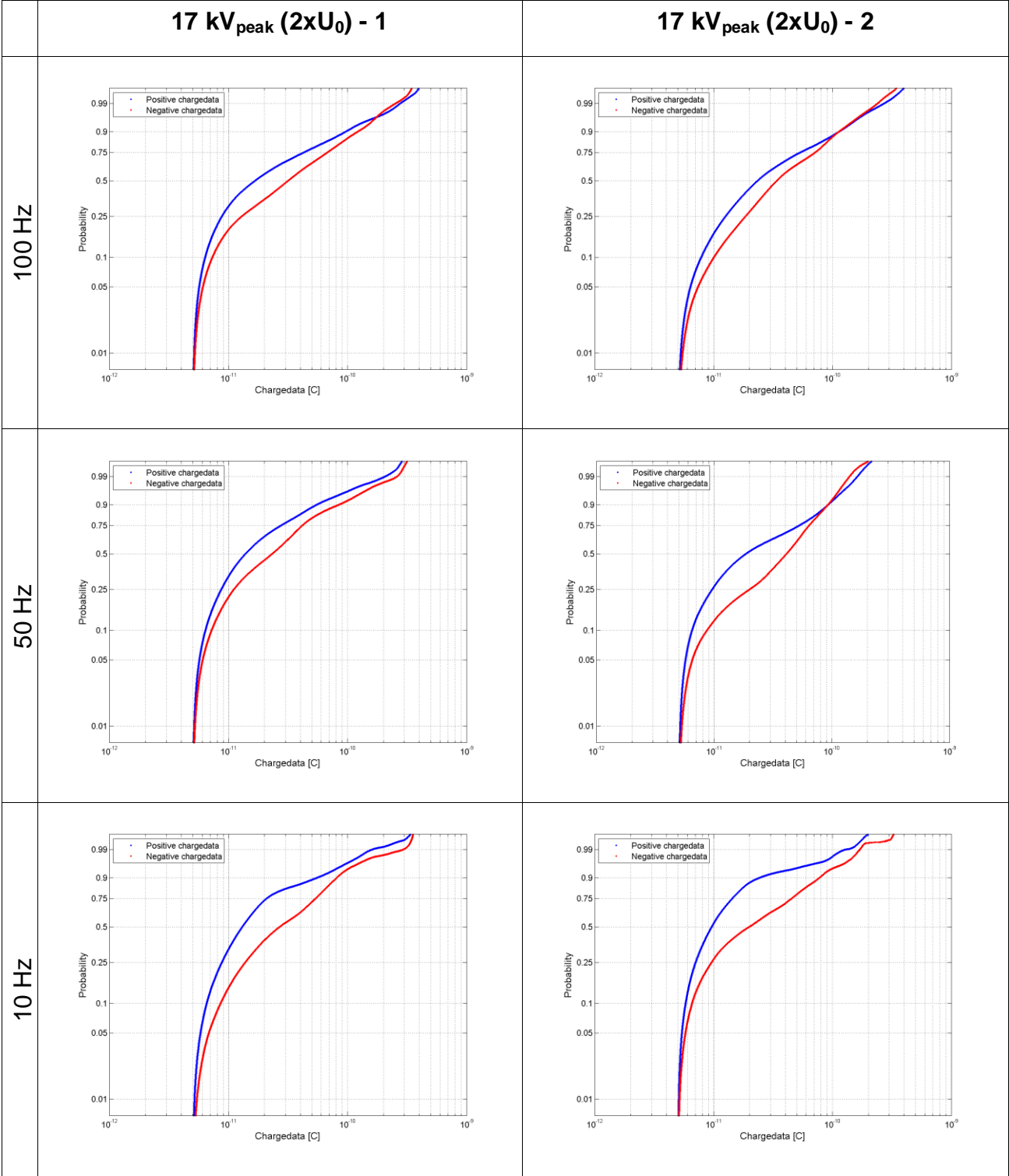
Joint #3 Aging: 256h / 14 cycles.

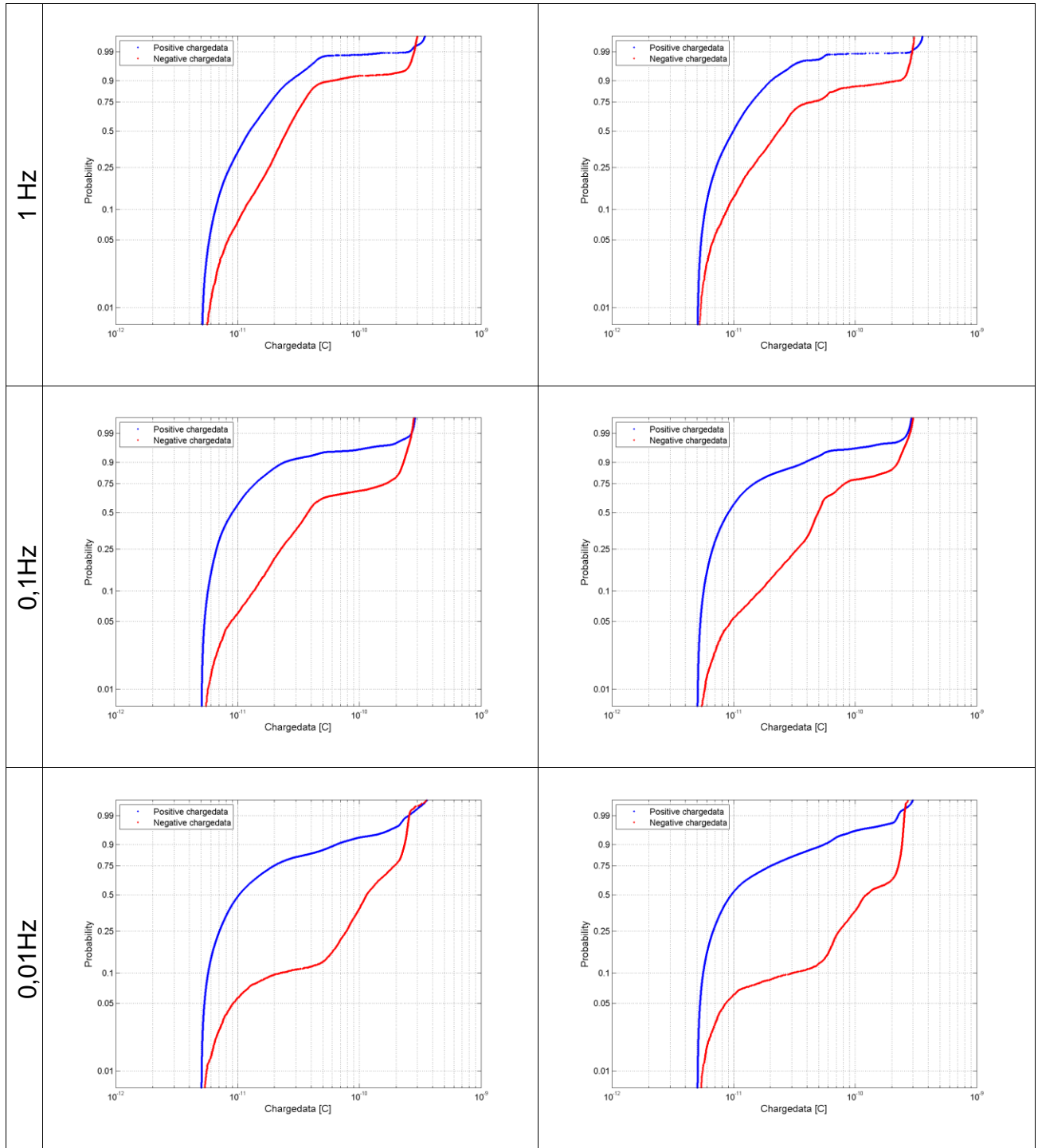


E. Weibull plots

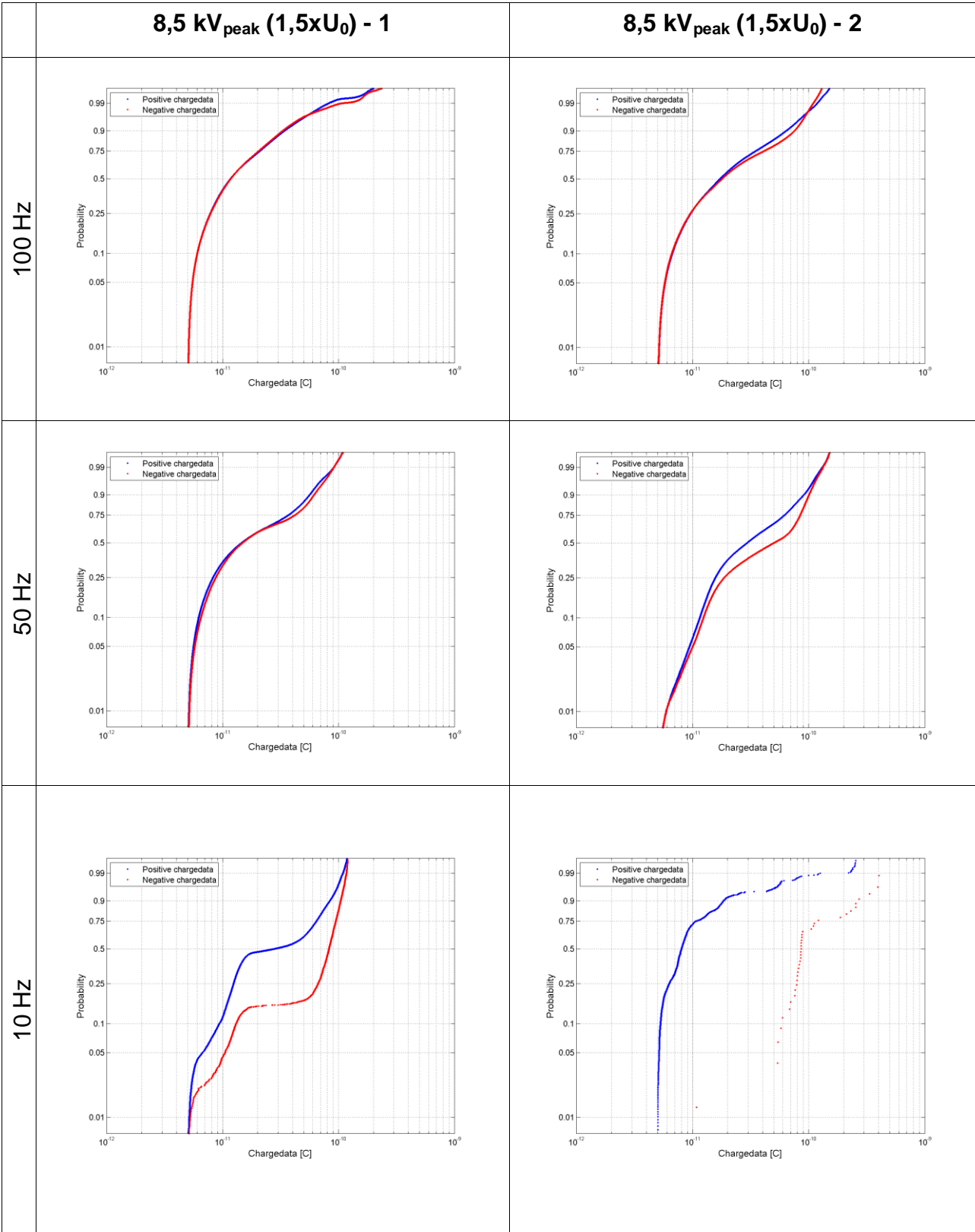
The following pages contain weibull plots from all PD measurements performed on the test objects. All measurements were performed twice.

Joint #1 Aging: 256h / 14 cycles

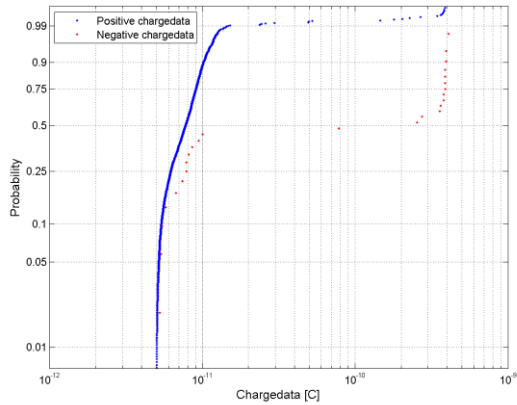
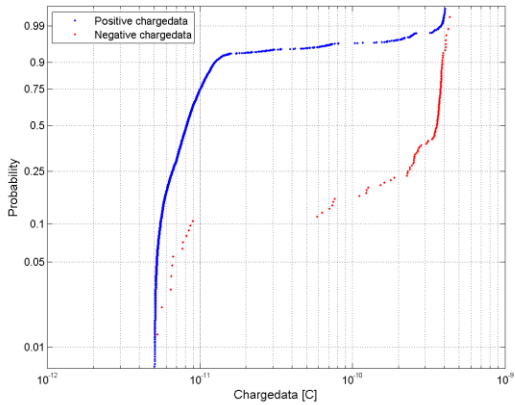




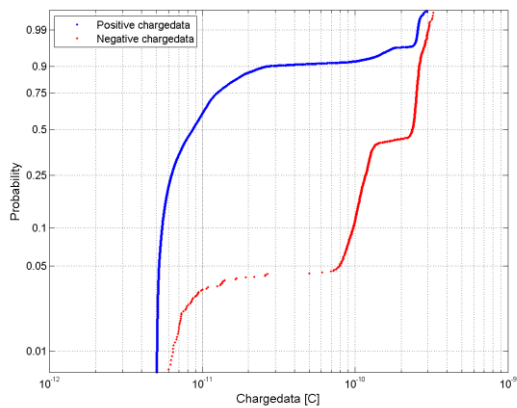
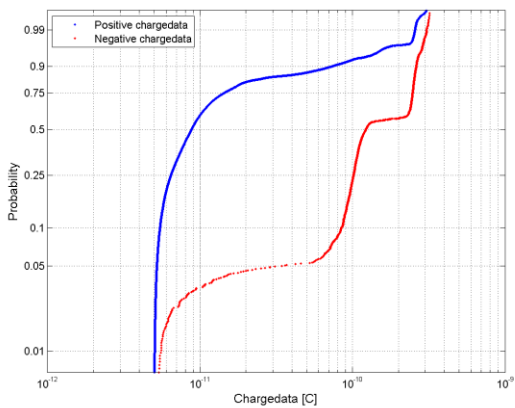
Joint # 1 Aging: 256h / 14 cycles.



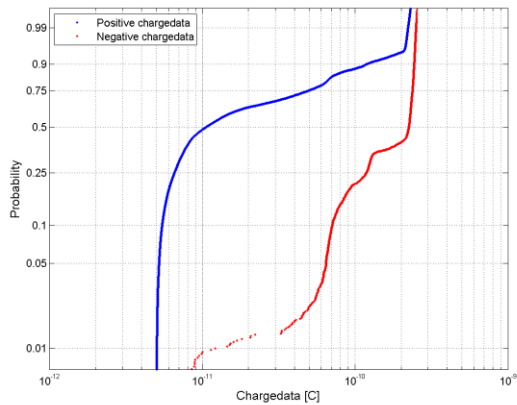
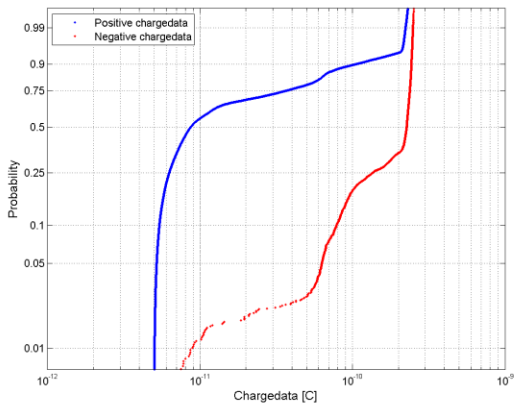
1 Hz



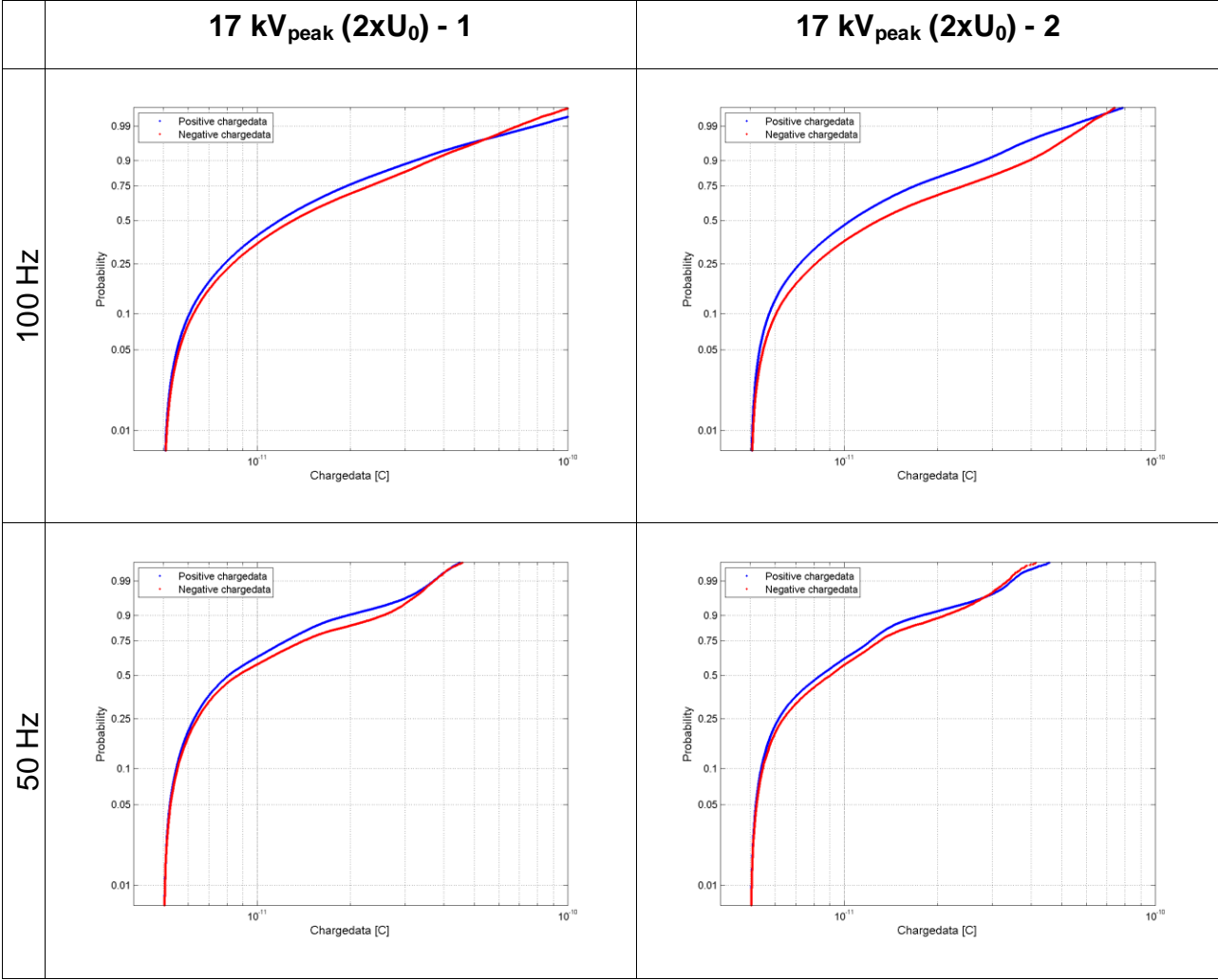
0,1 Hz



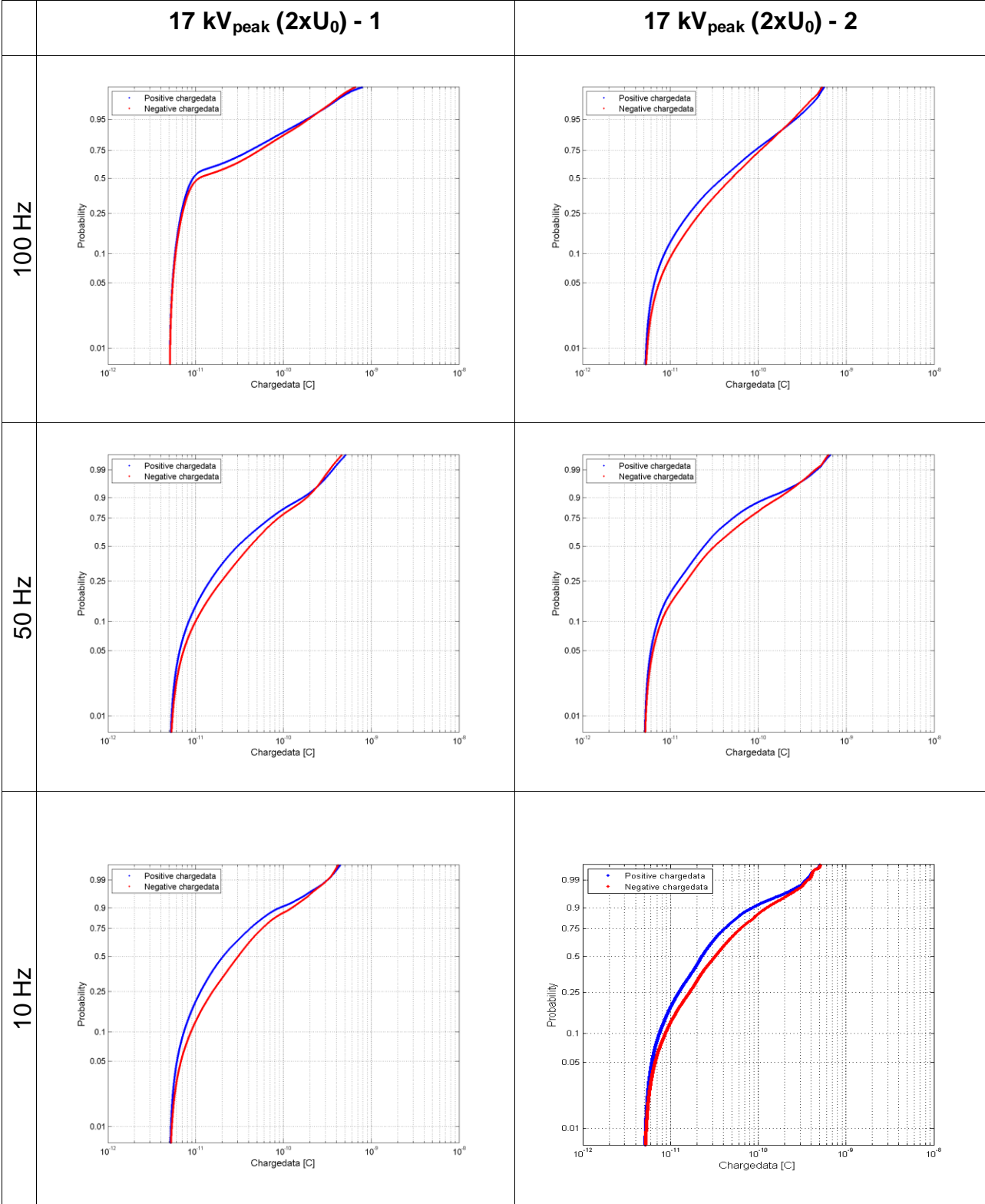
0,01 Hz



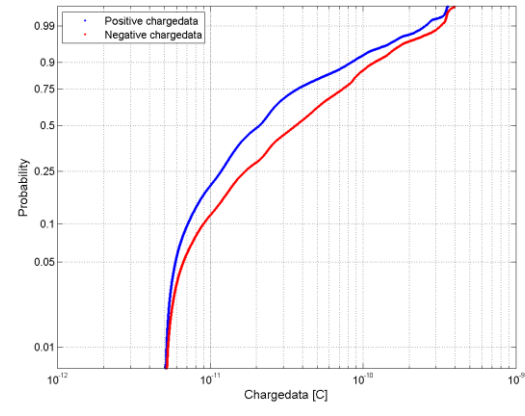
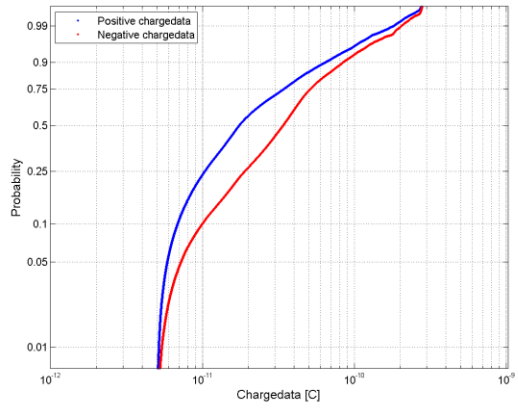
Joint #2 Aging: 136 h / 10 cycles



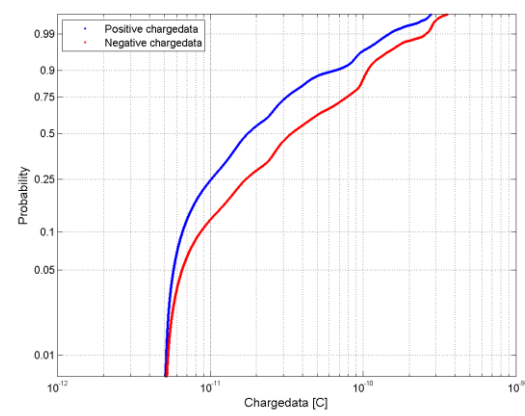
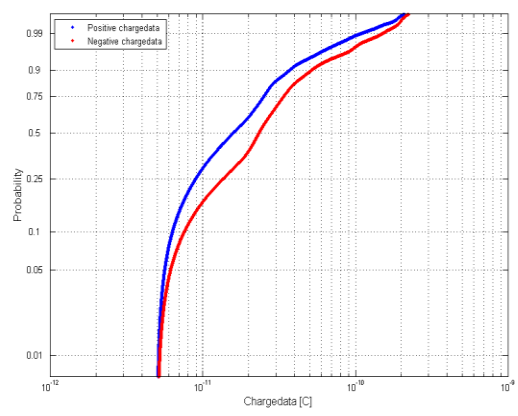
Joint #2 Aging: 256h / 14 cycles



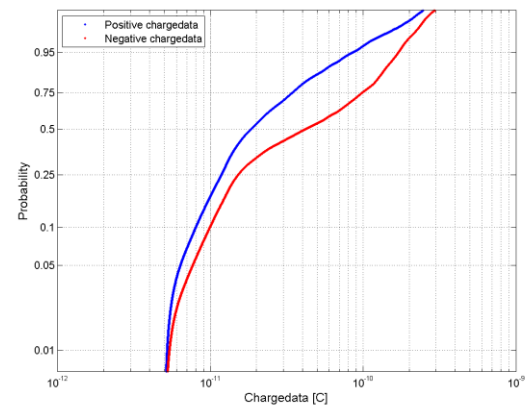
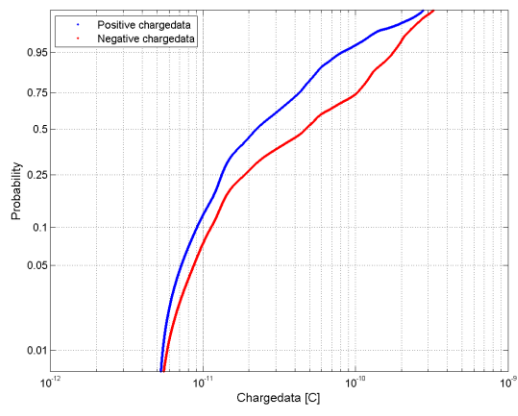
1 Hz



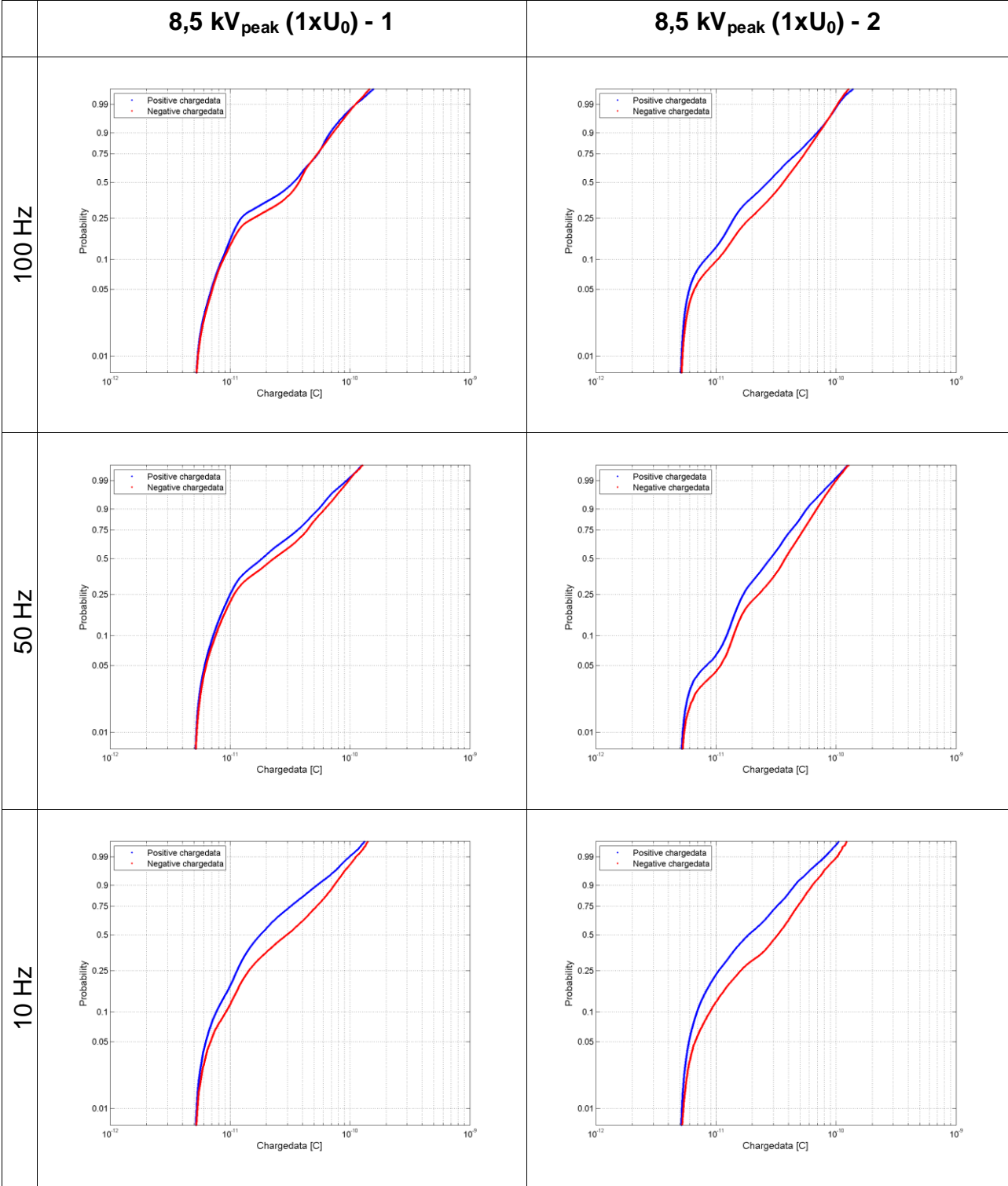
0,1Hz



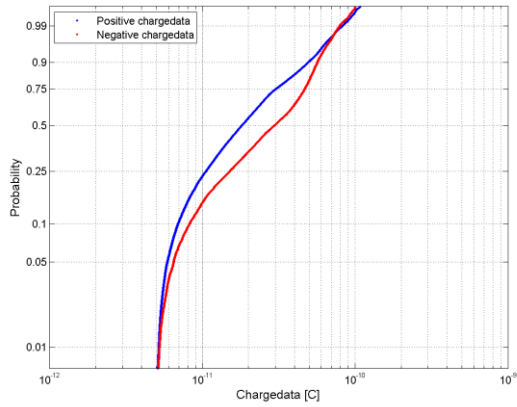
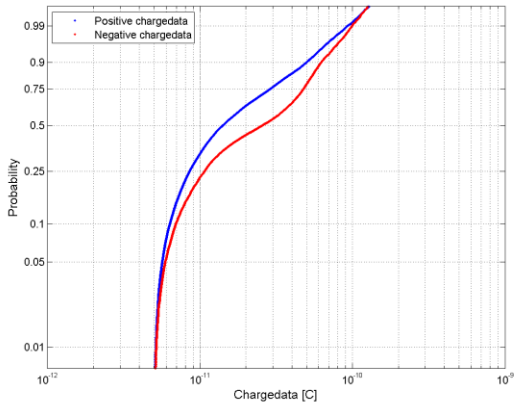
0,01Hz



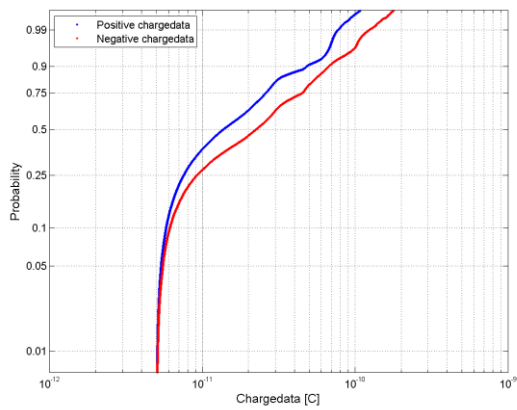
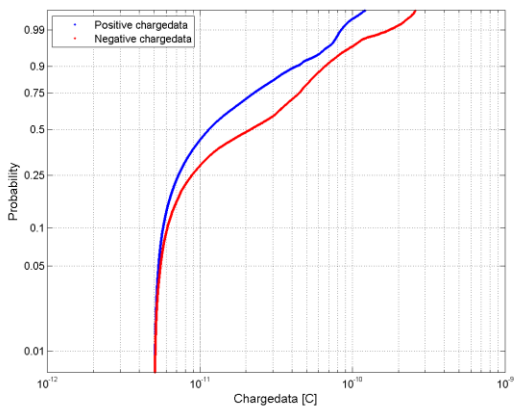
Joint #2 Aging: 256 h / 14 cycles



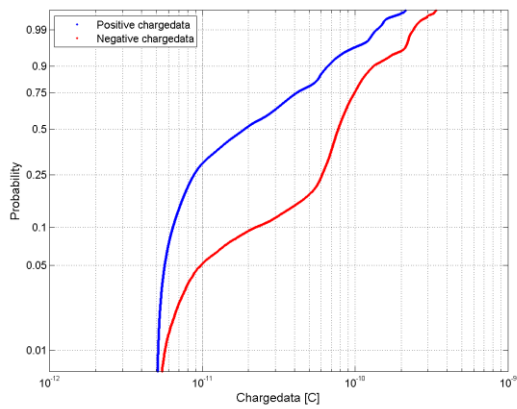
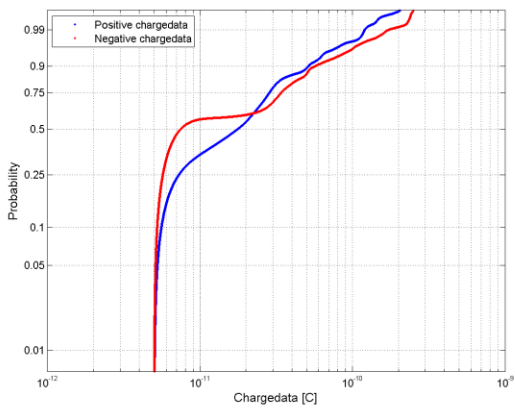
1 Hz



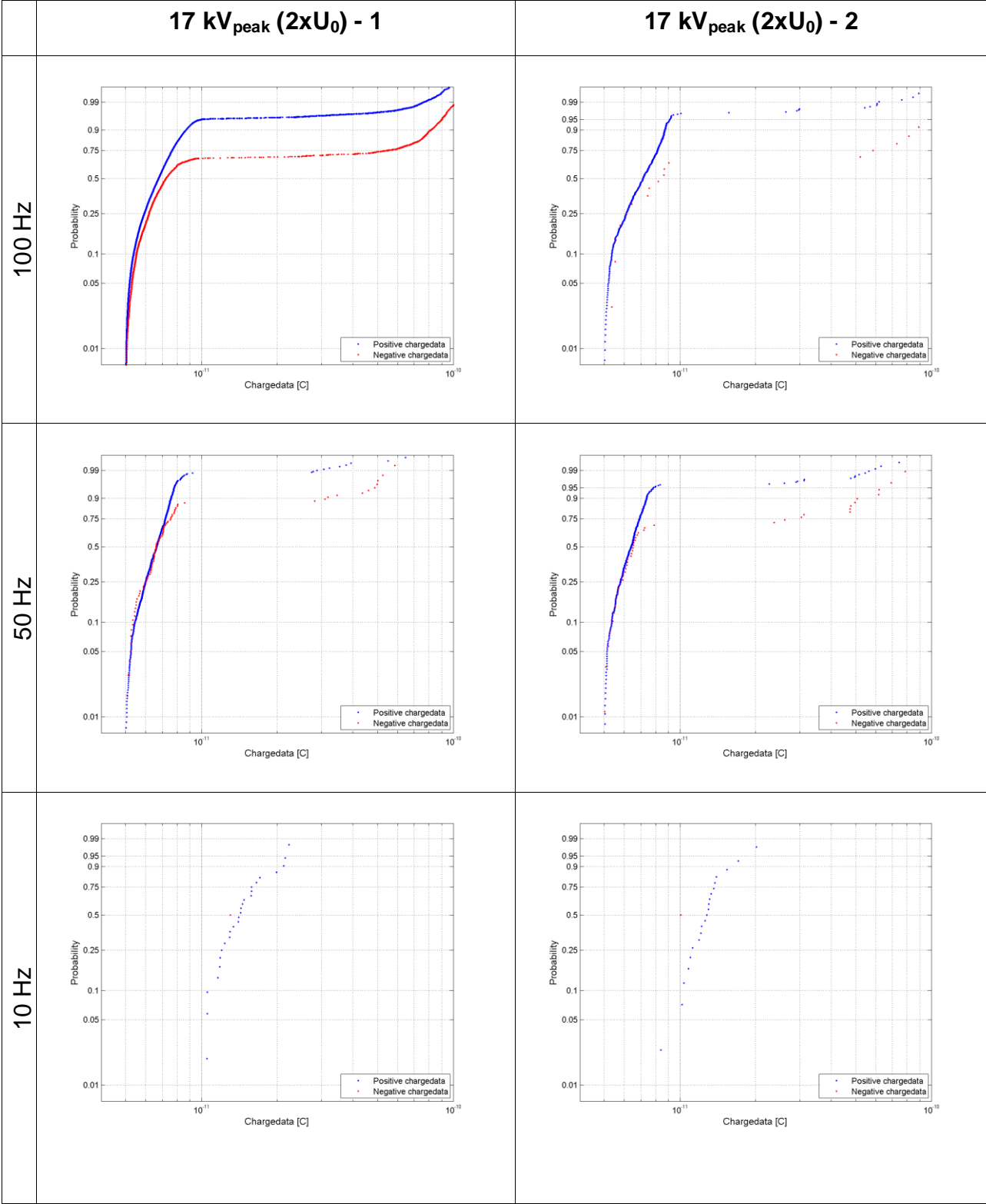
0,1 Hz



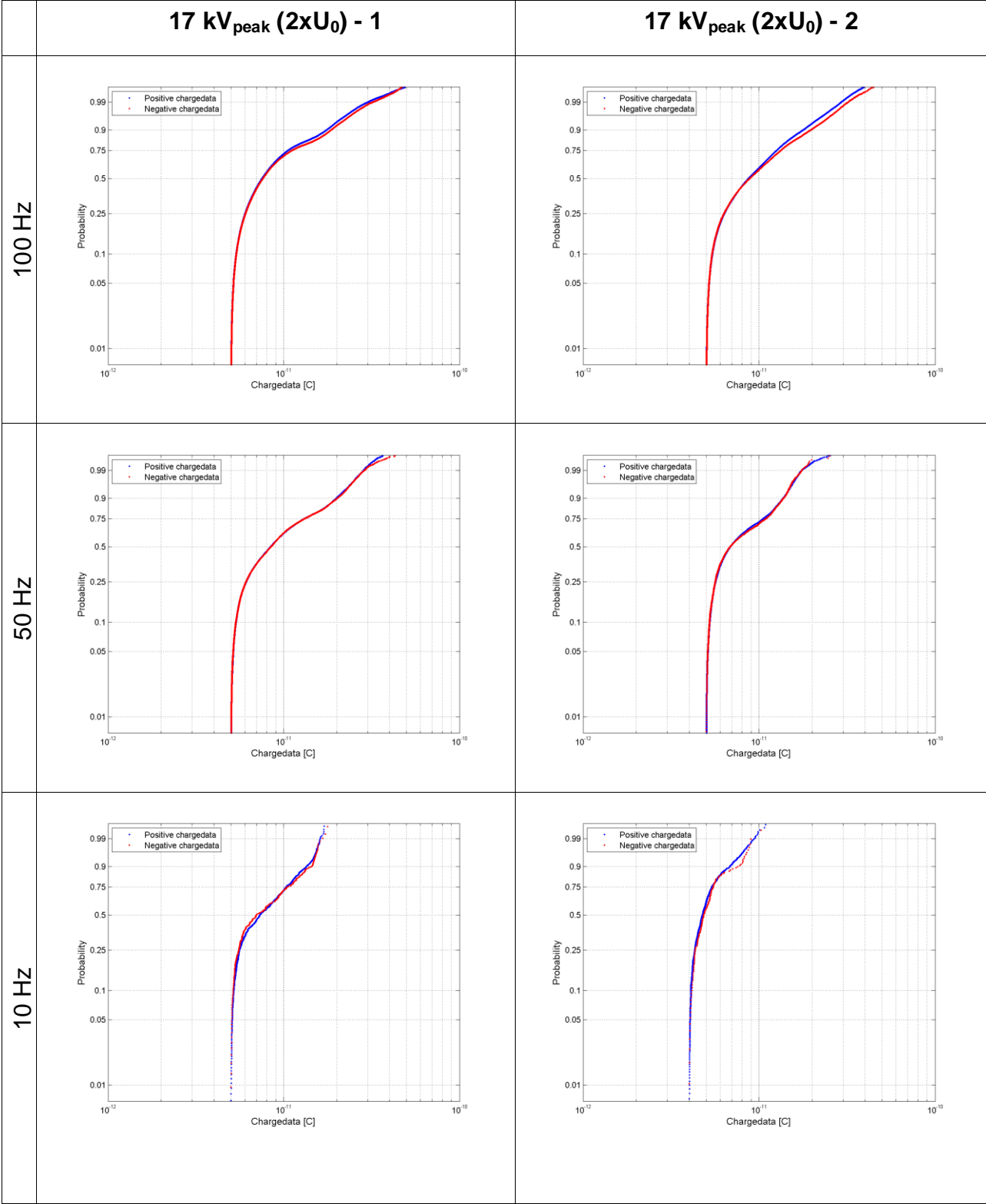
0,01 Hz

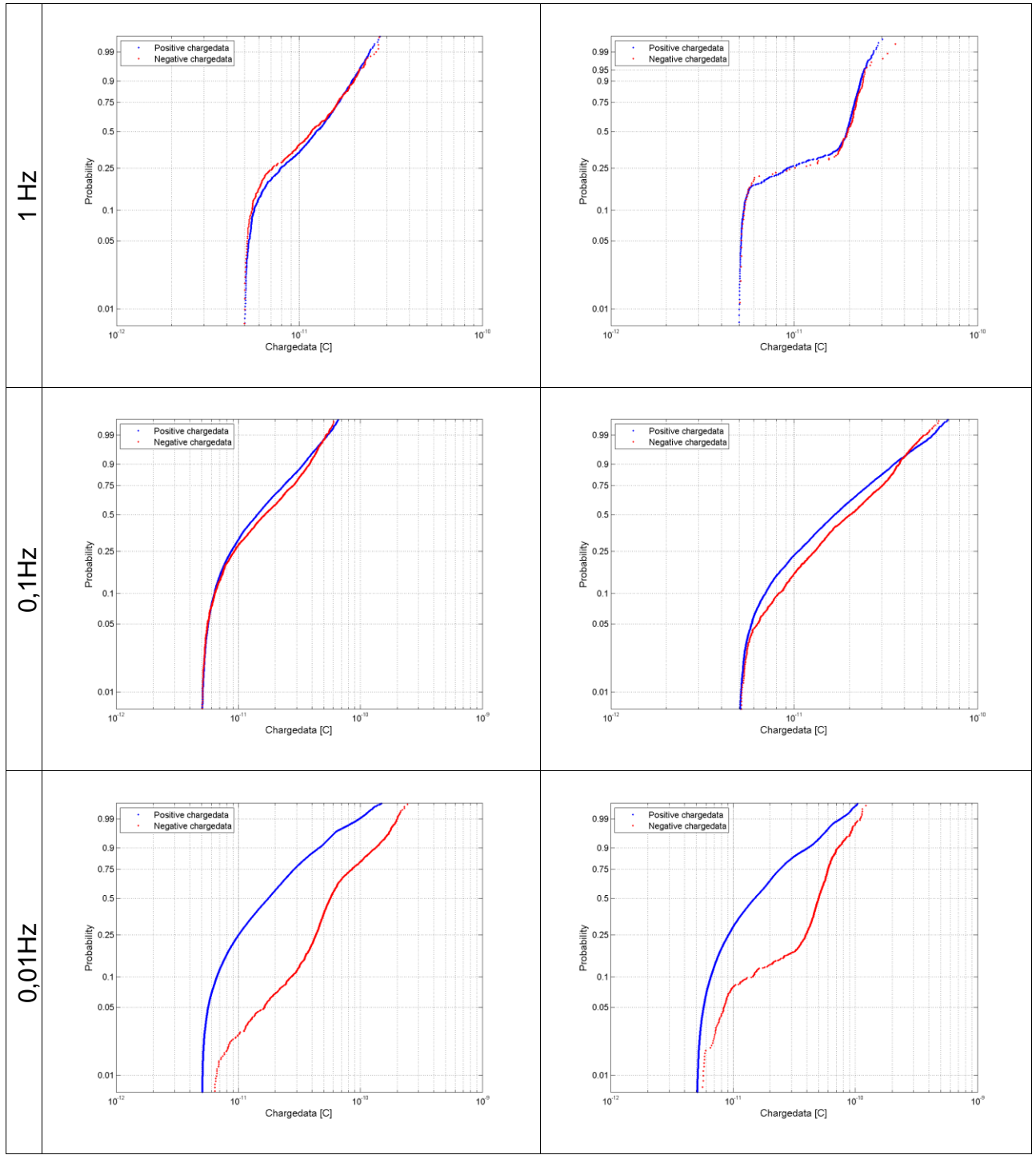


Joint #3 Aging: 136 h / 10 cycles

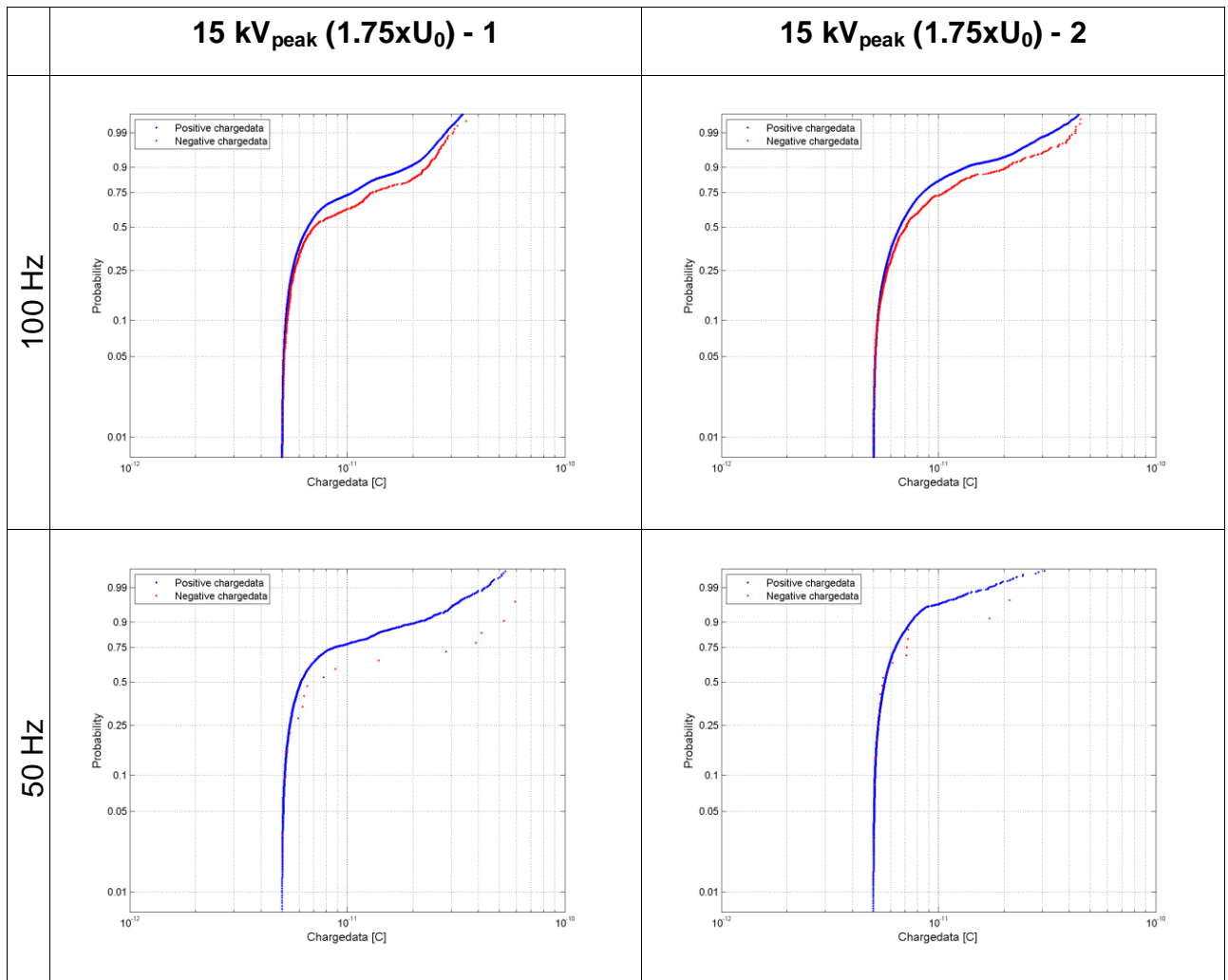


Joint #3 Aging: 256h / 14 cycles






Joint #3 Aging: 256h / 14 cycles.



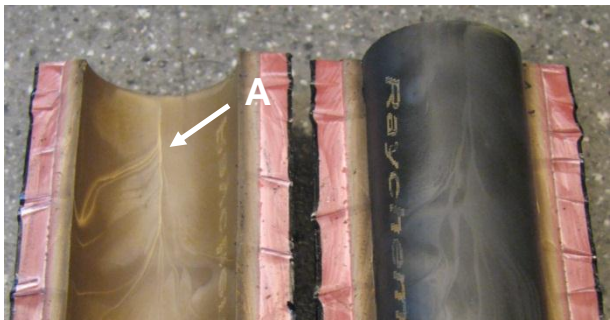
F. Dissection photos

Photos and comments from the dissection of the different test objects are presented on the following pages.

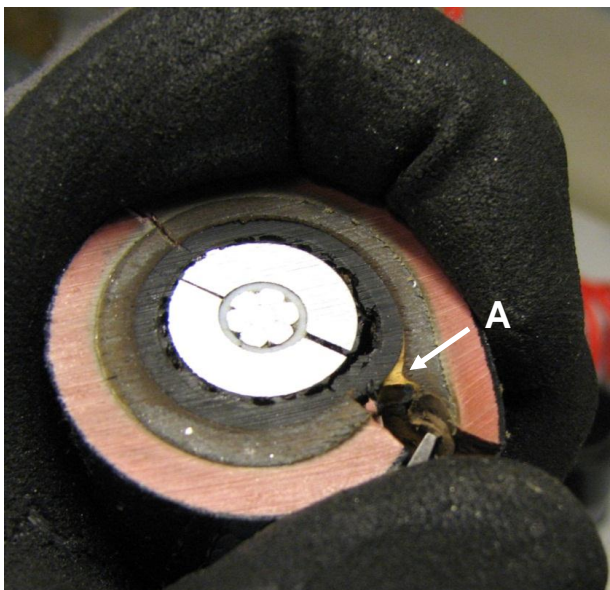
	<p>Glue has been pushed out from the protective outer sheath. The glue had accumulated between the joint and the thermal insulation. The thermal insulation had become brittle.</p>
	<p>Dried out glue inside aluminum foil on the outer sheath.</p>
	<p>Surface impressions from the aluminum foil on the insulating tube.</p>
	<p>Copper mesh fused into the insulating tube. No serious deformation or damage found.</p>



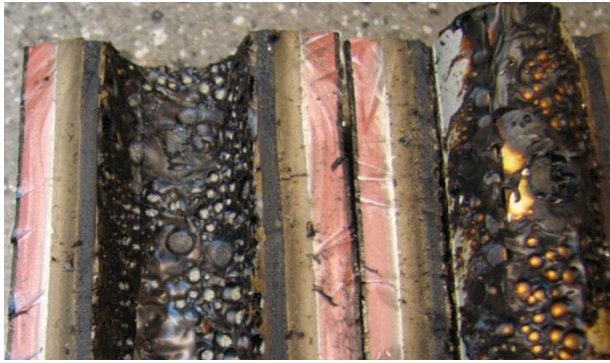
Copper mesh left impressions in the conducting layer outside the joint body. No punctures or holes could be detected.



The joint body and stress-control tube stuck very well together. Formations (A) in the layer between the joint body and stress-control tubing were made when pulling them apart. The inner part (grey/brown) of the joint body was still flexible. The outer part (red) had become harder.



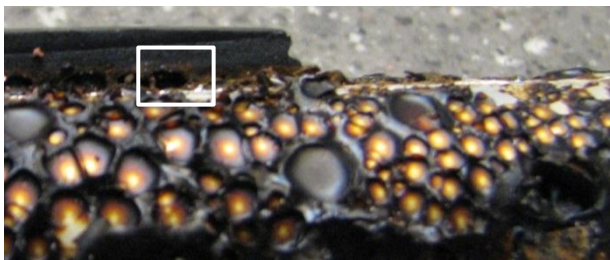
Joint body material stuck to stress-control tube (A). Picture shows how material stretches and changes color as it is pulled off.



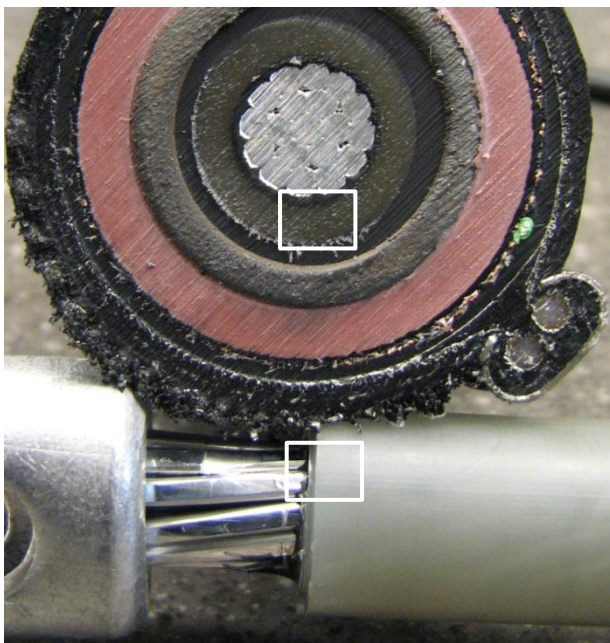
Pits and cavities in mastic between joint ferrule and stress-control tube. Mastic and stress-control is brittle.



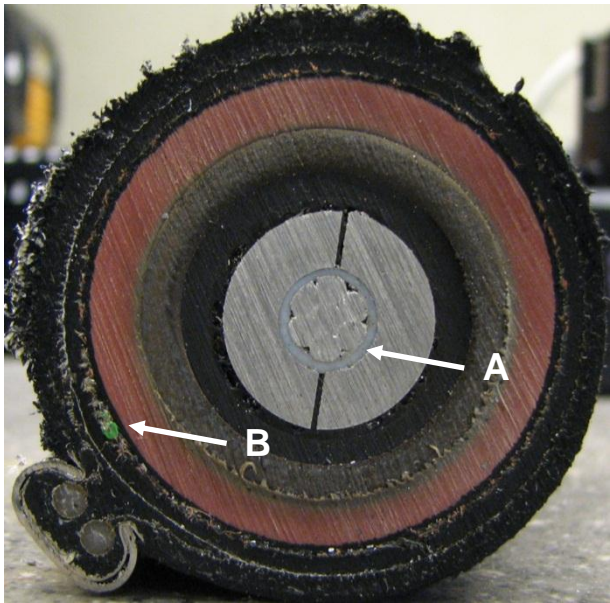
The stress-control tube broke off when removing joint ferrule leaving sharp edges (A).



Pits and cavities in mastic working their way towards the stress-control tube. Everything brittle and dried out.

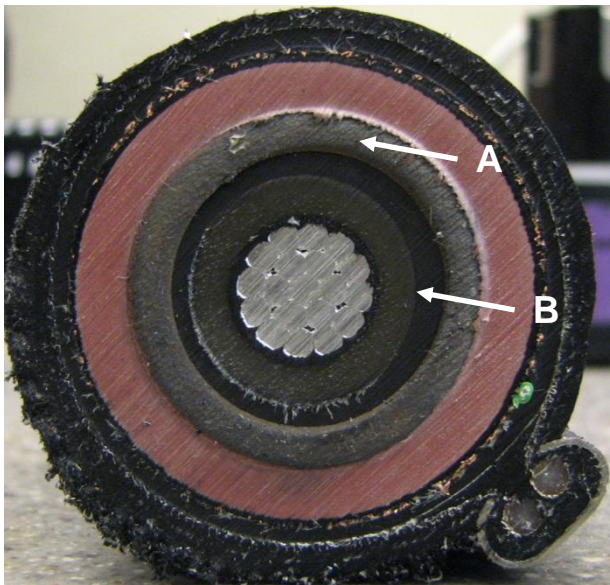


Discoloring of the XLPE inside the joint compared with the XLPE at the cable termination.

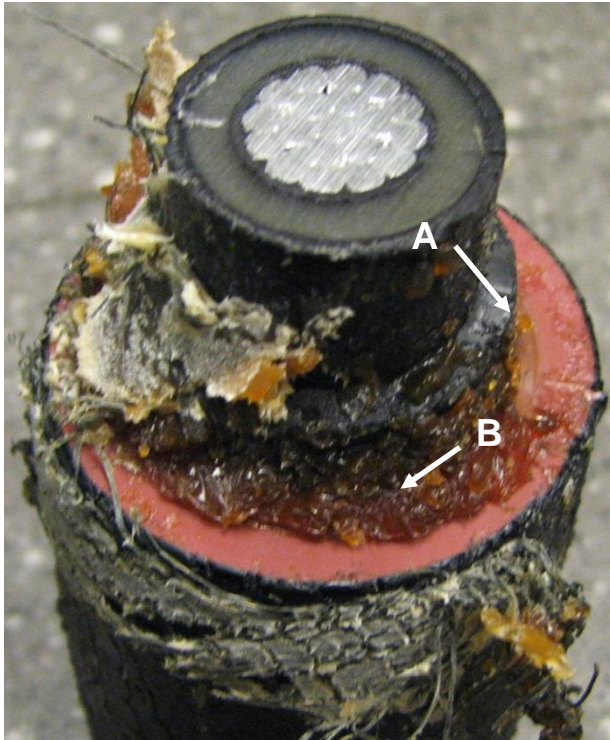


Joint ferrule with teflon between conductor and ferrule (A). The joint body colors had clearly changed in the inner part. The voids in the mastic inside the stress-control tube are visible.

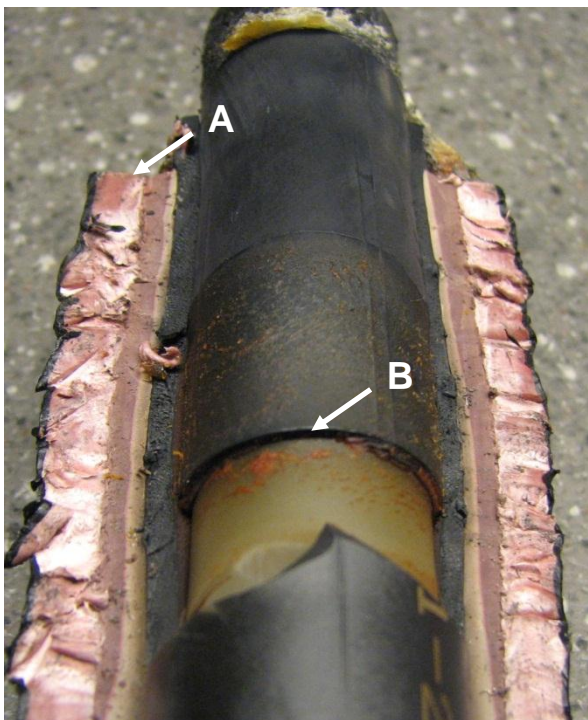
Thermocouple element can be seen in the copper mesh (B).



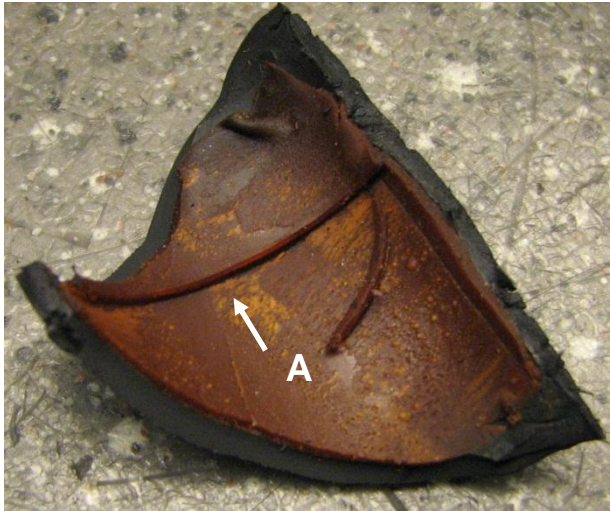
A cutaway close to the joint ferrule. Inner part of joint body bulging out, showing the flexibility (A). Stress control-tube with good adhesion to XLPE (B).



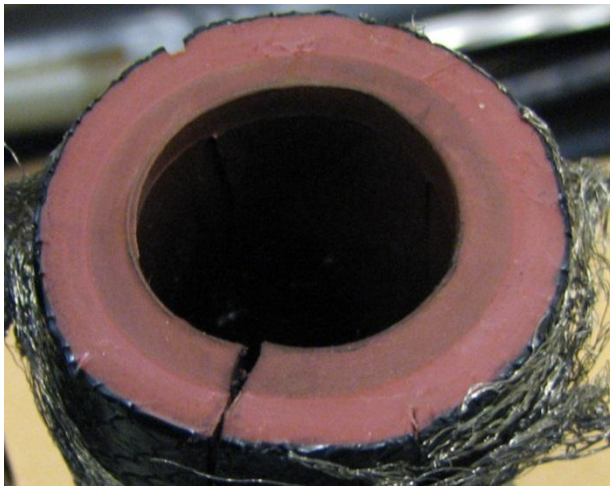
End of joint body and stress-control tube (A). Glue from insulating tube has accumulated in the corners (B). All materials seemed less brittle and aged compared to the middle of the joint. The materials were quite hard to pull apart.



End of joint body (A). XLPE-screen cut can be seen (B). Materials are far less aged and brittle compared to the center of the joint.



Mastic and stress-control tube taken from the XLPE-screen cut. The screen edge can be seen in the mastic (A). The material is not as aged and brittle as over the joint ferrule.



Joint #4 aged 12-15 hours. The colors are not changed in same degree as the joints aged 256 hours.



Joint #4 aged 12-15 hours. Stress-control tube still soft and flexible.

G. Equipment lists

Aging setup

Description	Name	Data	Sintef/NTNU ID
Variac	REO. RRTWMOG/TVR 6500.	32A 230V 7360W 50Hz	B01-07
Transformer one phase ring core	Noratel. N18068	1:47 40 A 75 V	B01-0816
Data logger	Agilent 34970A		G05-0142
Thermocouples	IEC type K	0-1100 °C.	n/a
DAQ	NI USB-6251		P08-0343
Terminal block	NI 7811R/7831RSCB- 68		P08-0203
Laptop		HP ProBook 6545b	Sintef
Ammeter	LEM Module. LT1000 S-1	0-1000A	I4-238
1/1 insulation transformer		3A 230V 175VA	B01-0703
Logger Software	BenchLink Data Logger 3. V3.10.00 2005		n/a
Variac Software	Labview 2011		n/a

Variable frequency PD measurement setup

Description	Name	Data	Sintef / NTNU ID
Quadripole/Measuring impedance	CPL 542A	Cn=30 μ F. I=0.5 A	H02-0133-16
Acquisition unit	MPD 600		H02-0132-02
Batteries	MPP 600		H02-0133-09 H02-0182-09
Fiber optics controller	MCU 502		H02-0133
Coupling capacitor	F & G Energie- technik GMBH. GSK150/800	Ck=800 pF, 150 kV	K03-0128
Calibrator	Cal1A. Power Diagnostix		H02-0172
Mixed Signal Oscilloscope	Tektronix MSO 2024	16ch. 200 MHz 1 GS/s	G04-0356
Function/Arbitrary waveform generator	Agient 33250A. 80MHz		B03-0410
Amplifier	TREK PD06035	\pm 30 kVDC or peak AC. \pm 40 mA peak AC \pm 20 mA DC Output impedance 47 Ω	B3-0404
Low-pass filter		20 kV 20 mA. No PD.	n/a
Laptop	HP	Running Omicron software	HP Compaq nc6000
Voltage Probe	Fluke	80K-40 HV 40 kV max	I06-0285

Acoustic PD measurement setup

Description	Name	Data	Sintef / NTNU ID
Preamplifier	Physical Acoustics Model 2/4/6	28 Vdc. 10kHz- 1.2MHz.	N07-0097
Preamplifier	Physical Acoustics Model 2/4/6	28 Vdc. 10kHz- 1.2MHz.	N07-0098
DC-Source		27 Vdc	NO7-0088-01
DC-Source		27 Vdc	NO-0070-07
Microphone	PAC D9241A- AA07		
Microphone	PAC D9241A- AA08		

H. Export data from MTRONIX to MATLAB

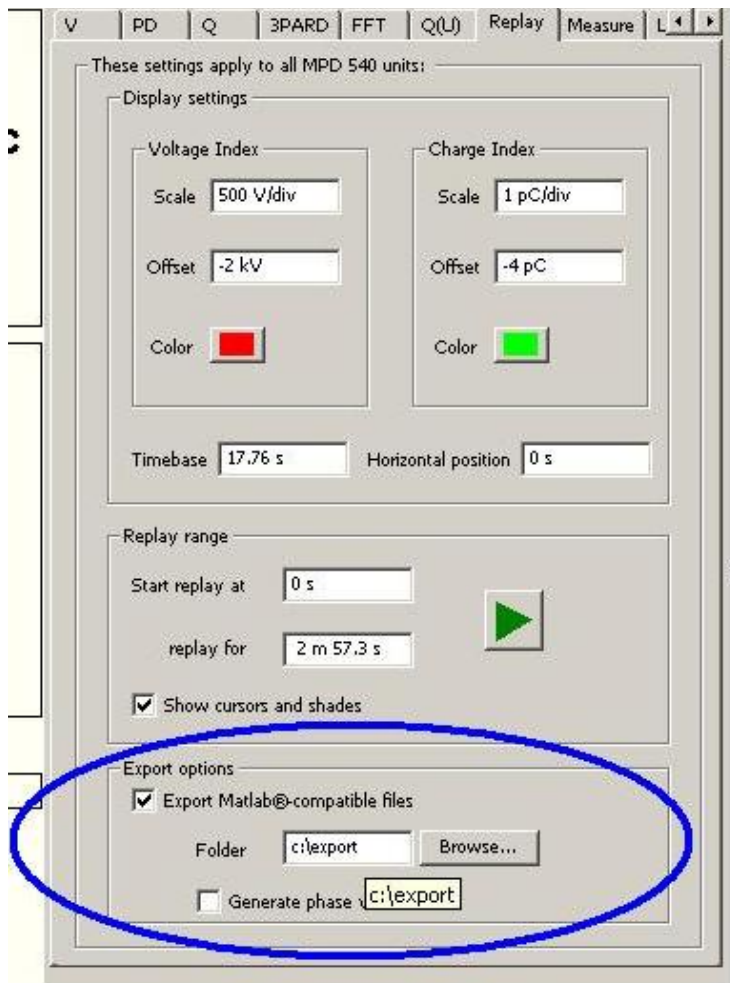


Figure 48. Mtronix software screen dump

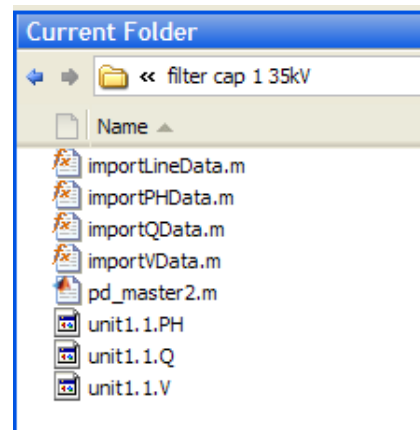


Figure 49. MATLAB folder content

To export data from the Mtronix software to MATLAB, first open the recorded Mtronix files in the Mtronix software. Check the boxes for **Export Matlab compatible files** and **Generate phase file**. When you press play under Replay Range, MATLAB readable files (unitx.y.PH, unitx.y.Q, unitx.y.V) will be created in the chosen folder during playback.

Put the export files in the same folder as the three m-files "importLineData.m, importPHData.m, importQData.m, importVdata.m. The mfiles converts the Mtronix-files to MATLAB tables using the three commands: (example on next page)

```
[q_tm,q]=importQData('folder','unitx.y.');
```

```
[phase]=importPHData('folder','unitx.y.');
```

```
[v_tm,v]=importVData('folder','unitx.y.');
```

Y:\TET5505 Fordypningsprosjekt\pex_endeavs_v3\40kV\importQData.m

```
1 function [q_tm, q] = importQData(folder, qUnit);
2
3 - fileName = sprintf('%s\\%s.Q', folder, qUnit);
4
5 - file = fopen(fileName, 'rb');
6
7 - if file == -1
8 -     msg = sprintf('file %s could not be opened', fileName);
9 -     error(msg);
10 - end
11
12 - fseek(file, 0, 'bof');
13 - q = fread(file, inf, 'float32', 8);
14 - fseek(file, 4, 'bof');
15 - q_tm = fread(file, inf, 'float64', 4);
16
```

Y:\TET5505 Fordypningsprosjekt\pex_endeavs_v3\40kV\importPHData.m

```
1 function phase = importPHData(folder, qUnit);
2
3 - fileName = sprintf('%s\\%s.PH', folder, qUnit);
4
5 - file = fopen(fileName, 'rb');
6
7 - if file == -1
8 -     msg = sprintf('file %s could not be opened', fileName);
9 -     error(msg);
10 - end
11
12 - fseek(file, 0, 'bof');
13 - phase = fread(file, inf, 'float64');
14
15
```

Y:\TET5505 Fordypningsprosjekt\pex_endeavs_v3\40kV\importVData.m

```
1 function [v_tm, v] = importVData(folder, vUnit);
2
3 - fileName = sprintf('%s\\%s.V', folder, vUnit);
4
5 - file = fopen(fileName, 'rb');
6
7 - if file == -1
8 -     msg = sprintf('file %s could not be opened', fileName);
9 -     error(msg);
10 - end
11
12 - fseek(file, 0, 'bof');
13 - v = fread(file, inf, 'float32');
14 - v_tm = 48e-6 * (0:size(v, 1) - 1);
```

I. Driving capacitive load

Cable (from termination to metall sleeve)

$$\epsilon_{c,r} := 2.5 \quad d_{c,y} := 19.5\text{mm} \quad d_{c,i} := 11.4\text{mm} \quad l_c := 1300\text{mm}$$

$$C_c := \frac{2 \cdot \pi \cdot \epsilon_0 \cdot \epsilon_{c,r} \cdot l_c}{\ln\left(\frac{d_{c,y}}{d_{c,i}}\right)} \quad C_c = 337 \cdot \text{pF}$$

Joint (over metall sleeve)

$$\epsilon_{j,r} := 3 \quad d_{j,y} := 25\text{mm} \quad d_{j,i} := 19.5\text{mm} \quad l_j := 170\text{mm}$$

$$C_j := \frac{2 \cdot \pi \cdot \epsilon_0 \cdot \epsilon_{j,r} \cdot l_j}{\ln\left(\frac{d_{j,y}}{d_{j,i}}\right)} \quad C_j = 114 \cdot \text{pF}$$

Joint (side of metall sleeve)

$$\epsilon_{s,r} := 3 \quad d_{s,y} := 25\text{mm} \quad d_{s,i} := 11.4\text{mm} \quad l_s := 200\text{mm}$$

$$C_s := \frac{2 \cdot \pi \cdot \epsilon_0 \cdot \epsilon_{s,r} \cdot l_s}{\ln\left(\frac{d_{s,y}}{d_{s,i}}\right)} \quad C_s = 43 \cdot \text{pF}$$

Capacitance in test object

$$C_{t,o} := C_c + C_j + C_s \quad C_{t,o} = 494 \cdot \text{pF}$$

Driving Capacitive Loads with Sine Waves

$$i = (C_{load} + 60 \text{ pF}) 2\pi f V_{peak}$$

where: i = the peak current needed from the amplifier

C_{load} = the load capacitance

60 pF = the internal capacitance of the P0622B

f = the maximum output frequency

V_{peak} = the peak voltage applied to the capacitive load

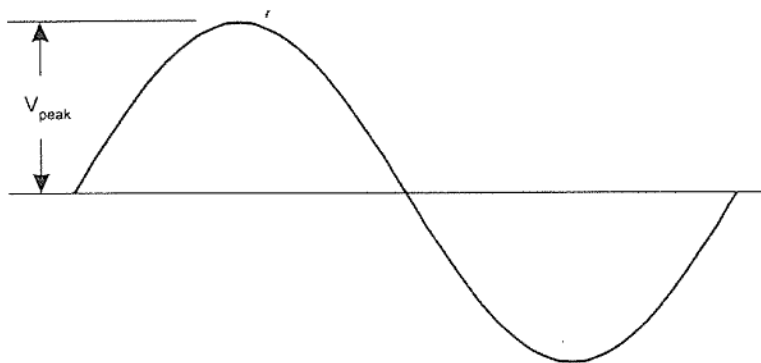


Figure 50. Calculation of current in capacitive load driven by TREK HV amplifier [33].

Driving the capacitive load (limit 40mA, 50pF internal)

$$C_{filter} := 700\text{pF} + 700\text{pF}$$

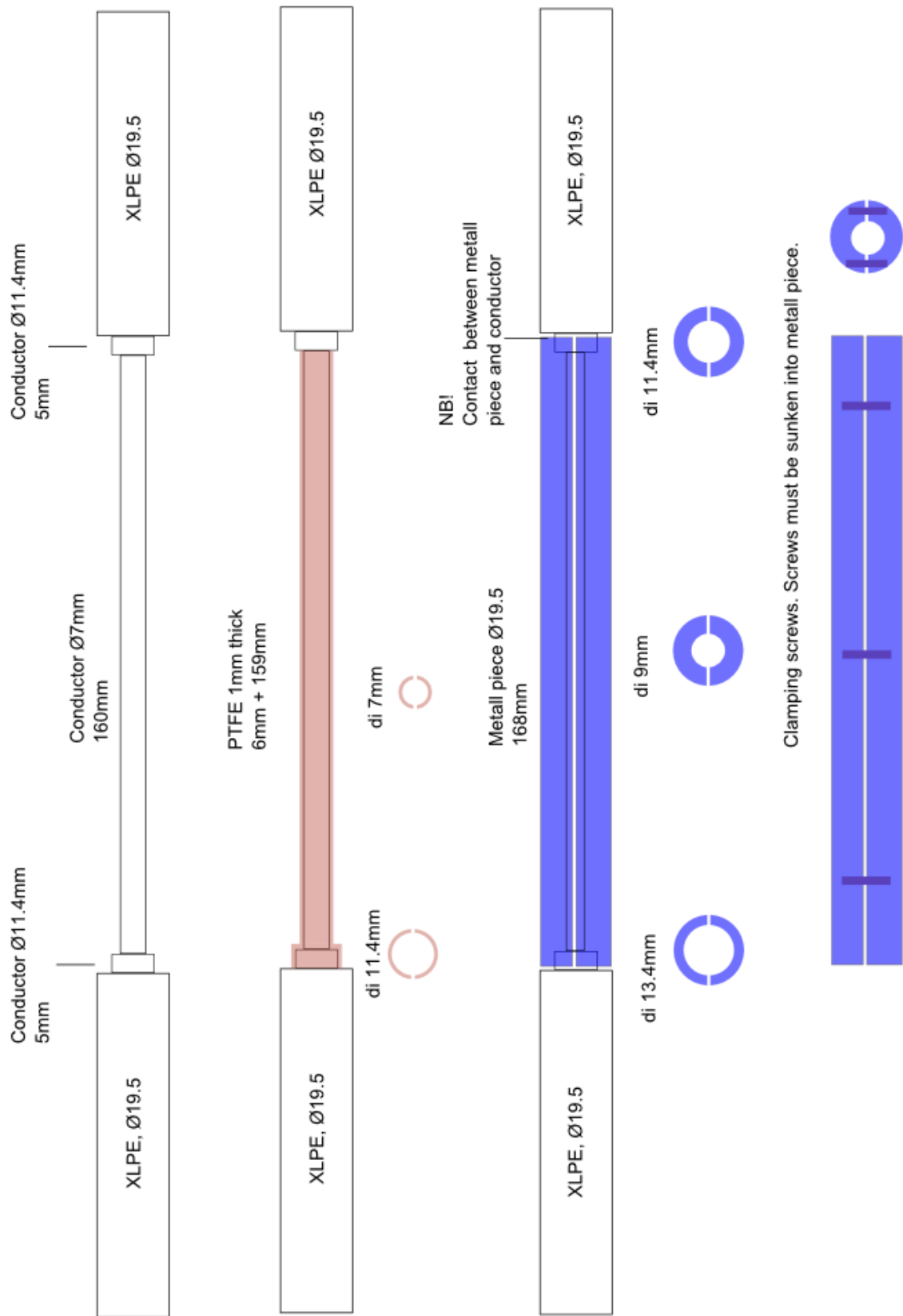
$$C_k := 800\text{pF}$$

$$C_{tot} := C_{t.o} + 50\text{pF} + C_{filter} + C_k \quad C_{tot} = 2.744 \text{ nF}$$

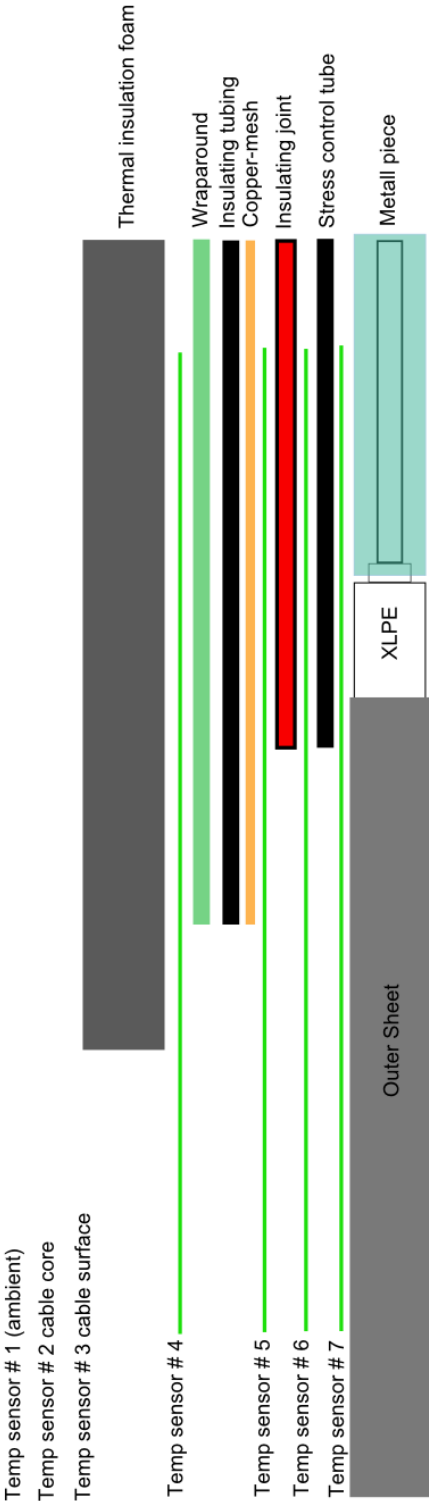
$$f := 100\text{Hz} \quad U_{peak} := 17\text{kV}$$

$$I_{peak} := C_{tot} \cdot 2 \cdot \pi \cdot f \cdot U_{peak} \quad I_{peak} = 29.3 \text{ mA}$$

J. Joint ferrule replacement



K. Temperature sensor placement in joint #4



L. Labview aging program

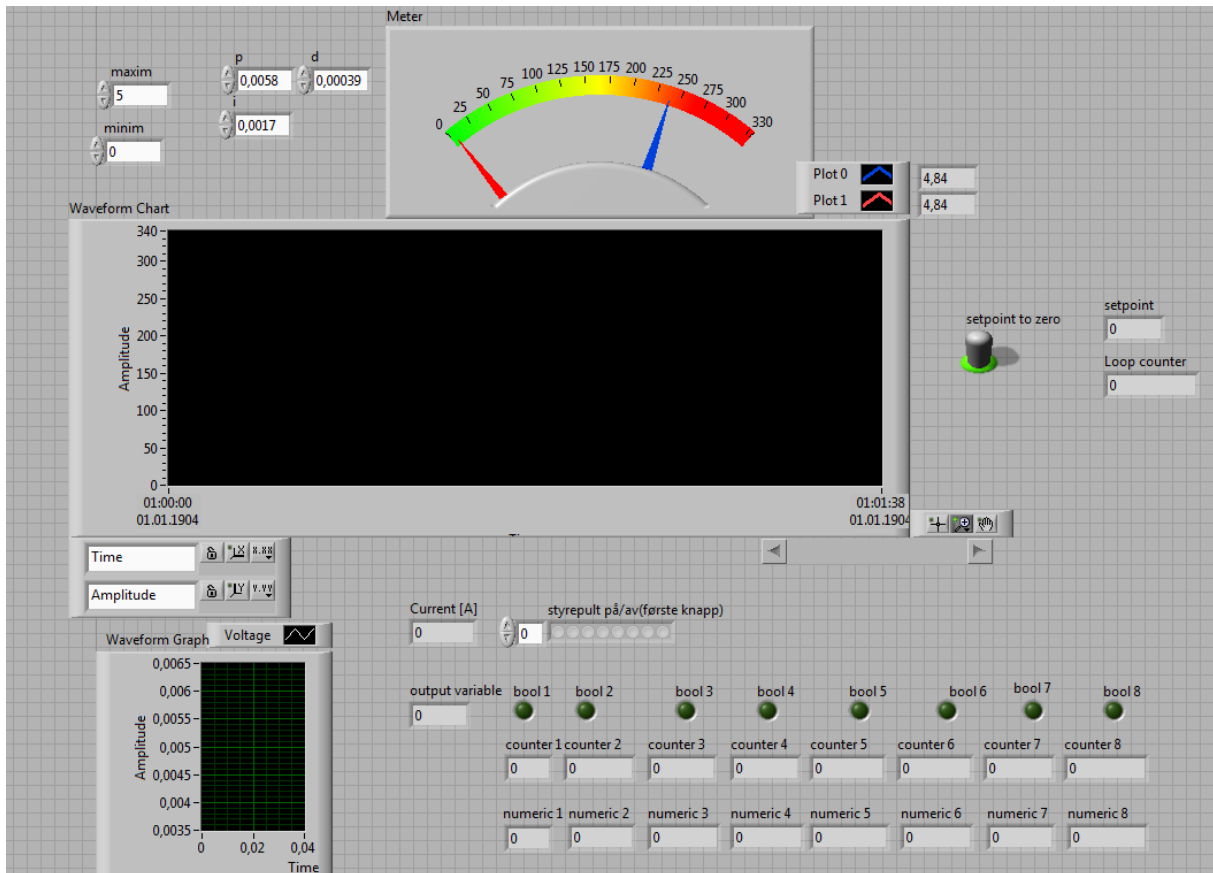


Figure 51. Front panel for Labview program used in aging setup. Functionality: -Turn on/off variac. -Set setpoint to zero -Monitor current waveform in test object - Monitor set point current and actual current values - Monitor counters - Set PID controller variables - Set output voltage min/max.

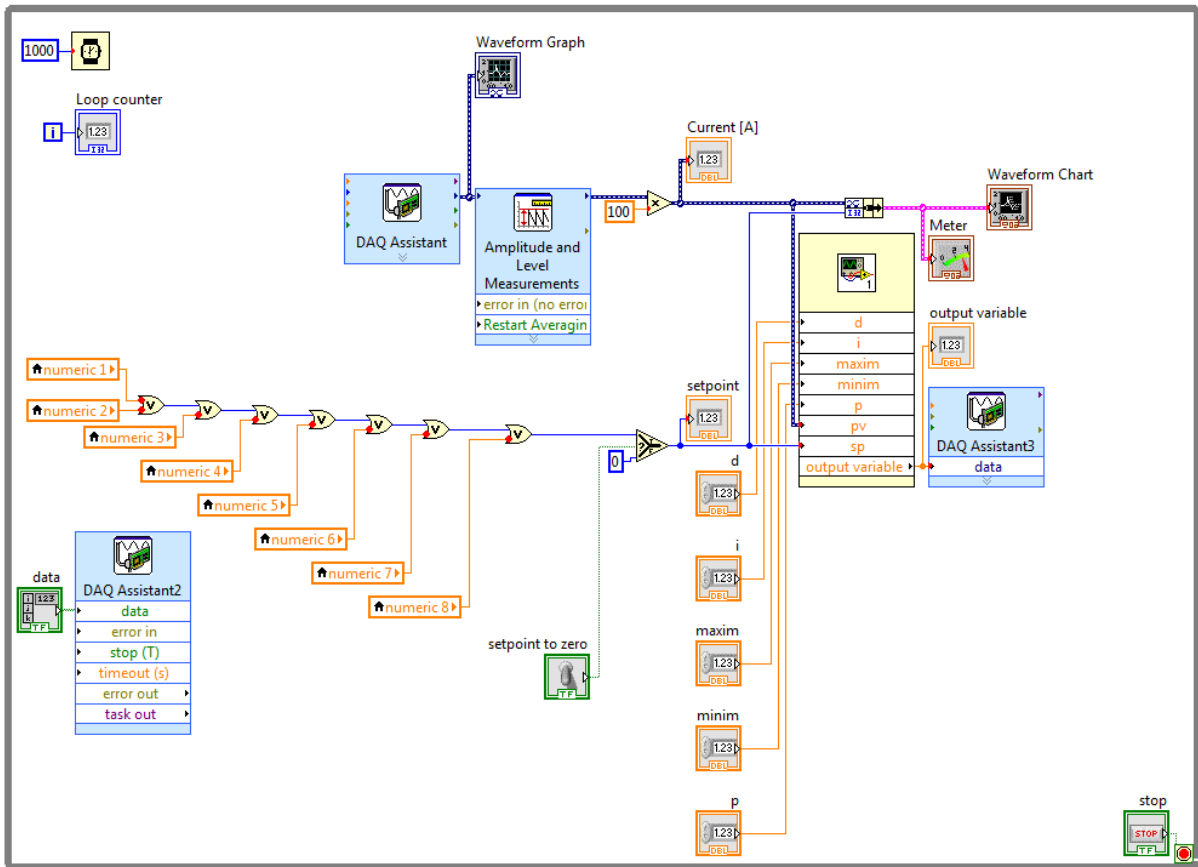
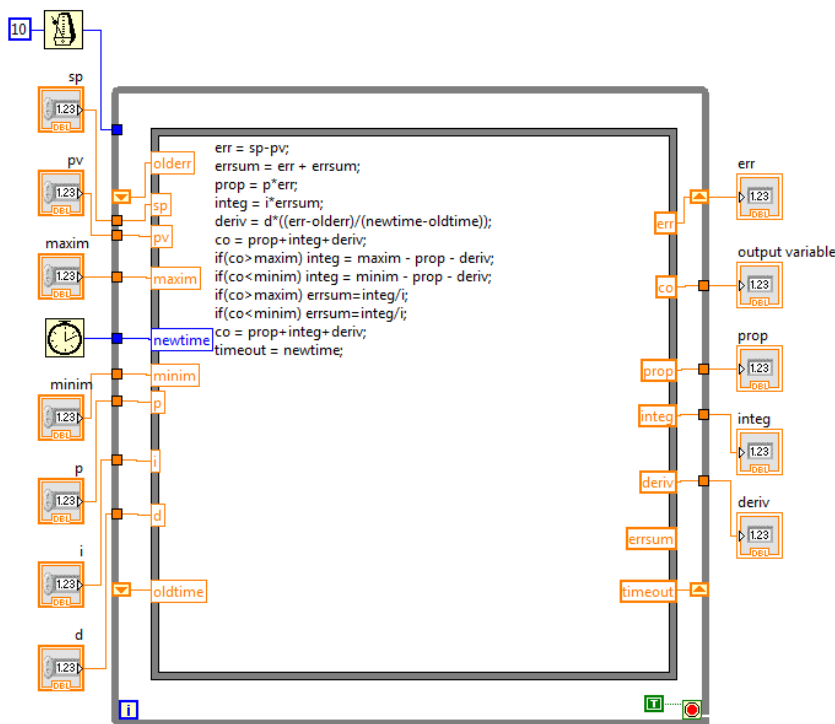


Figure 52. Block diagram for Labview program used in aging setup. Functionality: - Input from ammeter – Output to Variac (voltage set point, on/off)



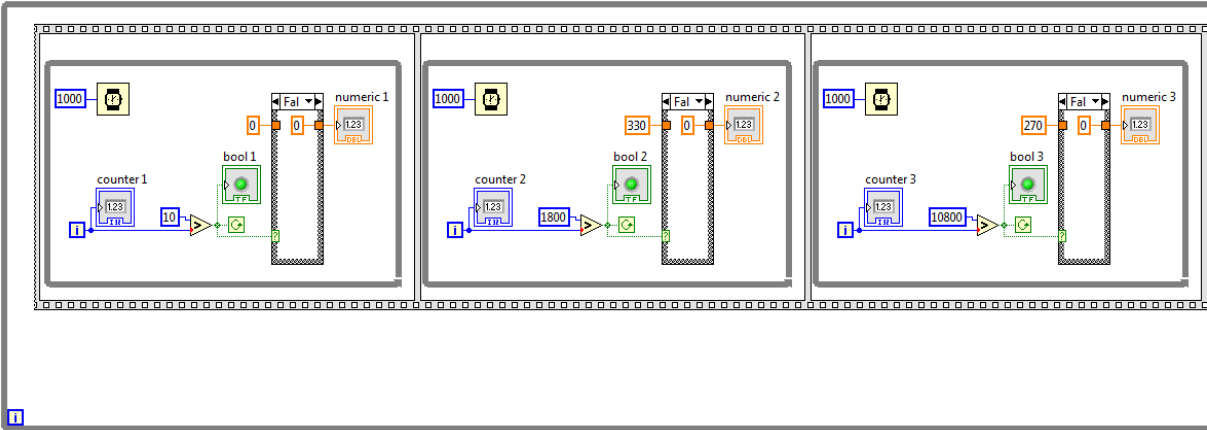


Figure 54. Block diagram for Labview program used in aging setup. Counter and set point. 1/3.

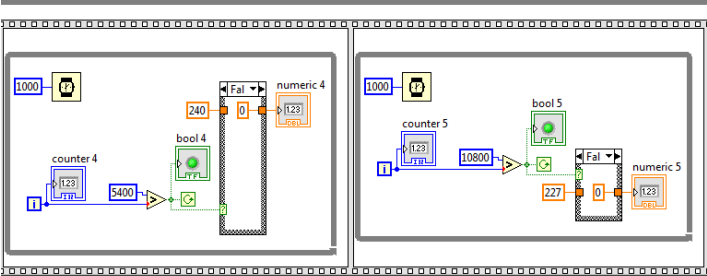


Figure 55. Block diagram for Labview program used in aging setup. Counter and set point. 2/3.

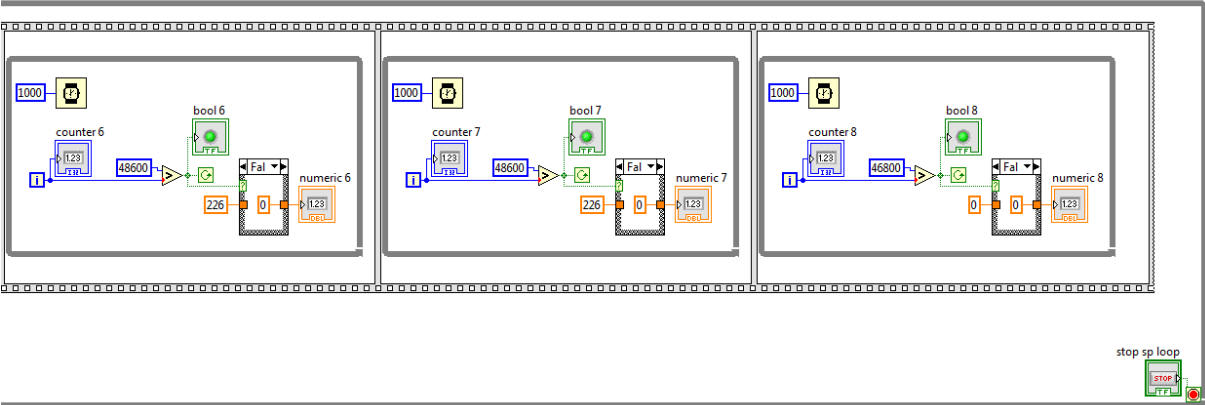


Figure 56. Block diagram for Labview program used in aging setup. Counter and set point. 3/3.

M. Wiring diagram aging setup

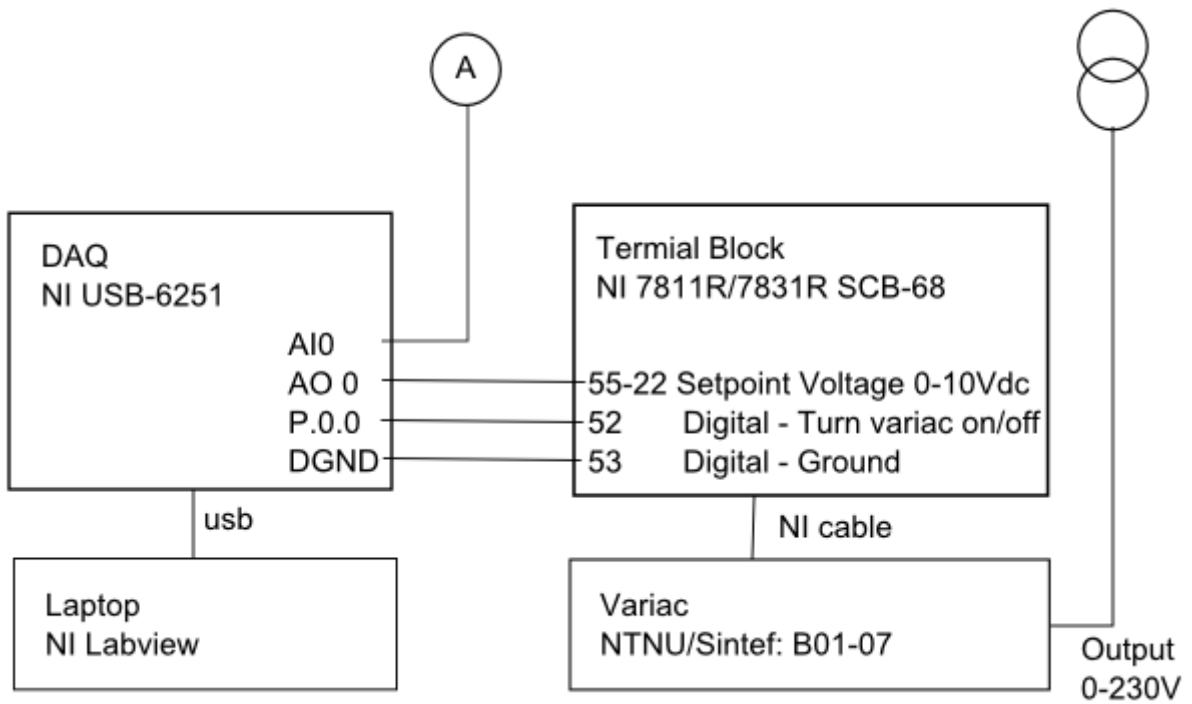


Figure 57. Wiring diagram for aging setup. Find complete component information in equipment list.